Longitudinal Diffusion-Weighted Imaging and T2 Relaxometry of the Hippocampus in Temporal Lobe Epilepsy

by

Seyed Amir Ali Adel

A thesis submitted in partial fulfillment of the requirements for the degree of

Master of Science

Department of Biomedical Engineering
University of Alberta

Abstract

Hippocampal sclerosis (HS) is an important predictor of surgical outcome in temporal lobe epilepsy (TLE). High-resolution (1 mm isotropic) diffusion tensor imaging (DTI) of the hippocampus in TLE patients has shown patterns of hippocampal subfield diffusion abnormalities which were consistent with HS subtype on surgical histology in a pilot sample of four patients. T2 relaxometry has also demonstrated focal hippocampal abnormalities which correlated with HS pathological features of neuron loss, gliosis, and granule cell dispersion. The objectives of this thesis were to determine the stability of focal hippocampus diffusion changes over time in TLE patients, compare diffusion and quantitative T2 abnormalities of the sclerotic hippocampus and correlate pre-surgical mean diffusivity (MD) and T2 maps with post-surgical histology.

To address these objectives, 19 TLE patients and 19 controls underwent two high-resolution ($1 \times 1 \times 1$ mm^3) DTI and ($1.1 \times 1.1 \times 1$ mm^3) T2 relaxometry scans (in a subset of 16 TLE patients and 9 controls) of the hippocampus at 3T, with a 2.6±0.8 year inter-scan interval. Within-participant hippocampal volume, MD and T2 were compared between the scans. Contralateral hippocampal changes 2.3±1.0 years after surgery and ipsilateral pre-operative MD maps versus post-operative subfield histopathology were evaluated in 8 patients who underwent surgical resection of the hippocampus.

The results showed significantly reduced volume and elevated MD and T2 of sclerotic hippocampi compared to healthy and non-HS hippocampi. These whole-hippocampus measures remained unchanged between the longitudinal scans. Focal regions of elevated MD and T2 in bilateral hippocampi of HS TLE were detected consistently at both scans. Regions of high MD and T2 correlated and remained consistent over time. Volume, MD and T2 remained unchanged in post-operative contralateral hippocampus. Regional elevations of MD identified subfield neuron

loss on post-surgical histology with 88% sensitivity and 88% specificity. Focal T2 elevations identified subfield neuron loss with 75% sensitivity and 88% specificity.

The findings of this work suggest no significant change in diffusion and T2 abnormalities in ipsilateral and contralateral hippocampi between the two scans, suggesting permanent micro-structural alterations. While both MD and T2 accurately predicted HS subtypes, MD was more sensitive than T2 in detecting neuron loss on post-surgical histology. Both DTI and T2 acquisitions were acquired using a clinically feasible protocol (at 3T in under 6 minutes each), potentially providing the opportunity to diagnose precise HS subtypes as well as detect subtle or regional contralateral hippocampal abnormalities, which may aide in predicting surgical outcomes preoperatively.

Preface

This thesis is an original work by Seyed Amir Ali Adel. The research project, of which this thesis is a part, received research ethics approval from the University of Alberta Research Ethics Board, Project Name “High Resolution Imaging in Epilepsy”, No. Pro00002937, 2021-2022.

Chapter 3 of this thesis has been submitted for publication

Acknowledgments

I would like to express my superior gratitude to my supervisors, Dr. Christian Beaulieu and Dr. Donald Gross. Christian, thank you for providing me with independence and critical feedback to learn and grow as a researcher. Don, thank you for always being extraordinary with your support and showing me what it means to be a brilliant physician scholar. A sincere thanks to Dr. Alan Wilman for his kindness and wisdom and Peter Seres for his patience to help me acquire my data.

I wanted to thank Sandy for her enormous support to organize data spreadsheets and recruit participants during the pandemic as without her this project would not be possible. I also wanted to thank amazing researchers and students in RTF: Luciana for her uplifting spirit and teaching me "Quero Café!"; Maria for listening to me complain and bringing me candies; Mi for providing me with LOTS of tea and making me laugh; Alejandro and Pablo for introducing me to beans and chips for breakfast and giving me a reason to be afraid of pikas!

I'm thankful and exteremly lucky to have my family supporting me: my mom and dad for always being there for me even though they are many many kilometres away; my brother Amir Reza for his honesty, sense of responsibility and unlimited support; my girlfriend Delaram for her unconditional love and kindness throughout this exciting and difficult journey.

Above all, I want to thank all epilepsy patients who volunteered to be part of this project, some of whom travelled 3-4 hours just to get to our center. I dedicate this work entirely to them and I hope that this research can some day make a positive impact on the lives of people with epilepsy.

Table of Contents

1. Introduction 1

1.1 Temporal Lobe Epilepsy 2

1.1.1 Hippocampus Anatomy 3

1.1.2 Hippocampal Sclerosis 5

1.1.3 Treatments and Surgical Intervention 8

1.2 Neuroimaging in TLE 10

1.2.1 Hippocampal Volumetry in Temporal Lobe Epilepsy 12

1.2.2 Hippocampal DTI in Temporal Lobe Epilepsy 16

1.2.3 Hippocampal T2 Relaxometry in Temporal Lobe Epilepsy 19

1.2.4 Neuroimaging Studies of Animal Models in Temporal Lobe Epilepsy 23

1.3 Fundamentals of Diffusion MRI 25

1.3.1 Diffusion Weighted Imaging 26

1.3.2 Diffusion Tensor Imaging 29

1.3.3 DTI Parameters 32

1.4 Relaxation-weighted and Quantitative T2 Imaging 34

1.4.1 T2 Relaxometry 36

1.4.2 Multi-echo Spin Echo sequence 37

1.5 Thesis Motivation 38

2. Methods 41

2.1 Participants 41

2.2 Image Acquisition 42

2.3 DTI Processing 43

2.4 T2 relaxometry Processing 46

2.5 Registration 48

2.6 Hippocampus Segmentation 52

2.7 Curved Multiplanar Reformatting 54

3. Longitudinal Hippocampal Diffusion-Weighted Imaging and T2 Relaxometry Demonstrate Regional Abnormalities Which are Stable and Predict Subfield Pathology in Temporal Lobe Epilepsy 56

3.1 Introduction 56

3.2 Methods 58

3.2.1 Participants/Study Demographics 58

3.2.2 Image Acquisition 61

3.2.3 Hippocampus Segmentation 61

3.2.4 Registration 63

3.2.5 Identification of Focal MD and T2 Abnormalities 64

3.2.6 Regional MD Changes Between the Scans 64

3.2.7 Statistical Analysis 64

3.2.8 Histology 66

3.3 Results 67

3.3.1 Whole-hippocampus MRI Measures Remain Stable 67

3.3.2 Heterogeneous Regional MD Abnormalities of the Sclerotic Hippocampus Persist 69

3.3.3 Regional T2 Relaxometry Increases Correspond to Regions with Elevated MD 72

3.3.4 Focal Regions of Elevated MD and T2 in Contralateral Hippocampus 73

3.3.5 MRI and Histological Assessment of Surgical Patients 74

3.3.6 Pre-surgical Regional Elevated MD and T2 Correspond with NeuN Loss on Post-Surgical Histology 76

3.4 Discussion 77

4. Conclusions 81

Appendix 96

List of Tables

Table 1.1. Histopathological features of HS in TLE. 7
Table 1.2. Engel surgical outcomes. 10
Table 1.3. Longitudinal volumetry studies of the hippocampus in HS TLE. 15
Table 1.4. Cross-sectional and longitudinal DTI studies of the hippocampus in HS TLE. 17
Table 1.5. Cross-sectional T2 relaxometry studies of the hippocampus in HS TLE. 20
Table 1.6. T2 relaxometry studies of the hippocampus with a surgical histology comparison ... 22
Table 2.1. Summary demographics and clinical information of participants. 42
Table 3.1. Characteristics and demographics of 19 TLE patients..... 60
Table 3.2. Hippocampus manual segmentation intra- and inter-rater reliability. 62
Table 3.3. Whole-hippocampus MRI measures and quantification of thresholded measures 69

List of Figures

Figure 1.1. The anatomy of the hippocampus 5
Figure 1.2. HS subtypes defined by the ILAE criteria 8
Figure 1.3. HS on coronal T2-weighted images 14
Figure 1.4. Spin echo sequence 27
Figure 1.5. Pulsed gradient spin echo (PGSE) sequence 29
Figure 1.6. Isotropic versus anisotropic diffusion 30
Figure 1.7. Quantitative DTI maps 33
Figure 1.8. T1 and T2 relaxation curves. 34
Figure 1.9. T1 and T2-weighted images 36
Figure 1.10. Multi-echo spin-echo sequence 38
Figure 2.1. Effect of GR artifact on diffusion images. 44
Figure 2.2. Average residual error maps of the tensor fit before and after processing 46
Figure 2.3. Multi-echo spin echo sequence and quantiative T2 48
Figure 2.4. Longitudinal registration of mean DWIs in control and bilateral HS TLE. 50
Figure 2.5. Longitduinal registration of mean DWIs in a surgical patient 51
Figure 2.6. Hippocampus ROIs on mean DWI in a control and unilateral HS patient 54
Figure 2.7. Curved multiplanar reformatting at hippocampal head-body junction 55
Figure 3.1. Longitudinal co-registration of processed mean DWIs 63
Figure 3.2. Flow chart of the hippocampus groups for the repeated-measures ANOVA 66
Figure 3.3. Longitudinal changes of whole-hippocampi MRI measures 68
Figure 3.4. Longitudinal co-registered regional MD maps of the hippocampus 71
Figure 3.5. Quantification of focal MD and T2 abnormalities of the hippocampus 72
Figure 3.6. Regional MD and T2 maps of the hippocampus 73
Figure 3.7. Longitudinal changes in MRI measures of the contralateral hippocampus 75
Figure 3.8. Comparison of pre-surgical MD and T2 maps with histology 76

Symbols and Abbreviations

ATL	Anterior Temporal Lobectomy
ADC	Apparent Diffusion Coefficient
B_0	Static Magnetic Field
B_1	Radiofrequency Magnetic Field
CA	Cornu Ammonis
CSF	Cerebrospinal Fluid
DTI	Diffusion Tensor Imaging
DWI	Diffusion-weighted Imaging
DG	Dentate Gyrus
EPI	Echo Planar Imaging
EPG	Extended Phase Graph
EEG	Electroencephalography
FA	Fractional Anisotropy
FLAIR	Fluid-Attenuated Inversion Recovery
FOV	Field of View
FN	False Negative
G	Gradient Amplitude
GCD	Granule Cell Dispersion
GFAP	Glial Fibrillary Acidic Protein
GR	Gibbs Ringing
HS	Hippocampal Sclerosis
H&E	Hematoxylin and Eosin
ICC	Intraclass Correlation Coefficient
ILAE	International League against Epilepsy
KA	Kainic acid
LFB	Luxol Fast Blue
MD	Mean Diffusivity
MESE	Multi-Echo Spin Echo
MRI	Magnetic Resonance Imaging
MPRAGE	Magnetization Prepared Rapid Gradient Echo
M_{xy}	Transverse Magnetization
M_z	Longitudinal Magnetization
NMR	Nuclear Magnetic Resonance
NeuN	Neuronal Nuclear Antigen
PET	Positron Emission Tomography
QL	Qualitative
QN	Quantitative
RF	Radiofrequency

ROI	Region of Interest
S_0	Baseline Signal without Diffusion Weighting
SAH	Selective Amygdalohippocampectomy
SF	Seizure Free
SNR	Signal-to-Noise Ratio
SPECT	Single Photon Emission Computer Tomography
T1	Longitudinal Relaxation Time
T2	Transverse Relaxation Time
T2*	Effective T2
TE	Echo Time
TP	True Positive
TLE	Temporal Lobe Epilepsy
TR	Repetition Time
TV	Total Variation
VBM	Voxel-based Morphometry
Δ	Time Between Diffusion Gradients
δ	Diffusion Gradient Duration
γ	Gyromagnetic Ratio
ε_1	Primary Eigenvector
λ_1	Primary Eigenvalues

1. Introduction

Epilepsy is characterized by the occurrence of repeated seizures or transient abnormal synchronous neuronal activity. Almost 300,000 Canadians live with epilepsy.[1] Collaborative advances in science and technology have allowed development of medical therapies to improve the lives of people with epilepsy. However, conventional anti-epileptic medications fail to control seizures in 30-40% of patients and these patients are referred to as having drug-resistant epilepsy.[2]

Temporal lobe epilepsy (TLE) is one of the most refractory to medical therapy as only 20% of patients respond to medications.[3] While temporal lobe surgery including the hippocampus can potentially relieve drug-resistant TLE patients from disabling seizures, about 50% of patients continue to experience seizures in long-term follow-up after their surgery.[4] Hippocampal sclerosis (HS) is the most common etiology associated with TLE.[5] Previous studies suggest that the poor success rate of temporal lobe surgery may be linked to injury in specific regions of the hippocampus.[5, 6] It would be better if one could see which hippocampal subregions are damaged prior to the surgery to improve patient selection to those most likely cured.

Magnetic resonance imaging (MRI) offers the best method of detection and treatment planning for epilepsy patients. While conventional in-vivo MRI can detect overall damage in the hippocampus, it does not identify injury in specific hippocampal subregions.[3] Diffusion tensor imaging (DTI) and T2 relaxometry are quantitative MRI techniques that have proven useful in the field of epilepsy by providing unique contrasts to assess the internal architecture of the hippocampus. This introductory chapter reviews key previous works and identifies the gaps in the literature that were explored in the original research outlined in Chapter 3.

1.1 Temporal Lobe Epilepsy

Epilepsy is one of the most common brain disorders worldwide as one in every 10 people experience seizures at some point in their lives and over a third of them develop epilepsy.[7] Epilepsy has been recognized since ancient times (the word is derived from the Greek roughly translating to "be taken hold of") and has been described in numerous different ways throughout history.[7] The International League Against Epilepsy (ILAE) describes epilepsy as "an enduring predisposition to generate epileptic seizures and by the neurobiologic, cognitive, psychological, and social consequences of this condition. The definition of epilepsy requires the occurrence of at least one epileptic seizure".[8] Seizures are transient signs/symptoms that occur due to abnormal excessive or synchronous neuron firing in the brain.[7, 8] Epilepsy is associated with increased mortality and morbidity[9] and many patients suffer from misconceptions and stigma.[10]

Temporal lobe epilepsy (TLE) is the most common form of focal epilepsy (named for its origin in one lobe) and one of the most refractory to medical therapy.[3] Previous ILAE classification categorized TLE under mesial temporal lobe and lateral temporal lobe epilepsy depending on the region where the seizures originated.[11] More recent studies using DTI,[12] functional MRI,[13] and invasive electroencephalogram (EEG)[14] suggest that structural and functional abnormalities extend beyond the temporal lobe regions. Nevertheless, it is generally accepted that mesial TLE is the most common form of TLE which involves brain structures such as the hippocampus, amygdala and parahippocampal gyrus.[6] In the revised ILAE classification, mesial TLE with HS was identified as a separate "constellations" and "electroclinical syndromes".[6, 15] HS is the most common underlying etiology in drug-resistant TLE accounting for 50-60% of cases.[5] HS is characterized by the loss of neurons and gliosis, though many other pathological features are found in the sclerotic hippocampus (discussed in Section 1.1.2). In a large pathological study of 5,392

epilepsy patients, 34% had HS and 5% showed dual pathology with HS in combination with cortical dysplasia, vascular lesions and tumours.[16] Focal cortical malformations (dysplasia) and low-grade neoplasms were identified as the other two common pathologies in mesial TLE, 27% and 13%, respectively. Other etiologies in TLE include perinatal injury, head trauma, central nervous system infections, limbic encephalitis, etc.[17]

The diagnosis of TLE is primarily based on the clinical history and a descriptive account of seizures. Standard scalp EEG measures the electrical activity of the brain and is routinely performed to detect abnormal neuronal discharges (e.g. spikes, slow waves) and lateralize seizure onset. Standard structural brain MRI is imperative to look for lesions and structural pathology in TLE patients. Patients with TLE typically present with an initial precipitating injury which may include febrile seizures, birth trauma, brain injury, or meningitis.[7]

TLE patients frequently experience focal onset seizures with impaired awareness.[18] Focal seizures without impaired awareness (sometimes referred to as aura) may also occur in isolation but the majority occur at the start of focal impaired awareness seizures.[17, 18] Some examples of auras include rising epigastric sensation, fear, déjà vu, visceral and auditory illusions, and oral and manual automatisms.[17] Patients can also experience secondary generalized seizures (focal onset seizure has spread to both brain hemispheres) yet these events are less common.[6, 18]

1.1.1 Hippocampus Anatomy

Resting in the medial temporal lobe, the hippocampus (hippocampi plural) is one of the most studied brain regions and is involved in many neurological disorders such as epilepsy, depression, Alzheimer's disease, etc.[19] Functionally, the hippocampus has been implicated in all aspects of the episodic, working, spatial and semantic memory as well as spatial planning.[20] Arantius in 1587 was the first person to compare the protrusion of the temporal horn to a hippocampus or seahorse.[21]

The structure of the hippocampus is complex and tubular-like made of cornu ammonis and dentate gyrus (Figure 1.1).

There are several ways to visualize the hippocampus. On a broad view, the hippocampus may be divided into head, body and tail. Pathologically, from the ventricular cavity to the hippocampus sulci, the cornu ammonis may be divided into 3 layers: stratum oriens, stratum pyramidale, and the molecular zone (strata radiatum, lacunosum, and moleculare).[21] When the hippocampus is viewed in cross-section through its mid-portion (coronal/transverse plane), the cornu ammonis can be divided into four subfields: CA1, CA2, CA3, and CA4 (Figure 1.1C). In this view, cornu ammonis and dentate gyrus show the characteristic interlocking "C" relation to each other.[22] While the hippocampus has many digitations and bulges which form a crescent shape, the interlocking C relation between the cornu ammonis and dentate gyrus remains intact along the entire length of the hippocampus.

The connections of the anterior and posterior regions of the hippocampus differ. The amygdala, involved in the regulation of emotional behaviour, lies at the anterior end of the hippocampus. From the posterior end, the hippocampus extends into the subiculum and forms the parahippocampal gyrus. The subiculum is the transition zone between the hippocampus and the entorhinal cortex. The glutamatergic fibers from the entorhinal cortex enter through the subiculum and reach the granule cell layer of the dentate gyrus. These fibers then project to the pyramidal cell layer of the CA3 and form Schaffer collaterals which reach the dendrites of CA1. The CA1 subfield is the main output of the hippocampus which projects to the alveus, fimbria and fornix.[23]

Importantly, disease processes such as TLE demonstrate regional specificity in how the hippocampus is affected at various locations along its longitudinal axis or within different subfields

(transverse axes).[24] This highlights the importance of visualizing and characterizing hippocampal subfields to better understand its role in disease pathogenesis.

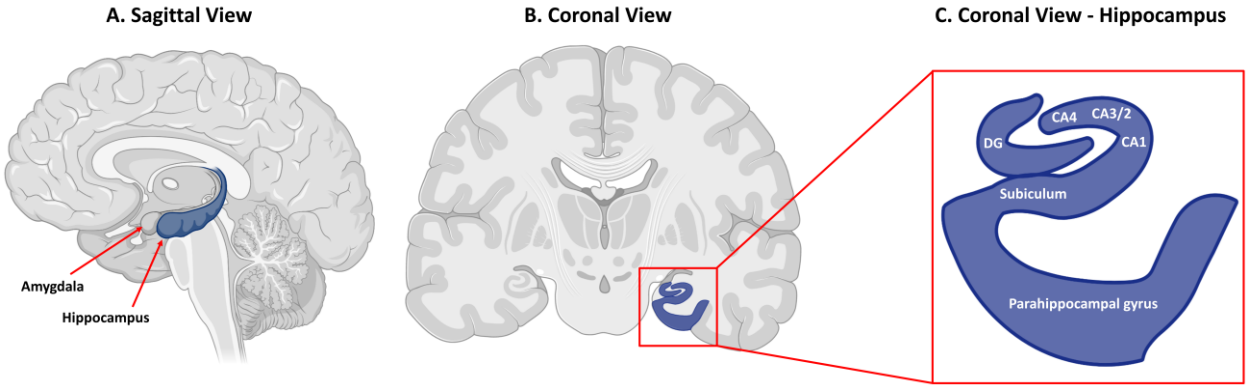

Figure 1.1. (A) Sagittal and (B) coronal view of the brain; the hippocampus is colored in blue. (C) Magnified coronal view of the hippocampal subfields, subiculum and parahippocampal gyrus. Cornu ammonis and dentate gyrus demonstrate the characteristic interlocking "C" relation on the coronal section. Created with BioRender.com.

1.1.2 Hippocampal Sclerosis

Hippocampal sclerosis was first characterized by Sommer in 1880 and it refers to regional pyramidal cell loss and gliosis in CA1, CA3 and CA4, whereas pyramidal cells in CA2 and granule cells in the dentate gyrus are the most resistant.[25] The histopathology of HS is complex and involves many cellular processes such as mossy fibre sprouting, disruption of interneuron network, dysregulation of neuropeptides and neurotransmitters, vasculature abnormalities and inflammation (Table 1.1).[5, 26-31] Among these processes, neuron loss and gliosis are clinically used to diagnose HS using post-surgical histology of the hippocampus tissue.

The ILAE categorizes three HS subtypes depending on which hippocampal subfield is predominately affected (Figure 1.2). In Type 1 HS (60-80% of all cases), CA1 is most severely affected (>80% cell loss) followed by substantial neuron loss in CA4 (40-90%). Type 2 HS refers to selective neuron loss in CA1 (>80%) with minor and barely visible neuron loss in CA2 (<20%). Type 3 HS refers to selective neuron loss in CA4 (~50%) whereas other subfields are moderately

affected (<30%). Type 2 and 3 HS are less common than Type 1 and account for ~20% of the cases.[25] While some patients display seizures originating from the mesial temporal lobe, about 20% of TLE cases do not show significant neuron loss and gliosis in the hippocampus and these are referred to as Non-HS. Granule cell dispersion (GCD), roughly defined as broadening of the granule cell layer >10 cells or 120 μm, commonly occurs in 50% of TLE patients, regardless of neuron loss and gliosis.[30]

The presence of HS is known to be associated with improved chances of a seizure free outcome (e.g. 54-70% of patients free of disabling seizures[6]) with temporal lobe resection compared to non-HS pathology which demonstrates 42-58% seizure-free surgical outcomes.[30] Further, different HS subtypes show different surgical outcomes. Type 1 HS demonstrates the highest rate of post-operative surgical seizure freedom (~70%) followed by Type 2 (~65%) and type 3 (~30%).[25, 30, 32] These findings highlight the importance of developing non-invasive methods to detect subhippocampal pathological changes in-vivo to allow for accurate prediction of seizure-free outcomes prior to surgery.

Table 1.1. Histopathological features of HS in TLE.

Pathological Features	Description	Example of Stains
Pyramidal cell loss[5, 30]	Subfield-specific loss of pyramidal neurons, subiculum is spared	NeuN, Luxol fast blue (LFB)
Gliosis (reactive astrogliosis)[5, 30]	Abnormal increase in the number of astrocytes in specific subfields or the dentate gyrus	astrocyte-specific markers (GFAP, etc.)
Granule cell dispersion and hypertrophy[5, 30]	Broadening of the granule cell layer (>10 cells or 120 μm) and hypertrophy in CA4	NeuN, LFB, Neurofilament,
Mossy fiber sprouting[29, 30]	Maladaptive plasticity resulting in extensive recurrent projection of mossy fibers into the dentate gyrus molecular layer	Timm stain, zinc transporter 3, dynorphin A
Interneuron network[30, 33]	Loss of interneurons, morphologic changes including abnormal dendrites	Parvalbumin, calbindin, calretinin
Neuropeptides[27, 30]	Loss or maladaptive axonal sprouting of anti-epileptic neuropeptide-containing neurons (neuropeptide Y, somatostating, galanin) or reorganization of pro-epileptic substance P-containing neurons	dynorphin, immuno-specific markers (Neuropeptide Y and galanin)
Neurotransmitters[27, 30]	Abnormal regulation of neurotransmitter release, receptor distribution (e.g. high expression of voltage-gated potassium channel, VgKC) and signaling	immuno-specific markers (e.g. KV1.1 to stain for VgKC)
Abnormalities of vasculature[28]	Loss of the blood brain barrier, proliferation of microvessels, vascular endothelial growth factor receptor expression	drug transporter protein, p-glycoprotein (stain for capillaries), Albumin
Inflammation[26, 31]	Upregulation of specific cytokines and chemokines (e.g. IL-1β, IL-18), accumulation of iron and reactive oxygen species	Immuno-specific markers (e.g IL-1β, IL-18 antibodies)

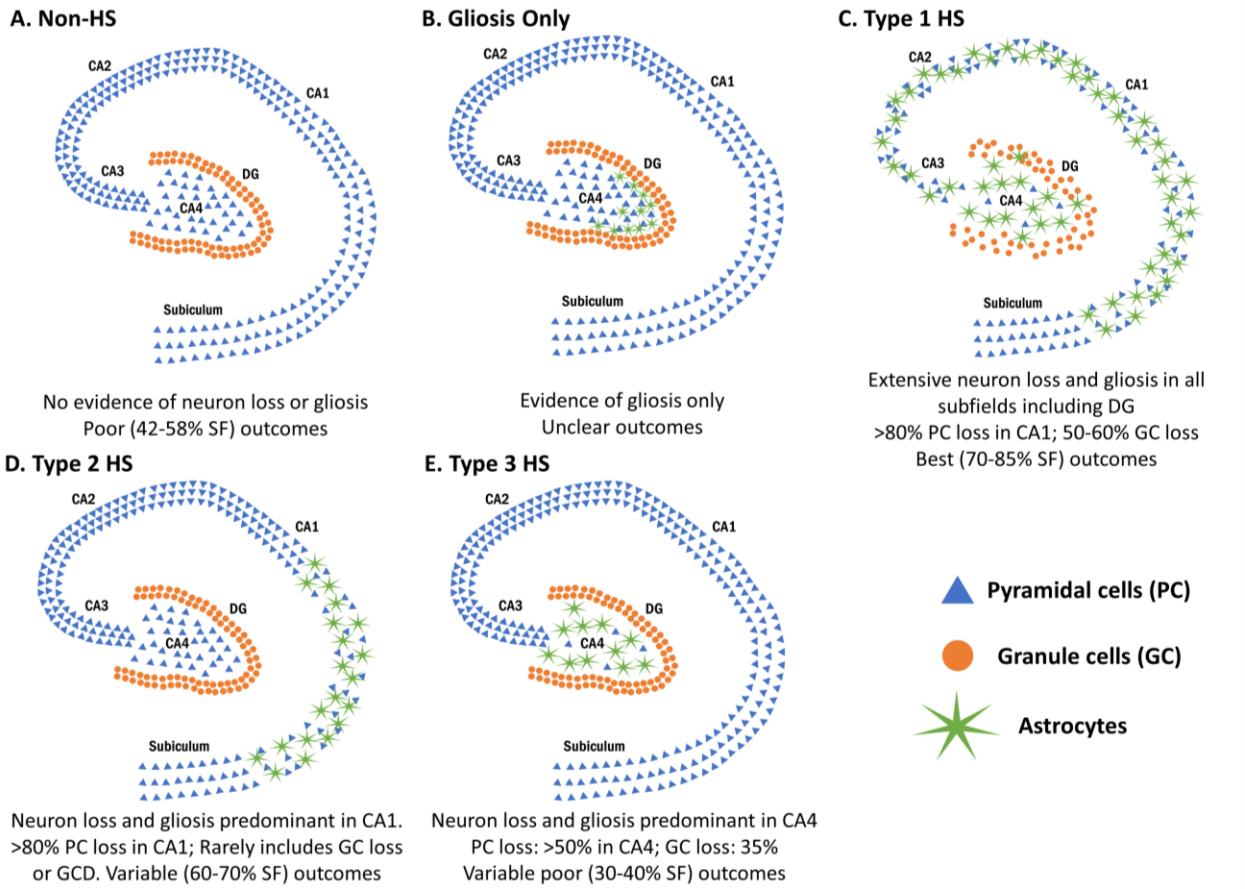

Figure 1.2. HS subtypes defined by the ILAE criteria: (A) non-HS, (B) gliosis only (C) type 1 HS, (D) type 2 HS, (E) type 3 HS. SF = seizure free.

1.1.3 Treatments and Surgical Intervention

Epilepsy can be managed in several ways including anti-epileptic medications, surgery, dietary therapy and neuromodulatory devices.[34] Anti-epileptic medications such as carbamazepine, phenytoin, lamotrigine and topiramate suppress generation, propagation and severity of seizures. However, as discussed, about 20-40% of TLE patients continue to experience seizures despite optimal medical therapy.[3] ILAE defines drug-resistance epilepsy as "failure of adequate trials of two tolerated and appropriately chosen and used antiepileptic drugs schedules (whether as monotherapies or in combination) to achieve sustained seizure freedom".[35] Failure of the first anti-epileptic drug is a robust predictor of patient developing drug-resistance.[36] Previous studies

demonstrate that 90-96% of patients who are controlled achieve seizure freedom after either the first or second drug tried.[36, 37]

While only 20% of TLE patients respond to medications, surgery can provide seizure freedom with resultant improvements in quality of life.[4] Patients with drug-resistant TLE may be referred to surgery including anterior temporal lobectomy (ATL) or selective amygdalohippocampectomy (SAH) following extensive assessments of semiology, EEG and neuroimaging findings. ATL is performed by the resection of anterolateral temporal neocortex, mesial amygdala and anterior hippocampus. SAH involves selective resection of the hippocampus and amygdala while the lateral temporal neocortex is spared.[38] In a landmark randomized controlled trial,[4] ATL was found to result in significantly more patients with seizure freedom (58%) versus those only receiving medical therapy (8% seizure freedom). Further clinical trials have supported these findings and highlighted the importance of early surgical intervention in relieving patients from disabling seizures.[39, 40] As an aside, seizure freedom outcomes after epilepsy surgery are commonly categorized according to Engel classification (Table 1.2).[41]

Long-term surgical outcome studies (e.g. 8 years post-operative) demonstrate that approximately 50% of patients experience seizure recurrence.[4] Certain predictors of favourable surgical outcome have been suggested including absence of focal seizures within 2 years of surgery, complete resection of the temporal lobe,[42] unilateral presence of a lesion detected by MRI,[43] and shorter epilepsy duration.[44] None of these factors alone has been found to sufficiently and accurately predict surgical outcomes.[6, 30, 41-45] As discussed in 1.1.2, post-surgical success has also been demonstrated to strongly correlate with the presence of HS and with a varying degree with different HS subtypes.[6] While HS can readily be diagnosed on clinical MRI (volume loss and increases in T2-weighted signal), the HS subtype is currently diagnosed on post-surgical histology.

Furthermore, animal and autopsy studies have demonstrated subtle HS pathology contralateral to the seizure focus which could also impact the surgical outcome.[46-48] However, the contralateral hippocampus can not be assessed with pathology as it is not resected during the surgery. Therefore, it has not been possible to use this information to predict seizure freedom in HS TLE patients prior to the surgery.

Table 1.2. Engel surgical outcomes.

Engel Outcome Scale
Class I: Free of disabling seizures
IA: Completely seizure-free
IB: Non disabling focal seizures without impaired awareness only
IC: Some seizures after surgery, but free of disabling seizures for at least 2 years
ID: Generalized convulsions with antiepileptic drug withdrawal only
Class II: Rare disabling seizures ("almost seizure-free")
IIA: Initially free of disabling seizures but has rare seizures now
IIB: Rare disabling seizures since surgery
IIC: More than rare disabling seizures after surgery, but rare seizures for at least 2 years
IID: Nocturnal seizures only
Class III: Worthwhile improvement
IIIA: Worthwhile seizure reduction
IIIB: Prolonged seizure-free intervals amounting to greater than half the follow-up period, but not less than 2 years
Class IV: No worthwhile improvement
IVA: Significant seizure reduction
IVB: No appreciable change
IVC: Seizures worse

1.2 Neuroimaging in TLE

Advances in brain imaging techniques have led to significant improvements in the visualization of different brain structures and insights into TLE processes. Pre-surgical evaluation of TLE patients relies heavily on video-EEG monitoring and neuroimaging findings from MRI, single photon emission computed tomography (SPECT) and positron emission tomography (PET) imaging. Routine scalp video-EEG monitoring enables lateralization of the epileptogenic zone, defined as the brain regions essential for the generation of seizures, as well as an evaluation of the seizure semiology. However, scalp EEG in many patients is not adequate to localize seizures to a particular

brain region. As such, intracranial electrodes may be surgically implanted to define the epileptogenic zone and allow for selective resection.[49]

SPECT and PET imaging help in lateralization of the seizure generator.[50] SPECT is used to measure regional cerebral blood flow by detecting gamma rays emitted by the injected radioactive tracers (e.g. technetium-99m propylene amine, etc.). During the ictal phase (during the seizure), increased neuronal activity is associated with increased metabolism and regional cerebral blood flow (hyperperfusion). If the radiotracer is injected close to the seizure onset (e.g. ideally within 20 seconds), ictal SPECT can identify regions of hyperperfusion involved in the seizure generation. During the interictal phase (in-between the seizures), cerebral blood flow is reduced (hypoperfusion) in the brain regions associated with seizures. These regions can be identified using interictal SPECT. However, SPECT imaging is limited by the spatial resolution of the images which limits percise localization of the seizure onset to a particular brain region. PET imaging detects positron decay of radiotracers injected intravenously. 18F-fluorodeoxyglucose PET is the standard method that provides an indirect marker of neuronal metabolism by measuring glucose consumption. PET can not be obtained during the ictal phase but interictal PET can reveal regions of hypometabolism that may be involved in seizure generation with a high degree of sensitivity.[51] One limitation of PET imaging is that it can not precisely determine the margins of surgical resection as the regions of hypometabolism extend beyond the epileptogenic zone.

While different centers use different imaging protocols, MRI is vital for accurate diagnosis and pre-surgical evaluation of TLE patients.[52] The ILAE has proposed the Harmonized Neuroimaging of Epilepsy Structural Sequences (HARNESS-MRI)[53] protocol for diagnosis and management of epilepsy which includes: high-resolution 3D T1-weighted (i.e., $1 \times 1 \times 1$ mm^3), high-resolution (i.e., $1 \times 1 \times 1$ mm^3) 3D fluid-attenuated inversion recovery (FLAIR), and high in-

plane resolution (i.e., 0.4 × 0.4 × 2 mm^3) 2D coronal T2-weighted. The HARNESS-MRI protocol recommends complete brain coverage with no interslice gap in all of the mentioned protocols. Also, DWI and quantitative T2 mapping are not included in this protocol.[53]

Based on the MRI findings, TLE patients can be categorized into mesial TLE with HS, lesional TLE, and non-lesional TLE. Lesional TLE may include evidence of extratemporal lesions, temporal lesions besides HS or HS associated with additional lesions termed dual pathology.[34] HS can be qualitatively detected on high quality MRI with high sensitivity using hippocampal volume loss, increased hippocampus signal on T2-weighted or FLAIR images and loss of hippocampal architecture.[6] While qualitative analysis allows detection of HS using these features, subtle abnormalities of the hippocampus may be missed.[5, 6] Quantitative MRI techniques such as hippocampal volumetry, DTI and T2 relaxometry have shown better sensitivity and specificity to detect subtle structural abnormalities of the hippocampus. As discussed below in Sections 1.3 and 1.4, DTI and T2 relaxometry, in particular, can provide essential quantitative information about the internal architecture of the hippocampus. The following sections review the relevant literature on hippocampal volumetry, diffusion MRI and T2 relaxometry in TLE patients and animal models.

1.2.1 Hippocampal Volumetry in Temporal Lobe Epilepsy

One of the most striking MRI features of the sclerotic hippocampus is volume loss which can be readily visualized on high-resolution T1-weighted or coronal T2-weighted scans (Figure 1.3).[54-56] Numerous studies have highlighted the diagnostic importance of hippocampal volumetry (quantification of the hippocampus volume) to increase sensitivity and specificity of HS detection.[5, 53, 57-60] The gold-standard hippocampal volumetry method is by manual delineation of the hippocampus on magnetization prepared rapid acquisition gradient echo (MPRAGE) T1-weighted images. Since manual segmentation of the hippocampus can be time consuming,

previous studies have developed automated hippocampal segmentation protocols in TLE patients to allow implementation of hippocampal volumetry in the clinical setting.[57, 58, 60]

Focal loss of volume in the ipsilateral hippocampus has been found to correlate with histological degree of neuron loss and gliosis, suggesting sensitivity of hippocampal volumetry in detection of HS pathology.[61-65] It is unclear whether volume abnormalities of the ipsilateral hippocampus progress over time. Some cross-sectional studies have reported correlations between seizure frequency[66, 67] and epilepsy duration[68-70] with ipsilateral hippocampus atrophy. However, within-individual progression of seizure-induced damage can not be assessed using the cross-sectional design. Some longitudinal imaging studies (Table 1.3) have reported atrophy of the ipsilateral hippocampus, supporting necessity of early surgical intervention.[71-73] However, a more recent volumetry study did not find any changes in the ipsilateral hippocampus over ~3 years.[74]

In addition to the characteristic atrophy of the ipsilateral hippocampus, subtle volume loss of the hippocampus contralateral to the seizure focus has also been reported by some studies on whole and regional hippocampal levels.[66, 75-78] A review of voxel-based morphometry studies in TLE reported atrophy of the contralateral hippocampus in 17% of all cases.[79] These results are consistent with the autopsy studies[46-48] demonstrating neuron loss and gliosis in the unresected contralateral hippocampus. However, it is unclear what the effect of surgery is on the contralateral hippocampus. While some studies report progressive post-operative atrophy of the contralateral hippocampus,[73, 80, 81] a more recent study did not find any changes.[82] Therefore, more studies with a longitudinal design are needed to improve understanding of hippocampal volume changes following TLE surgery.

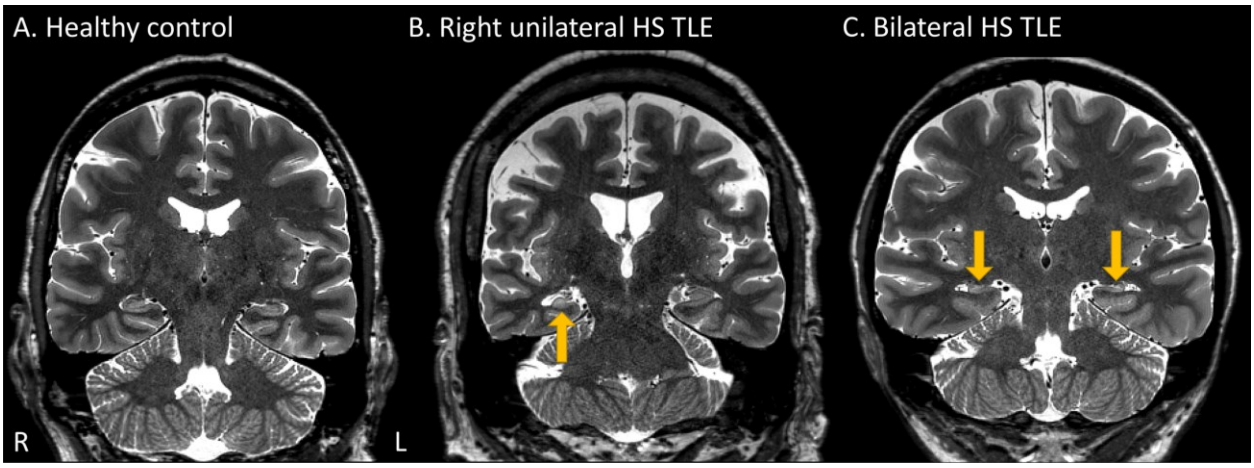

Figure 1.3. Coronal T2-weighted images of a (A) control (50 years-old male), (B) right unilateral HS (44 years-old male) and (C) bilateral HS patient (59 years-old male). Yellow arrows point to the ipsilateral sclerotic hippocampus with marked atrophy and enhanced T2-weighted signal.

Table 1.3. Longitudinal volumetry studies of the hippocampus in HS TLE.

Study	B_0/Sequence /Resolution	Subjects	Age (years)	Inter-scan gap	Analysis method	Main findings
Briellmann et al. 2002	1.5T /MPRAGE/ 1.4 mm thickness*	TLE: 25	30±9	3.5 years (range 3-4)	Manual ROI	No change in contralateral volume. ↓ in ipsilateral volume by 9%
Fuerst et al. 2003	1.5T/ MPRAGE/ resolution not stated	TLE: 12	40 (21-73)	3.5 years (range 2-5)	Manual ROI	No change in contralateral volume. ↓ in ipsilateral volume only in patients with ongoing seizures
Conz et al. 2011	2T/ MPRAGE/ 1.2×0.7×3 mm^3	TLE: 33 Control: 14	36 (21-70)	TLE: 45 months (7-85) Control: minimum 7 months	Manual ROI	↓ volume of bilateral hippocampi
Fernandes et al. 2014	2T/ MPRAGE/ 1×1×1 mm^3	TLE: 47 Control: 28	TLE: 45±9 Control: 41±8	TLE: 4 years (0.5–10) Control: 5 (0.3–12)	Manual ROI	Post-operative ↓ in contralateral volume
Alvim et al. 2016	3T/ MPRAGE/ 1×1×1 mm^3	TLE: 21 Control: 11	TLE: 46 (19-61) Control: 41 (27–54)	TLE: 18 months (18-56)	VBM	↓ in contralateral volume. Ipsilateral hippocampus remained unchanged
Elliott et al. 2016	1.5T/ MPRAGE/ 1×1×1 mm^3	Group 1: TLE: 25 Control: 12 Group 2: TLE: 10 Control: 3	Group 1: TLE: 39 (19–59) Control: 33 (23–58) Group 2: TLE: 39 (24-59) Control: 25 (22-33)	Group 1: TLE: 4 (0.4–9); Control 7 (4–9) Group 2: TLE: days 1, 2, 3, 6, 60 and 120 post-operative Control: 1, 2, 3, 6 and 60 after baseline	Manual ROI	Group 1: Post-operative ↓ in contralateral volume, prominent in hippocampus body. Group 2: post-operative ↓ in contralateral starting on day 1, then progressing over the first week before stabilizing over the long-term
Li et al. 2021	3T/ MPRAGE/ 1×1×1 mm^3	TLE: 28 Control: 29	TLE: 26 (15-44) Control: 27 (19-42)	Baseline, 3 months, 12 months (post-operative for TLE)	Manual ROI	No post-operative change in contralateral hippocampus.

* In-plane resolution is not stated. Abbreviations: EPI: echo planar imaging; MESE: multi-echo spin echo; MPRAGE: magnetization prepared rapid acquisition gradient echo; ROI: region of interest; TLE: temporal lobe epilepsy; VBM: voxel-based morphometry.

1.2.2 Hippocampal DTI in Temporal Lobe Epilepsy

DTI has been extensively used to study white matter connectivity in TLE demonstrating bilateral and extratemporal white matter abnormalities.[12] DTI has also been used to demonstrate microstructural diffusion abnormalities of the hippocampus in TLE patients (Table 1.4). These studies consistently demonstrate an increase in the ipsilateral hippocampal mean diffusivity (MD)[83-96] and a reduction in fractional anisotropy (FA)[83, 85, 89, 92, 94] compared to the healthy hippocampi of the controls. Further, ex-vivo surgical resection studies provide a basis for investigation of hippocampal diffusion abnormalities by demonstrating a profound rearrangement and disorganization of the internal fiber bundles in HS pathology.[97] MD of the resected sclerotic hippocampus has also been demonstrated to correlate with pyramidal cell density in CA4/DG.[61] However, more studies are needed to provide a better understanding of the pathological basis of hippocampal diffusion abnormalities in HS TLE patients.

Low resolution of DTI acquisitions has been a significant shortcoming in previous diffusion studies (typically >2 mm isotropic; >8 mm^3 voxel volume). This limitation has exacerbated partial volume effects and limited regional specificity of hippocampal analysis. One recent study has acquired 1 mm isotropic DTI to address these limitations.[94] This study demonstrated patterns of hippocampal subfield diffusion abnormalities in TLE patients which were consistent with HS subtype on post-surgical histology. Also, consistent with some of the low-resolution DTI studies[92, 98] and pathological studies[46-48], high-resolution DTI has shown regional diffusion abnormalities in the contralateral hippocampus of some TLE patients, suggesting bilateral hippocampal pathology which is more readily visualized with high resolution imaging.

It is unclear whether these diffusion abnormalities change or remain stable over time, highlighting the need for longitudinal studies. The only two surgical studies (~8 mm^3 voxel volume) demonstrated changes in MD in the post-operative contralateral hippocampus however

with conflicting findings (one showing an increase in MD[99] and other showing a decrease[100]). Thus, more studies with a longitudinal design are needed to explore these inconsistencies.

Table 1.4. Cross-sectional and longitudinal DTI studies of the hippocampus in HS TLE.

Study	B_0/ Resolution	Subjects	Age (years)	Analysis	Main findings
			Cross-sectional studies		
Wieshmann et al. 1999	1.5T/ 2.5×2.5×5 mm^3	TLE: 14 Control: 6	TLE: 33 (20-50) Control: 31 (29-36)	Manual ROI on DWIs	↑ ipsilateral MD compared to contralateral and control hippocampi.
Hugg et al. 1999	4.1T*/ 1.6×1.6×5 mm^3	TLE: 8 Control: 5	TLE: 30±10 Control: 28±8	Manual ROI on T1 weighted	↑ ipsilateral MD compared to contralateral and control hippocampi.
Yoo et al. 2002	1.5T/ 1.6×1.6×5 mm^3	TLE: 18 Control: 19	TLE: 30 (16-42) Control: 28 (19-39)	Manual ROI on DWIs	↑ ipsilateral MD compared to contralateral hippocampi. ↑ contralateral MD compared to control hippocampi.
Assaf et al. 2003	1.5T/ 2.4×1.9×3 mm^3	TLE: 12 Control: 14	TLE: 41 (27–59) Control: 31 (24-49)	Manual ROI on DWIs	↑ ipsilateral MD and ↓ FA compared to contralateral hippocampi. ↑ ipsilateral MD compared to control hippocampi.
Thivard et al. 2005	1.5T/ 1.2×1.2×5 mm^3	TLE: 35 Control: 36	TLE: 34±9 (19-53) Control: 33± 9 (18-57)	Manual ROI on DWIs	↑ ipsilateral MD compared to control hippocampi. ↓ contralateral MD compared to control hippocampi.
Lui et al. 2005	1.5T/ resolution not stated	TLE: 20 Control: 20	TLE: 34 (18-48) Control: 34 (19-47)	Manual ROI on DWIs	↑ ipsilateral MD compared to contralateral and control hippocampi. Negative correlation between hippocampal MD and multiple memory tests.
Gonçalves Pereira et al. 2006	1.5T/ 2.5×2.5×5 mm^3	TLE: 55 Control: 20	TLE: 33±10 (18-57) Control: 34±11 (19-52)	Manual ROI on DWIs	↑ ipsilateral MD compared to contralateral and control hippocampi. Bilateral MD increases found in 7% of cases.
Salmenpera et al. 2006	1.5T/ 1.4×1.4×5 mm^3	TLE: 7 Control: 13	TLE: median 30 Control: median 34	Manual ROI on T2 weighted images	↑ ipsilateral MD compared to contralateral and control hippocampi. ↓ ipsilateral FA from posterior to anterior regions.
Focke et al. 2008	3T/ 1.9×1.9×2.4 mm^3	TLE: 33 Control: 37	TLE: median 42 (17-62) Control: median 39 (18-70)	Automated (FreeSurfer)	↑ ipsilateral MD compared to contralateral and control hippocampi. Small clusters of reduced FA in contralateral hippocampus.
Liacu et al. 2010	1.5T/ 1.9×1.9×4 mm^3	TLE: 17 Control: 10	TLE: 33±8 Control: 29±4	Manual ROI on T1 weighted images	↑ ipsilateral MD and ↓ FA compared to contralateral and control hippocampi. ↓ contralateral FA in HS patients compared to control hippocampi.

Nazem-Zadeh et al. 2014	3T/ 2.0×2.0×2.6 mm^3	TLE: 23 Control: 48	TLE: 42±13 Control: 33±10	Manual ROI on T1 weighted images	↑ ipsilateral MD compared to contralateral and control hippocampi. Ipsilateral MD showed 90% true detection rate without any wrong lateralization.
Chiang et al. 2016	3T/ 2×2×2.2 mm^3	TLE: 28 Control: 28	TLE: 37±12, Control: 38±9	Manual ROI on T1 weighted images	↑ bilateral MD compared to control hippocampi.
Ercan et al. 2016	1.5T/ 2×2×2.7 mm^3	TLE: 14 Control: 15	TLE: 34±12 (19-66) Control: 35±12 (21-52)	Manual ROI on T1 weighted images	↑ ipsilateral MD and ↓ FA in HS patients compared to contralateral and control hippocampi. Ipsilateral FA negatively correlated with epilepsy duration. History of febrile convulsion correlated with ipsilateral MD.
Treit et al. 2019	3T/ 1×1×1 mm^3	TLE: 18 Control: 19	TLE: 42±14 (18-67) Control: 44±14 (18-70)	Manual ROI on mean DWIs	↑ ipsilateral MD and ↓ FA in HS patients compared to contralateral and control hippocampi. Heterogeneous regional MD elevations in ipsilateral hippocampus. Regional MD elevations also observed in contralateral hippocampus.
Sala-Padro et al. 2020	3T/ 2.5×2.5×2.5 mm^3	TLE: 22 Control: 18	TLE: 45±11 Control: 49±12	Automated on MPRAGE	↑ contralateral MD in subiculum compared to control hippocampi. ↑ contralateral MD in patients with uncontrolled seizures in CA1, molecular layer, dentate gyrus compared to seizure-free patients. ↓ contralateral FA in parasubiculum, subiculum and CA4 compared to control hippocampi.
			Longitudinal Studies		
Thivard et al. 2007	1.5T/ 1.25×1.25×5 mm^3	TLE: 24 Control: 36	TLE: 32±9 (20-50) Control: 33±9 (18-57)	Manual ROI on DWIs	Post-operative ↓ in contralateral MD
Elliott et al. 2018	1.5T/ 2×2×2 mm^3	Group 1: TLE 25 Control: 12 Group 2: TLE: 10 Control: 3	Group 1: TLE: 39.3 (19–59) Control 33 (23–58) years Group 2: TLE: 39 (24-59) Control 25 (22-33)	Manual ROI on MPRAGE	Group 1: ↑ MD and ↓ FA in contralateral hippocampus. Group 2: diffusion abnormalities were observed only after 1-3 years

*whole-body imaging spectrometer. Abbreviations: DWI: diffusion-weighted imaging; FA: fractional anisotropy; MD: mean diffusivity; MPRAGE: magnetization prepared rapid acquisition gradient echo; ROI: region of interest; TLE: temporal lobe epilepsy; VBM: voxel-based morphometry.

1.2.3 Hippocampal T2 Relaxometry in Temporal Lobe Epilepsy

Increases in T2 relaxation time of the ipsilateral hippocampus has consistently been found in HS dating back to early 1990s (Table 1.5 and Table **1.6**).[57, 62, 94, 101-117] While visual detection of increased T2-weighted signal can reliably detect HS in TLE patients,[6, 52, 53] quantification of T2 relaxation time has shown better accuracy in detection of HS[62, 102, 103, 106, 111-113, 115] with some studies reporting up to 100% sensitivity and specificity.[111, 115] Further, increased hippocampal T2 relaxation time has been shown to correlate with neuron loss in the CA1 and CA3,[62, 117] gliosis in CA1,[62] glial cell count in DG,[109] and GCD[116] in HS pathology. These studies used histology stains including NeuN and H&E stains which are used as markers of neuron loss, GFAP as a marker of astrogliosis and LFB as a marker for myelin. These findings provide a strong basis for using quantitative T2 to accurately detect HS in vivo. In fact, recent studies have developed automated segmentation and processing methods to implement T2 relaxometry in the clinical setting.[57, 107]

Some studies have looked at regional T2 mapping of the hippocampus (anterior to posterior profile[67, 108] or head, body tail[57]). For example, one recent study[57] found higher hippocampal T2 in head, body, and tail of ipsilateral hippocampus of unilateral HS patients and in the body and head of bilateral hippocampi of bilateral HS patients. However, similar to DTI studies, T2 relaxometry studies have been limited by the low spatial resolution of acquisitions due to relatively long scan times and the need for large voxel volume with high signal-to-noise ratio to adequately measure T2 values. While recent studies acquired T2 scans with higher in-plane resolutions,[57, 94, 107, 111, 113, 115, 116] these studies still acquired thick slices (>3 mm except one study[94]) which can result in missed lesions/abnormalities on a regional hippocampal level. Therefore, more studies are needed to explore focal T2 profile of the hippocampus and potentially correlate regional T2 abnormalities with histopathological features of HS.

Longitudinal T2 relaxometry studies in TLE patients are lacking. There is currently one study that looked at T2 changes over one year in newly diagnosed TLE patients.[118] Their results indicated an increase in hippocampal T2 in only one patient who was consequently diagnosed with HS based on clinical MRI findings. It is therefore unclear whether T2 abnormalities of the hippocampus progress over time and more studies are needed.

Table 1.5. Cross-sectional T2 relaxometry studies of the hippocampus in HS TLE.

Study	B_0/ Sequence/ resolution	Subjects	Age (years)	Analysis method	Main findings
			Cross-sectional Studies		
Van Paesschen et al. 1997	1.5T/ MESE, 16 echos/8 mm thickness*	TLE: 100 Control: 22	TLE: median 33 (16- 64) Control: median 29 (21-37)	Manual ROI	↑ ipsilateral T2 compared to contralateral and control hippocampi. Combination of T2 and volume revealed previously undetected bilateral HS in few cases
Kälviäinen et al. 1998	1.5T/ MESE, 16 echos/8 mm thickness*	TLE: 32 Control: 25	TLE: 32±15 (15-62) Control: 33±12 (21-64)	Manual ROI	↑ T2 in the body of the ipsilateral hippocampus
Woermann et al. 1998	1.5T/ Dual echo spin echo/ 0.9×0.9×5 mm^3	TLE: 30 Control: 20	TLE: median 34 (19-49) Control: median 31 (20-59)	Manual ROI	↑ T2 in ipsilateral hippocampus with 16/30 patients showing diffuse abnormalities and 6/30 showing focal anterior abnormalities
Briellmann et al. 2004	3T/ MESE, 8 echo/ 0.9×1.9×6 mm^3	TLE: 40 Control: 55	TLE: 30±12 Control: 34±9	Manual ROI	↑ T2 in ipsilateral hippocampus. T2 abnormality did not correlate with epilepsy duration or the estimated seizure load.
Mueller et al. 2007	1.5T/ Dual-echo spin echo, 1×1×3 mm^3	TLE: 42 Control: 30	TLE: 35±11 Control: 30±8	Manual ROI	↑ T2 in ipsilateral hippocampus of HS. No T2 change in hippocampi of non-HS.
Coan et al. 2014	3T/ MESE, 5 echos/ 0.9×1×3 mm^3	TLE: 20	TLE: median 46 (17-74)	Manual ROI	Combination of volumetry and T2 demonstrated abnormalities in 99% patient with visually detected HS and in 28% with visually normal MRI.

Kubota et al. 2015	3T/ MESE, 5 echos/ 0.9×1×3 mm^3	TLE-HS: 124 TLE MRI negative: 79 Control: 59	TLE: median 45 (17-74)	Manual ROI	↑ T2 in ipsilateral (76% of patients), contralateral (5% of patients) and bilateral hippocampi (19% of patients). T2 sensitivity was 74% for patients with TLE-HS and 14% for non-HS TLE. T2 specificity was 95% for patients with TLE-HS and 97% for non-HS TLE.
Winston et al. 2017	3T/ Dual-echo spin echo/ 0.4×0.4×4 mm^3	TLE: 50 Control: 50	TLE: median 40 (18-76) Control: median 37 (17-66)	Manual ROI on MPRAGE	↑ T2 in ipsilateral hippocampus of unilateral HS and bilateral hippocampi of bilateral HS. ↑ T2 in contralateral hippocampus.
Treit et al. 2019	3T/ MESE, 16 echos/ 1.1×1.1×1 mm^3	TLE: 18 Control: 19	TLE: 42±14 (18-67) Control: 44±14 (8-70)	Manual ROI	↑ T2 in ipsilateral hippocampus. No T2 changes in contralateral hippocampus
Vos et al. 2020	3T/ Dual-echo spin echo/ 0.4×0.4×4 mm^3	TLE: 69 Control: 111	TLE: 43±15 (18-76) Control: 40±13 (17-67)	Automated ROI on MPRAGE	↑ T2 in ipsilateral hippocampus of unilateral HS and bilateral hippocampi of bilateral HS. ↑ T2 in ipsilateral head, body, and tail of unilateral HS and in bilateral body and head in bilateral HS. ↑ T2 in the body and head of contralateral hippocampus in some examples
			Longitudinal T2 Studies		
Van Paesschen et al. 1998	1.5T/ MESE,16 echo/8 mm thickness*	TLE: 36 Control: 12	TLE: median 26 (14-50) Control: median 29 (21-38)	Manual ROI	↑ T2 only in 1/4 patients with HS on follow-up. No hippocampal T2 changes in other patients.

* In-plane resolution is not stated. Abbreviation: MESE: multi-echo spin echo; ROI: region of interest; TLE: temporal lobe epilepsy.

Table 1.6. T2 relaxometry studies of the hippocampus with a surgical histology comparison in HS TLE patients.

Study	B0/sequence/ resolution	Patients/ Surgery/ Resection	Stains	Comparison method	Main findings
Jackson et al. 1993	1.5T/ MESE, 16 echos/ 8 mm thickness*	14/ATL	not stated	Qualitative	↑ T2 in ipsilateral hippocampus of unilateral HS. T2 values >116 ms associated with HS. Bilateral abnormalities in 29% of cases of HS
Van Paesschen et al. 1995	1.5T/ MESE, 16 echos/ 8 mm thickness*	32/ATL & SAH/ En-bloc	H&E LFB	Qualitative	↑ T2 in 31/32 ipsilateral and 5/32 contralateral hippocampi with classical HS. Type 3 HS patients 3/32 showed normal T2 in ipsilateral hippocampus
Van Paesschen et al. 1997	1.5T/MESE, 16 echos/ 8 mm thickness*	59/ATL/ En-bloc	H&E, LFB, GFAP	Quantitative	↑ T2 associated with neuron loss and glosis in the CA1
Von Oertzen et al. 2002	1.5T/dual echos spin echo/ 0.9×0.9×4 mm^3	12/SAH/ En-bloc	NeuN	Quantitative	Diffuse T2 abnormalities in ipsilateral and contralateral hippocampus. T2 correlated with neuronal density in CA1 and CA3
Briellmann et al. 2002	1.5T/MESE, 16 echos/ 8 mm thickness*	44/ATL/ En-bloc	H&E, GFAP	Quantitative	T2 correlated with glial cell count in the dentate gyrus
Briellmann et al. 2004	3T/MESE, 8 echos/ 0.9×1.9×6 mm^3	17/ATL/ En-bloc	H&E, GFAP	Qualitative	Elevated T2 on the ipsilateral side identified HS accurately
Gonçalves Pereira et al. 2006	1.5T/MESE, 4 echos /0.9×1.25×4 mm^3	28/ATL/ En-bloc	H&E, GFAP	Qualitative	T2 relaxometry classified 96% of HS patients.
Rodionov et al. 2015	3T/dual-echo spin echo/ 0.9×0.9×5 mm^3	27/ATL	not stated	Qualitative	T2 relaxometry classified HS with 100% sensitivity and specificity.
Sato et al. 2016	3T/MESE, 8 echos/ 0.9×1.9×5 mm^3	30/ATL & SAH	NeuN, GFAP, H&E	Qualitative	T2 relaxometry detected non-atrophic hippocampal abnormality and correlated with gliosis and GCD
Chen et al. 2016	3T/MESE/ 0.9×0.9×3 mm^3	17/ATL	H&E	Qualitative	T2 relaxometry classified HS with 92% sensitivity and 100% specificity.
Goodkin et al. 2021	3T/dual echo spin echo/ 0.4×0.4×5 mm^3	43/ not clear	not stated	Qualitative	T2 relaxometry classified unilateral HS with 92% and identified 91% of bilateral HS cases.

* In-plane resolution is not stated. Abbreviation: MESE: multi-echo spin echo; ATL: anterior temporal lobectomy; SAH: selective amygdalohippocampectomy; NeuN: neuronal nuclear antigen; LFB: Luxol fast blue; H&E: hematoxylin and eosin stain; GFAP: glial fibrillary acidic protein; GCD: Granule cell dispersion.

1.2.4 Neuroimaging Studies of Animal Models in Temporal Lobe Epilepsy

While several animal models of TLE have been developed, the most widely used models involve administration of chemoconvulsants (kainic acid and pilocarpine).[119] Kainic acid (KA) is an analog of glutamate and acts on ionotropic kainate receptors to cause neuronal depolarization. Pilocarpine activates the cholinergic system by acting on the muscarinic acetylcholine receptors.[120] Systemic or intraventricular injection of KA or pilocarpine results in recurrent secondary generalized seizures mostly originating from the hippocampus/amygdala with a similar pathological correlate of HS in humans.[119] Patients with TLE commonly present with an initial precipitating injury, some of whom have experienced status epilepticus.[7] Status epilepticus can be defined as abnormally prolonged seizure activity (e.g. 30 minutes) which can have negative long-term consequences such as neuronal death/injury and network imbalance.[18, 119] Injection of KA/pilocarpine "reproduces" status epilepticus and the animals then develop chronic epilepsy with repeated seizures after a period of time (days to weeks depending on the animal strain, injection method, etc.).[120-122]

Volumetric MRI has been extensively used in animal TLE studies to demonstrate hippocampal atrophy. Rodent hippocampal volume (in some studies bilateral hippocampal[120, 121] and in others only the ipsilateral hippocampus[123]) has been found to significantly shrink following the injection of KA or pilocarpine as early as 24 hours.[120] During the chronic phase (roughly 1 month after status epilepticus in mice), some studies suggest a progressive reduction in regional hippocampal volume (e.g. CA1, CA3 and dentate gyrus) which correlated with the degree of neuron loss on hippocampal histology, seizure frequency and worse memory outcomes.[121, 124, 125] This has led to the hypothesis that repeated seizures could result in a cumulative loss of neurons in the hippocampus over time.[122] This hypothesis is controversial and is not supported by other animal studies that demonstrate no relationship between the progression or development of

hippocampal atrophy and recurrent repeated seizures[126-128]. These studies suggest that the majority of neuronal loss in these animals occurs before presentation of the first behavioural seizures.[128]

KA/pilocarpine-injected animals demonstrate a significant reduction in hippocampal MD (by ~20%) within the first hour of injection.[129] This initial reduction has been suggested to be related to cytotoxic edema which is defined as energy failure in the tissue leading to an imbalance of Na^+ concentration across the cell membrane.[130] As a result of higher intracellular Na^+ concentration compared to the extracellular Na^+ concentration, water moves into the cell leading to swelling. Cytotoxic edema is resolved within a day or few days and accordingly MD values increase on mature lesions after several weeks to months giving rise to a biphasic profile of hippocampal MD changes over time.[130, 131] Recent high-resolution animal DTI studies (e.g. 136 × 136 × 700 μm^3 at 9.4T[132]) suggest an immediate increase in FA in hippocampal subfields (e.g. dentate gyrus) which correlate with histopathological features of mossy fiber sprouting and reorganization of axons of the molecular layer.[132, 133] Both hippocampal subfield MD and FA have also been found to correlate with neuron loss and gliosis in CA1, CA3 and dentate gyrus[129, 130, 132, 133], providing a basis for investigating these markers in TLE patients.

Rodent models of KA and pilocarpine injection demonstrate increased T2-weighted signal in the hippocampus beginning 2 hours after status epilepticus and peaking at 12-24 hours after status epilepticus.[130] The enhanced T2-weighted signal can return to the baseline levels over subsequent weeks/months as the water is reabsorbed from the lesion/edema.[129, 130] Quantitative T1 and T2 values have also been found to increase to a peak level 24 hours following status epilepticus but remain under the baseline levels 2 months later.[129-131] Increased quantitative T2 in the hippocampus of rodent models of KA and pilocarpine has been shown to correlate with neuron loss, gliosis, edema, and breakdown of the blood-brain barrier.[123, 131]

1.3 Fundamentals of Diffusion MRI

Magnetic resonance imaging (MRI) is a powerful non-invasive in-vivo tool in medical diagnosis and biomedical research. The potentials of MRI are astonishing considering the fact that there are many different ways that the images of the human body can be obtained and manipulated. There are numerous MRI techniques that have proven highly effective in the management of neurological diseases. In this thesis, diffusion-weighted imaging (DWI) and T2 relaxometry MRI were used to study the brain of TLE patients with the future hope of detecting changes in the brain that allow patients make more informed decisions about their treatment plan; specifically regarding epilepsy surgery.

MRI relies on the fundamentals of nuclear magnetic resonance (NMR) by taking advantage of the abundance of hydrogen atoms embedded within the water molecule to create detailed images of the human body. The MRI scanner consists of four main components: the magnet, gradient coils, radiofrequency (RF) coils and a computer system. An NMR experiment involves three stages: polarization, excitation and relaxation. In the polarization step, a strong and uniform magnetic field (labelled B_0) probes the protons to line up in the same direction—similar to how a magnet pulls the needles of a compass—giving rise to a net longitudinal magnetization. In the excitation step, purposeful application of transient bursts of RF pulses (labelled B_1) disturb the alignment of protons which can result in a net transverse magnetization. The transverse magnetization precesses with a certain characteristic frequency known as the Larmor frequency. This rotating magnetization produces an oscillating magnetic field which induces movement of charged particles (current) in the RF coil, giving rise to the MR signal. When the RF pulse is turned off, the excited spins relax back to their original alignment due to T1 and T2 relaxation as discussed in 1.4. Three sets of gradient coils (e.g. in X, Y and Z direction) are used in MR systems to cause

a linear variation of the magnetic field in different directions and encode the spatial location of the protons. The computer console takes the signal from the protons in the body and creates detailed images of the tissue inside the body. Different arrangements of RF pulses and gradients, known as MRI sequences, allow for manipulation of the protons in the desired way to produces images with different contrasts. Considering this brief introduction to MRI, the next few sections will cover basics of diffusion and T2 relaxometry as the main focuses of this work.

1.3.1 Diffusion Weighted Imaging

DWI is a powerful MRI technique that allows for an indirect measurement of molecular diffusion within the brain. While the basic contrasts in conventional MRI (T1, T2 and proton density) can reveal essential structural information about the brain, DWI provides qualitative and quantitative information regarding properties of the tissue microenvironment such as structural connectivity and white matter tract orientations.

Diffusion is described by the random motion of molecules (also known as Brownian motion) from one part of a system to another. Einstein's equation (Equation 1.1) relates diffusion (labelled D) to the mean square of the distance (labelled X) travelled by molecules in a given interval of time (labelled T_d):

$$< X^2 > = 2\, DT_d \tag{1.1}$$

Isotropic diffusion describes unhindered and random movement of molecules within a medium such as a glass of water. However, in biological tissues, molecular diffusion is affected by different processes such as physical arrangement of cell structures (e.g. axonal membrane in neurons etc.). This gives rise to apparent diffusion coefficient (ADC) as the molecular movement is reduced by interaction of water molecules with the tissue microstructure. Since diffusion is dependent on the direction of displacement of water molecules, DWI uses this fundamental property to probe the microstructural environment of the underlying tissue.

The most common approach to acquire DWIs is the pulsed gradient spin echo (PGSE) sequence first demonstrated by Stejskal-Tanner in 1965.[134] The basic structure of the PGSE sequence is based on the spin echo sequence first demonstrated by Hahn in 1950[135] (Figure 1.4). In a spin echo sequence, an excitation 90° RF pulse is followed by a refocusing 180° RF pulse. Following the 90° RF pulse, the longitudinal magnetization (M_z) is tipped into the transverse plane giving rise to transverse magnetization (M_{xy}). Over time, the spins dephase due to T2 relaxation, resulting in the decay of M_{xy}. The 180° RF pulse is then applied that refocuses the spins and results in production of an echo with the maximum signal occurring at the echo time (TE). The sequence is then repeated with the application of another 90° RF pulse at time TR, the repetition time.

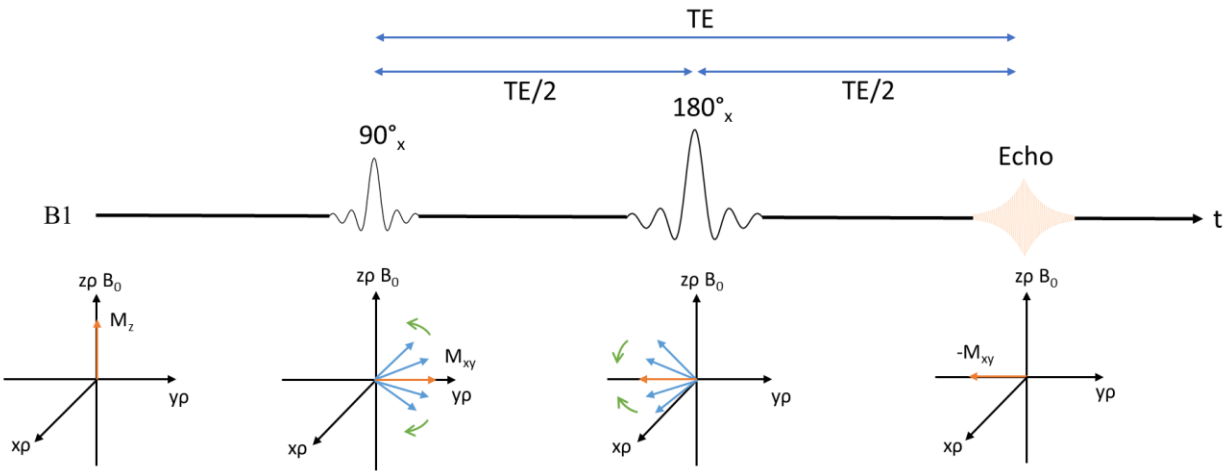

Figure 1.4. In a spin echo sequence, following the 90° excitation pulse, longitudinal magnetization (M_z; orange arrow) is tipped into the transverse plane (M_{xy}). The 180° pulse is then used to refocus the individual spins (blue arrows), resulting in an echo at time TE. Note that the spins are shown in the rotating frame of reference (axes denoted by subscript ρ). For simplicity, this figure ignores the decay of M_{xy} due to T2 relaxation.

In the PGSE sequence, two symmetric diffusion encoding gradients are applied: one between the 90° pulse and 180° refocusing pulse and the other after the 180° pulse and before the signal readout (Figure 1.5). The first diffusion encoding gradient dephases M_{xy}, labelling the position of the spins

by the phase of the transverse magnetization. Considering the individual spins, variation in the magnetic field caused by the gradient results in some spins precessing faster than others and thus becoming out of phase. The second 'rephasing' gradient is applied to reverse the phase incoherence of individual spins and results in the recovery of the signal. Assuming a stationary hydrogen spin, the effect of first and second gradient cancels out and the spin will not accumulate phase. Considering a diffusing molecule in the direction that the diffusion gradients are applied, there will be a net phase difference because the gradient experienced during the first and second diffusion gradients will not cancel out; this will result in signal loss.

To simplify and characterize the effect of diffusion sensitizing gradients, *b*-value (Equation 1.2) was introduced by Le Bihan in 1986[136]:

$$b = \gamma^2 G^2 \delta^2 (\Delta - \frac{\delta}{3}) \tag{1.2}$$

Where *b*-value is in units of s/mm^2, γ is the gyromagnetic ratio, G is the gradient strength, δ is gradient length, and Δ is the time between the two diffusion gradients. Consequently, signal attenuation ($\frac{S}{S_0}$) can be measured in the experiment and used to calculate ADC for a given *b*-value using Equation 1.3:

$$\frac{S}{S_0} = \exp(-b\ ADC) \tag{1.3}$$

Equations 1.2 and 1.3 imply that as the strength of diffusion gradients increase, *b*-value increases and more signal is lost.

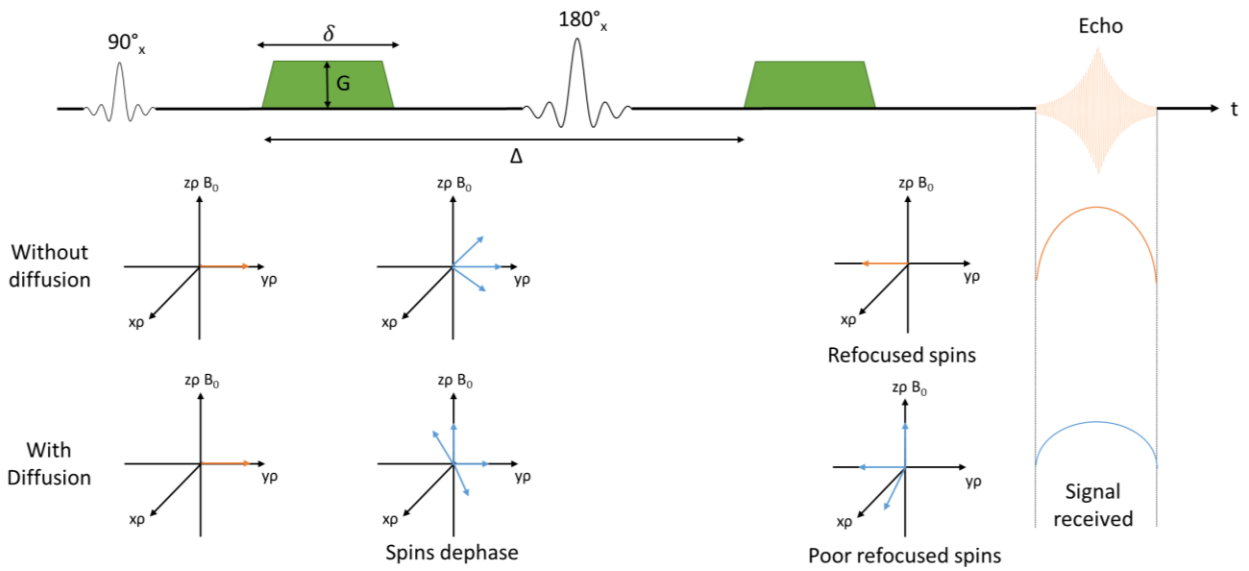

Figure 1.5. The pulsed gradient spin echo (PGSE) sequence uses the basic structure of a spin echo sequence with the addition of two diffusion sensitizing gradients of size G, duration δ, and separated by time Δ. Diffusing spins will accumulate shift which results in a net attenuation of the echo amplitude. For simplicity, this figure ignores the decay of M_{xy} due to T2 relaxation.

The images obtained from the PGSE sequence are diffusion-sensitized (defined by the *b*-value) and for that reason they are known as 'diffusion-weighted'. DWIs of brain areas with higher rates of diffusion such as the cerebrospinal fluid (CSF) exhibit more signal loss and appear darker. Conversely, brain regions with lower diffusion rate such as the gray matter appear brighter. Note that the diffusion-weighted images do not reflect "pure" diffusion values as they are also T2-weighted given the typically long TE used in the acquisition. To remove relaxation contrast, images are obtained with at least two differing *b*-value, b_0 and b, to calculate the ADC. The b_0 images are obtained without diffusion sensitising gradients (b=0) but with all other sequence parameters identical to those used in the DWIs. Commonly, *b*-values of 1000-1500 s/mm^2 are used in diffusion MRI studies.

1.3.2 Diffusion Tensor Imaging

Diffusion is dependent on the direction of movement of the molecules which may not be the same in all directions in tissue. Considering diffusion as a three-dimensional process, it can be described

using a tensor model (Figure 1.6).[137] In this model, diffusion is considered a symmetric tensor, D, that describes molecular movement along each principal axis and correlation between displacements along these axes. Applying a mathematical procedure known as decomposition, the tensor matrix can be represented by three 3 eigenvectors (ε_1, ε_2, ε_3) that describe the axes/orientation of the diffusion tensor ellipsoid and 3 eigenvalues (λ_1, λ_2, λ_3) that describe the magnitude of the diffusion for the axes (Equation 1.4):

$$\begin{bmatrix} D_{xx} & D_{xy} & D_{xz} \\ D_{yx} & D_{yy} & D_{yx} \\ D_{zx} & D_{zy} & D_{zz} \end{bmatrix} \xrightarrow{eigendecomposition} \begin{bmatrix} \lambda_1 & 0 & 0 \\ 0 & \lambda_2 & 0 \\ 0 & 0 & \lambda_3 \end{bmatrix} \quad (1.4)$$

Similar to how MRI gradients can be applied in different directions (e.g. along the X, Y and Z direction), diffusion sensitizing gradients can be applied in different directions. In diffusion tensor imaging (DTI), the diffusion sensitizing gradients are applied in at least 6 different directions to estimate the diffusion matrix. The tensor is then calculated for each voxel in the image by acquiring b0 images and DWIs sampled in different directions.

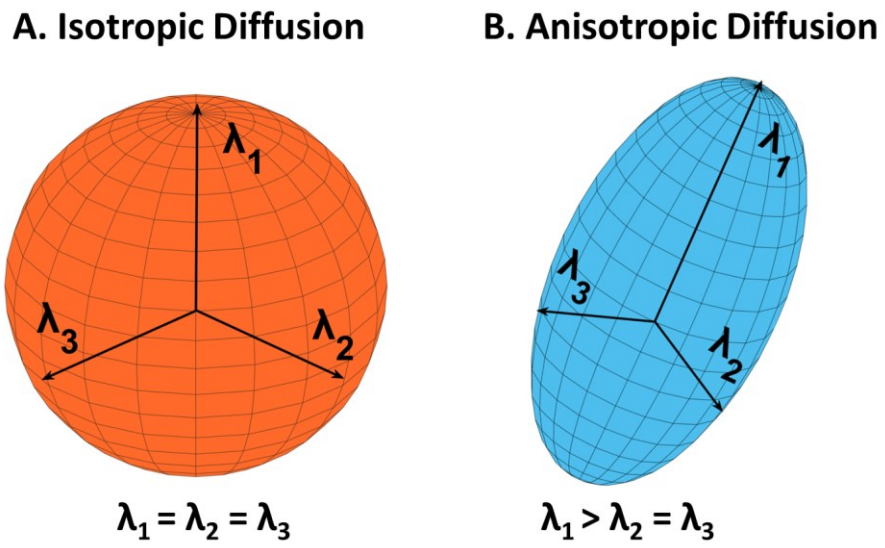

Figure 1.6 (A) Isotropic diffusion tensor with equal eigenvalues. (B) Anisotropic diffusion tensor (e.g. λ_1 larger than λ_2 and λ_3).

Echo-planar imaging (EPI) is the most common method to acquire DTI in which an entire slice is acquired following a single excitation ('single-shot'). This rapid acquisition of slices (in a fraction of a second) is beneficial for diffusion imaging because it reduces subject motion artifacts and consequently inconsistencies in diffusion measurements. However, EPI has several setbacks: 1- eddy current distortions induced by rapidly switching diffusion gradients, 2- local magnetic field inhomogeneities (largely in areas of air-tissue interface) caused by susceptibility-induced off resonance of precessional frequencies, 3- inevitable subject motion artifact still exist, and 4- low spatial resolution because only a limited number of frequency or phase encoding steps (e.g. matrix size) can be obtained before the signal decays in a short acquisition time. Most of these limitations can be addressed to a certain degree via post-processing methods (further explored in Chapter 2).

The fourth limitation, namely low spatial resolution, is more difficult to deal with as it requires modification to the DTI protocol at the time of the scan. Spatial resolution is particularly important for improved and detailed visualization of the brain structures and more accurate calculation of the quantitative diffusion parameters (discussed in Section 1.3.3) by reducing the partial volume effect. The partial volume effect is an artifact where more than one tissue type occurs in a voxel due to limited image sampling and spatial resolution.[138] There is an inherent signal-to-noise ratio (SNR) loss in DTI acquisitions due to the combined effect of diffusion gradients and long TE. Reducing the voxel volume (increasing the spatial resolution) further compromises the SNR as the signal is proportional to voxel size. As a result, the typical voxel volumes in conventional clinical DTI of the human brain at 3T have been 8 mm^3 or larger. One solution to low DTI SNR is to select lower *b*-values while making sure that there is still enough diffusion contrast. Another method is to acquire a 'slab' of images (e.g. reduced number of slices) covering the region of interest as opposed to whole-brain coverage. This allows for the acquisition

of a larger number of averages in a given scan for the same slice that increases the SNR as the square root of the averages. This method is useful if the focus of the study is on a particular brain region of interest such as the hippocampus. The trade-off, however, is the loss of potentially important information in regions that were not covered in the acquisition.

1.3.3 DTI Parameters

The two main quantitative diffusion parameters are mean diffusivity (MD) and fractional anisotropy (FA) which are calculated based on eigenvalues. MD provides a non-directional estimate of molecular diffusion rate and is calculated by the mean of the three eigenvalues independent of fiber orientation and gradient directions:

$$MD = \frac{\lambda_1+\lambda_2+\lambda_3}{3} \tag{1.5}$$

FA describes the degree of anisotropy and is calculated by taking standard deviation of 3 eigenvalues normalized to a value of 0 (isotropic diffusion) to 1 (fully restricted diffusion along one axis):

$$FA = \sqrt{\frac{3}{2}} \sqrt{\frac{(\lambda_1-\mathrm{MD})^2+(\lambda_2-\mathrm{MD})^2+(\lambda_3-\mathrm{MD})^2}{\sqrt{\lambda_1{}^2+\lambda_2{}^2+\lambda_3{}^2}}} \tag{1.6}$$

Measurements of MD and FA in the tissue (e.g. calculated for all voxels; Figure 1.7) provide an indirect estimate of the underlying microstructure. An increase in MD may reflect elevated extracellular water content and increased intracellular spaces which may be due to pathology such as neuron loss, cell hypertrophy, Wallerian degeneration, etc. A decrease in MD may also reflect pathology; for example, following acute stroke, loss of ion homeostasis leads to an influx of water from the extracellular space into the intracellular space, contributing to the observed decrease in MD. In ordered white matter, anisotropy has been shown to correlate most strongly with membrane density, specifically axonal membrane.[139] Presence or absence of myelin can also influence the

degree of anisotropy. Interpretation of FA in heterogeneous tissues such as the hippocampus is difficult. This is because FA does not account for crossing fibers (e.g. run in different directions) that may exist within a single voxel. Nonetheless, as discussed before in Sections 1.2.2 and 1.2.4, hippocampal FA has been shown to correlate with HS pathological features of neuron loss and gliosis in high-resolution ex-vivo DTI in human studies as well as animal models of epilepsy. In this thesis, MD and FA values were used to yield information about the epileptic hippocampus and were compared to the healthy hippocampi of the controls.

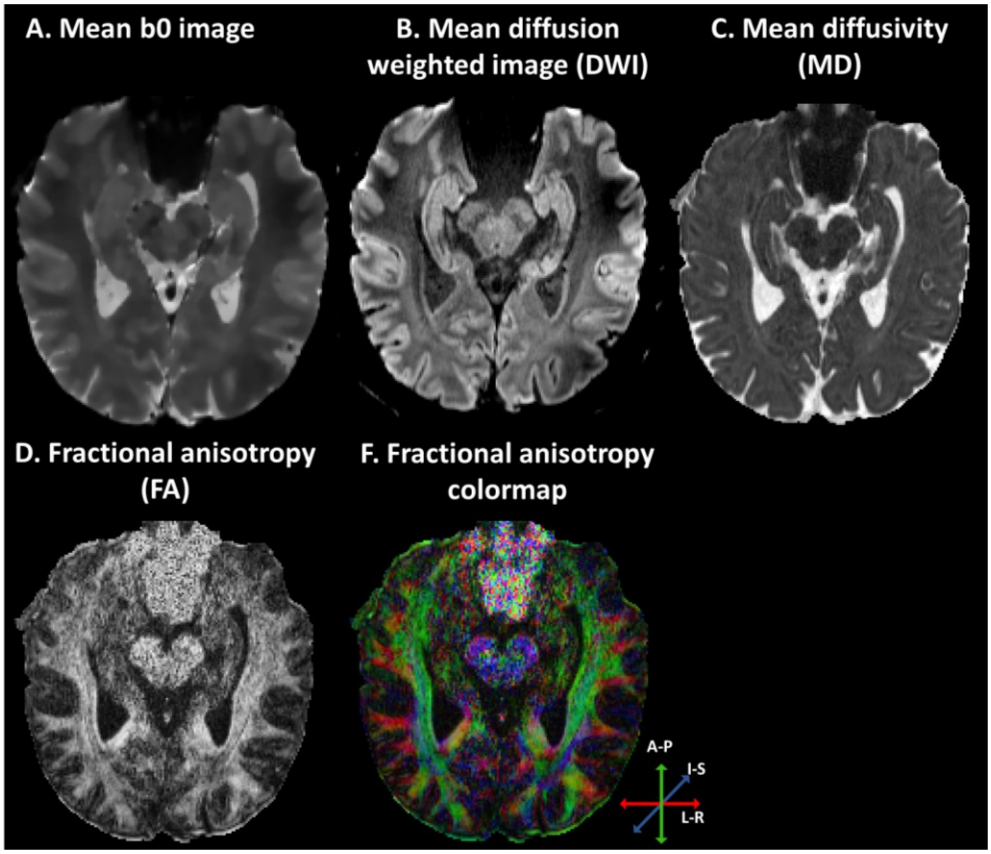

Figure 1.7 Processed DTI maps. (A) Mean b0 image (average of 10 b0 images) and mean DWIs (10 averages of 10 directions with b=500 s/mm^2) acquired with slices along the long axis of the hippocampus. (C) MD map reflects overall diffusion—brighter regions correspond to higher diffusion (e.g. CSF) and darker regions correspond to lower diffusion (e.g. gray matter structures such as the hippocampus). (D) FA map reflects the degree of anisotropy—higher anisotropy observed in white matter tracts. (F) FA map colored based on the directionality (primary eigenvector) of white matter tracts—red reflects left-right orientated fibers, green reflects anterior-posterior fibers, and blue reflects superior-inferior fibers.

1.4 Relaxation-weighted and Quantitative T2 Imaging

As previously described, after the B_1 field is turned off, the magnetization relaxes back to the equilibrium due to two separate but simultaneous processes, T1 and T2. T1 relaxation, also known as the spin-lattice relaxation, is the recovery of the longitudinal magnetization (M_z) due to the interactions between the nuclear spins and the surrounding environment. Mathematically, T1 relaxation time is the time needed for the *z* component of the magnetization to reach 63% of its maximum value (Figure 1.8A). T2 relaxation, also known as spin-spin relaxation, is the decay of the transverse magnetization (M_{xy}) due to the interactions of individual spins and the resultant dephasing of the nuclear magnetic moments. T2 relaxation time is the time required for the transverse magnetization to decay to 37% of its maximum value (Figure 1.8B).

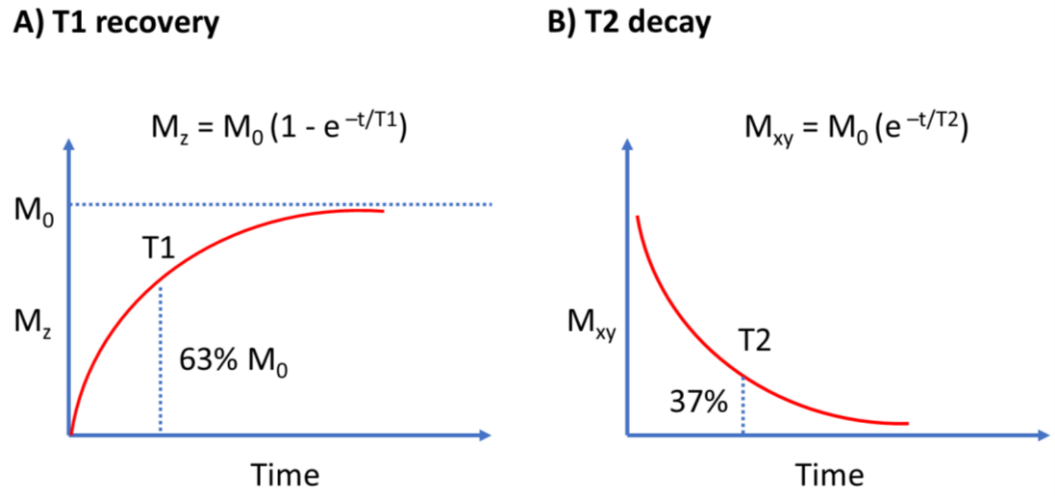

Figure 1.8. (A) T1 relaxation time is the time needed for the longitudinal magnetization (M_z) to reach 63% of its maximum value (M_0). (B) T2 relaxation time is the time required for the transverse magnetization (M_{xy}) to decay to 37% of its maximum value (M_0).

The most common method to create an MR image is to use relaxation-weighted imaging (T1- or T2-weighted) by sensitizing the MRI sequence to a range of relaxation times (Figure 1.9). T2-weighted images are created when TE is kept long relative to T2 relaxation times and TR is kept long so that M_z has fully recovered. T1-weighted images are created when TR is kept short relative

to T1 relaxation times and TE is short so that T2 differences do not evolve. T1-weighted images can also be acquired using an inversion recovery sequence. In the magnetization prepared rapid acquisition with gradient echo (MPRAGE) sequence first proposed by Mugler and Brookeman in 1990,[140] an initial 180° inversion RF pulse is followed by a number of rapidly acquired gradient echoes (a sequence known as spoiled gradient echo sequence) with small flip angles (5°-12°) and short TE's (2-4 ms). After the inversion pulse, the longitudinal magnetization recovers via T1 relaxation mechanisms toward the equilibrium for a specified inversion time (typically 600-900 ms). The rapid data collection following the inversion using the spoiled gradient echo sequence creates a T1-weighted contrast with high gray-white matter tissue differentiation. T1 and T2-weighted images provide structural information about the brain, essential to qualitative diagnosis of many neurological diseases. Importantly, a weighted image is not a true reflection of actual relaxation times because of other effects (e.g. proton density, diffusion).

T1 and T2 relaxation times are intrinsic properties of the tissue. Pure T1 and T2 relaxation values can be computed using various techniques. Damadian in 1971 first demonstrated that tumour cells have longer T1 and T2 values compared to normal cells.[141] Many studies have demonstrated alterations in T1 and T2 values in various brain regions in multiple sclerosis[142], Alzheimer's disease[143], epilepsy[54] and other neurological conditions. Changes in the relaxation times reflect non-specific alterations in the tissue microenvironment and local water content such as demyelination, tumour-related changes, injury or presence of macromolecules such as iron[54, 142-145]. Specifically, quantitative T2 values have been extensively used in TLE to demonstrate hippocampal pathology in hippocampus sclerosis patients (see Table 1.5 and Table 1.6). Increased T2 in the sclerotic hippocampus has been shown to correlate with the HS pathology (e.g. neuron loss, gliosis, granule cell dispersion) in both human (Table 1.5) and animal studies (Section 1.2.4).

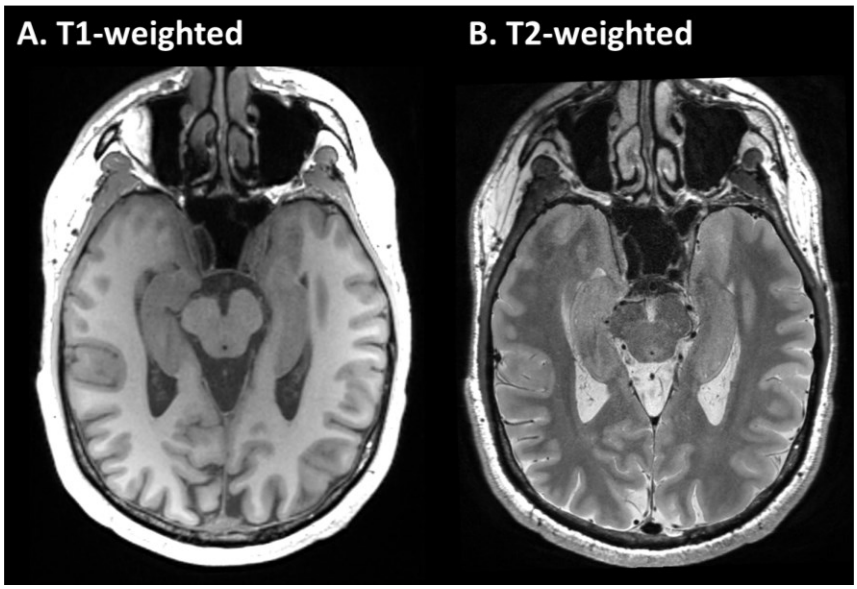

Figure 1.9 (A) Example of a T1-weighted magnetization prepared rapid acquisition with gradient echo (MPRAGE) image and (B) T2-weighted images. Both images were acquired with 1 mm isotropic resolution. The MPRAGE image was reconstructed along the long axis of the hippocampus to match with the axial hippocampus T2-weighted image.

1.4.1 T2 Relaxometry

T2 Relaxometry refers to the measurement of T2 relaxation times from MR images. T2 relaxation is caused by a combination of dynamic (denoted T2) and static (denoted T2$'$) processes. The apparent transverse relaxation (T2*) is the combination of these processes:

$$\frac{1}{T2^*} = \frac{1}{T2} + \frac{1}{T2'} \tag{1.7}$$

The dynamic processes are thermodynamic in nature and are explained by the interactions between the individual spins resulting in fluctuations in the local magnetic field and loss of phase coherence. The static processes are induced by the external field and include susceptibility sources. Static processes can be removed with a 180° refocusing pulse as used in a standard spin echo sequence (discussed in 1.3.1). In fact, the spin echo sequence can be used to quantify T2 by obtaining images at multiple echo times and fitting for T2 exponential decay using this equation:

$$S = S_0 \, exp \frac{-TE}{T2} \tag{1.8}$$

where S and S_0 denote the magnitude of echo peak and equilibrium magnetization, respectively. However, this equation ignores the effect of spin diffusion. At long TE, diffusion results in premature decay of the T2 signal and variability in signal loss at different echo times. Also, T2 relaxometry using the spin echo sequence in a clinical setting is challenging due to long scan times.

1.4.2 Multi-echo Spin Echo sequence

To overcome the limitations of the spin echo sequence to quantify T2 values, the Carr Purcell Meiboom Gill (CPMG) or multi-echo spin echo (MESE) sequence was developed in which a 90° RF pulse is followed by a train of 180° refocusing pulses (Figure 1.10).[146, 147] In a MESE, the first echo with short TE produces proton density contrast while images produced at longer TE provide T2-weighted contrast. Short echo spacing also limits the effect of diffusion. The train of 180° pulses are 90° out of phase which reduces the effect of imperfect 180° pulses. The MESE sequence allows sampling of T2 signal decay curve at multiple time points (echo times) for each K-space line during a single excitation.

In practice, a precise 180° RF pulse is not achievable due to slice-profile variation, RF inhomogeneity and B_1 calibration errors. As a result, following two or more imprecise refocusing pulses, stimulated echoes arise resulting in overestimation of T2 relaxation times. To explain what stimulated echoes are, consider a train of three 90° RF pulses. Following the first pulse, M_z is deflected to the transverse plane and then decays with T2 relaxation rate over time. After the second 90° pulse, M_{xy} is stored in the longitudinal plane and the T2 relaxation decay is halted. After the third pulse, the magnetization is again deflected to the transverse plane which continues to decay with T2. For a period of time between the second and third pulse, magnetization is stored in the longitudinal plane. The resulting echo from these spins that did not fully undergo T2 relaxation is called a stimulated echo. While this example is an overestimation of the reality, the resulting stimulated echo increases the amplitude of later echoes and results in an overestimation

of T2 relaxation times. While much of the previous T2 relaxometry literature has ignored the effect of stimulated echoes, other methods have been developed to compensate for the effect of stimulated echoes which can provide more accurate measurements of the T2 (discussed in Chapter 2).

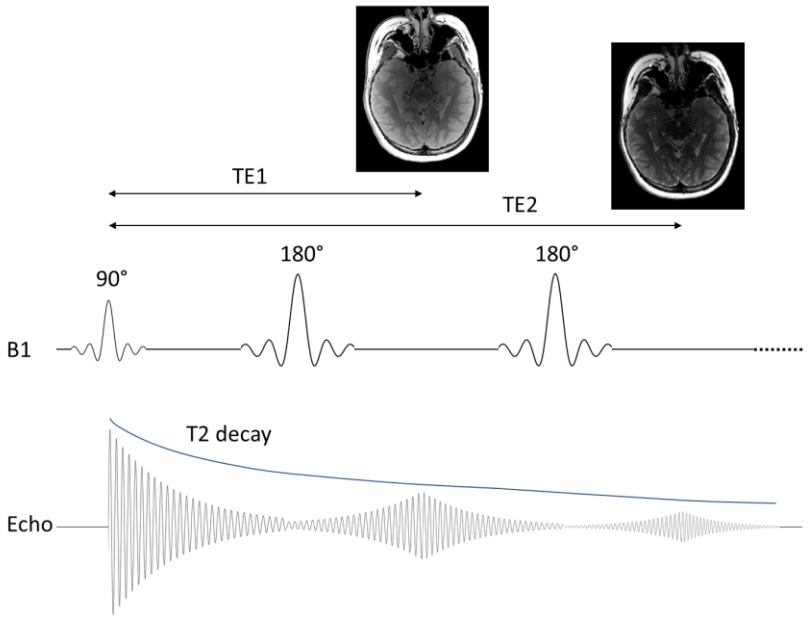

Figure 1.10 In a multi-echo spin-echo sequence, two or more 180° refocusing pulses are applied after the initial 90° excitation pulse. As time passes during the experiment, the acquired images possess lower signal due to the decay of the net transverse magnetization with time T2. This allows sampling of the T2 decay curve at different echo times (e.g. TE1, TE2, etc.).

1.5 Thesis Motivation

The introduction of MRI to the field of epilepsy has revolutionized the diagnosis and management of patients. MRI is routinely used to select surgical candidates for TLE surgery. HS can be readily detected on structural MRI using hippocampal atrophy and increased T2-weighted signal.[6] However, more subtle abnormalities may be detected using quantitative techniques such as hippocampal volumetry, diffusion MRI and quantitative T2.[5, 6] Also, regional hippocampal (i.e. specific subfield) abnormalities that have clinical implications may not be recognized with the

current clinical MRI acquisitions.[52, 65, 98, 113] Diffusion MRI offers a unique insight into the TLE processes by evaluating the internal architecture and structural integrity of the hippocampus. Increases of MD, in particular, have consistently shown sensitivity to detect abnormalities in the ipsilateral hippocampus, correlating with neuronal loss in CA4 and dentate gyrus (see Table 1.4). T2 is a non-specific measure of the tissue microenvironment. Increased quantitative T2 relaxation time in the hippocampus of TLE patients has been shown to correlate with neuronal loss in CA1 and CA3, gliosis in the dentate gyrus and granule cell dispersion (see Table 1.6).

DTI and T2 relaxometry studies have been limited by the low spatial resolution of acquisitions and while recent studies acquired T2 scans with high in-plane resolutions (e.g. 0.43 × 0.43 mm^2), these studies still acquired thick slices (4 mm or above) which can result in missed lesions/abnormalities on a regional hippocampal level.[107, 113, 116] Our lab has developed fast and efficient methods of acquiring high resolution (1 × 1 × 1 mm^3) diffusion MRI and (1.1 × 1.1 × 1 mm^3) T2 relaxometry of the hippocampus.[94, 148] High-resolution DTI has demonstrated focal diffusion abnormalities of the hippocampus pre-surgery that agreed with subfield neuron loss in post-surgical histology in a pilot cohort of 4 patients.[94] However, T2 relaxometry and histology correlations were not performed in this study and to characterize and validate TLE diffusion and quantitative T2 findings, a larger sample size of patients with post-surgical histology is required.

Furthermore, the review of the literature in Section 1.2 suggested a need for more longitudinal diffusion and T2 relaxometry studies to provide a better understanding about the disease progression or lack thereof in TLE patients as well as the impact of surgery on the unresected contralateral hippocampus. Specifically, some previous longitudinal MRI studies have suggested progressive atrophy of the sclerotic hippocampus[71, 72, 149] as well as a post-operative reduction in volume and an increase in MD of the contralateral hippocampus.[80, 81, 99, 150] However,

these findings are not supported by other MRI and histological studies[82, 127, 128, 151] which suggest limited change over time in the hippocampus. Thus, more longitudinal studies are needed to explore these inconsistencies.

The objectives of this work were three-fold: 1- to assess the stability of whole and focal hippocampus diffusion and T2 changes of the ipsilateral and contralateral hippocampus over time in TLE patients; 2- to compare diffusion and quantitative T2 abnormalities of the sclerotic hippocampus; 3- to compare the location of pre-operative MD and T2 abnormalities of the hippocampus with areas identified as abnormal (e.g. containing neuron loss) in subfield histopathology following surgery. It was hypothesized that hippocampal diffusion and T2 changes will persist in TLE patients, implying permanent neuron loss, and that the location of these MRI findings will correlate with subfield histopathology following the surgery. These results would help to assess the potential clinical utility of high-resolution diffusion and T2 relaxometry MRI in TLE to characterize hippocampal subfield pathology pre-surgically that would have significant implications for patient selection in TLE.

2. Methods

This chapter provides more detailed explanations of the methodologies employed to conduct the longitudinal imaging study presented in Chapter 3.

2.1 Participants

This study included 19 controls (mean age 44±13 years; 18-70 years; 10 females) and 19 patients with TLE (mean age 43±13 years; 19-71 years; 9 females) who had two research MRI scans. The clinical information of all participants are outlined in Table 2.1 and Table 3.1. Based on qualitative review of the clinical MRI by the clinical radiologist, 19 TLE patients were subdivided into unilateral HS (n=11), bilateral HS (n=2) and non-HS (n=6). Unilateral and bilateral HS patients demonstrated evidence of unilateral or bilateral hippocampal atrophy, loss of internal architecture or enhanced T2 signal on clinical MRI. Non-HS patients did not have any evidence of hippocampal atrophy, loss of internal hippocampus architecture or other obvious structural abnormalities, except for one patient who had a low grade ganglioglioma (with normal appearing hippocampus). There was no significant difference in age of seizure onset between different TLE subtypes. Disease duration was significantly longer in HS (25±16 years) compared to non-HS patients (9±10 years) (U=11, p=0.012; Mann-Whitney Test).

Eight out of 19 TLE patients (seven unilateral HS and one non-HS patient with ganglioglioma) had hippocampal resection surgery at 6.6±7.5 months (1 day-18 months) after scan 1 and then had a follow-up scan at 2.3±1.0 years (1-4 years) after their surgery. Of those who had surgery, two patients had selective amygdalohippocampectomy (SAH) and six had anterior temporal lobectomy (ATL). The Engel surgical outcomes included 5/8 patients with Engel IA outcome (‘Completely seizure-free”), 1/8 with Engel ID (“Generalized convulsions with antiepileptic drug withdrawal only”) and 2/8 with Engel IIIA (“Worthwhile seizure reduction”).

Histological samples of the hippocampus were available for all 8 surgical patients. Histology stains included NeuN as a marker of neuronal loss, GFAP as a marker of gliosis, and LFB as a marker for myelin density. The HS subtypes were assigned by a neuropathologist based on the degree of neuronal loss (NeuN expression) in hippocampus CA1 and CA4 subfields as per ILAE criteria.[25]

Table 2.1. Summary demographics and clinical information of participants.

Group	**Control (n=19)**	**TLE (n=19)**		
TLE subtype	n/a	Non-HS (n=6)	Unilateral HS (n=11)	Bilateral HS (n=2)
Mean age at baseline (years, range)	44 (18-70)	39 (18-53)	44 (19-71)	36, 59
Sex	9M:10F	5M:1F	4M:7F	1M:1F
Mean inter-scan gap (years, range)	2.7 (1.1-4.0)	2.9 (2.3-3.0)	2.5 (1.0-4.4)	2.4, 2.6
Handedness	18R:1L	4R:2L	10R:1L	1R:1L
Mean age of seizure onset (years, range)	n/a	30 (17-51)	20 (2-44)	0.7, 5
Disease duration (years, range)	n/a	9 (1-29)	25 (5-53)	36, 54

2.2 Image Acquisition

All MRI images were acquired on a Siemens Prisma 3T with 80 mT/m gradient strength per axis using a 64-channel RF coil. Diffusion images were acquired with single-shot 2D EPI (GRAPPA R = 2; 6/8 PPF; A/P phase encode), FOV = 220 × 216 mm^2, matrix = 220 × 216, 20 slices at 1 × 1 × 1 mm^3 resolution with no interpolation, TE = 72 ms, TR = 2800 ms, b = 500 s/mm^2, 10 averages of 10 gradient directions and 10 b0s in 5:18 minutes as per Treit et al.[94] The slices were manually aligned along the long axis of the hippocampus using a whole-brain 3D T1-weighted MPRAGE as reference. The 3D MPRAGE images were acquired aligned to the anterior-posterior commissural line with TE = 2.37 ms, TR = 1800 ms and 0.9 × 0.9 × 0.9 mm^3 resolution in 3:39 minutes. T2 relaxometry scans were acquired using a 16-echo spin-echo sequence with TE = 10.7-171.2 ms, 10 ms inter-echo spacing, TR = 3560 ms and 1.1 × 1.1 × 1 mm^3 resolution in 5:47

minutes. T2 scans included the same 20 slices on the DTI acquisition and were obtained along the long axis of the hippocampus. Lastly, coronal T2-weighted images were acquired with TE = 52 ms, TR = 9550 ms, 70 slices, 0.5 × 0.5 × 1 mm^3 resolution in 7:40 minutes and this scan was used to assist with hippocampus segmentation as discussed in Section 2.6.

2.3 DTI Processing

Prior to computing quantitative diffusion metrics (MD and FA), post-processing steps are necessary to ensure high quality data by minimizing the effect of MRI artifacts. In this work, the first processing step was to average diffusion images of repeated directions to obtain 1b0 and 10 DWIs in MATLAB R2020b. The rest of the steps included Gibbs-ringing, eddy current and motion corrections, and tensor parameter estimations performed in ExploreDTI v4.8.6.[152]

Gibbs ringing (GR) artifact occurs as a result of finite and insufficient sampling of K-space frequencies using Fourier transform.[138] GR commonly appears as parallel dark lines in the image around high-contrast interfaces (e.g. CSF-tissue border) where the signal possess an oscillating behaviour. GR artifacts are most pronounced on b0 images due to sharp signal differences at the bright CSF interface with dark adjacent tissue. The effect of GR artifacts on quantitative diffusion measures include higher variability of MD and FA (generally an overestimation of FA and an underestimation of MD).[138] ExploreDTI uses the total-variation (TV) approach to lessen the effect of GR artifact.[153] In this dataset, GR correction using the TV method was applied in ExploreDTI with the following parameters: number of non-DWIs = 1 (the default value is set to 10), lambda = 100, iterations = 100, and step size = 0.01. This processing step reduced the number of voxels with MD values at the lower end of the distribution (Figure 2.1). However, GR correction also resulted in some degree of image smoothing in the b0 image which contributed to the narrow MD distribution seen in Figure 2.1D. Image blurring also resulted in a false MD increase in the stratum

lacunosum moleculare (SLM), as a consequence of higher signal intensity of the SLM on the b0 but not on mean DWIs (Figure 2.1). Increasing the number of non-DWIs and/or reducing lambda (the weighting factor) exacerbated image blurring. Increasing the lambda reduced image blurring but instead cropped out parts of the image. Further work is needed to develop a more suitable method to correct for GR in either ExploreDTI or other software (e.g. MRtrix3).

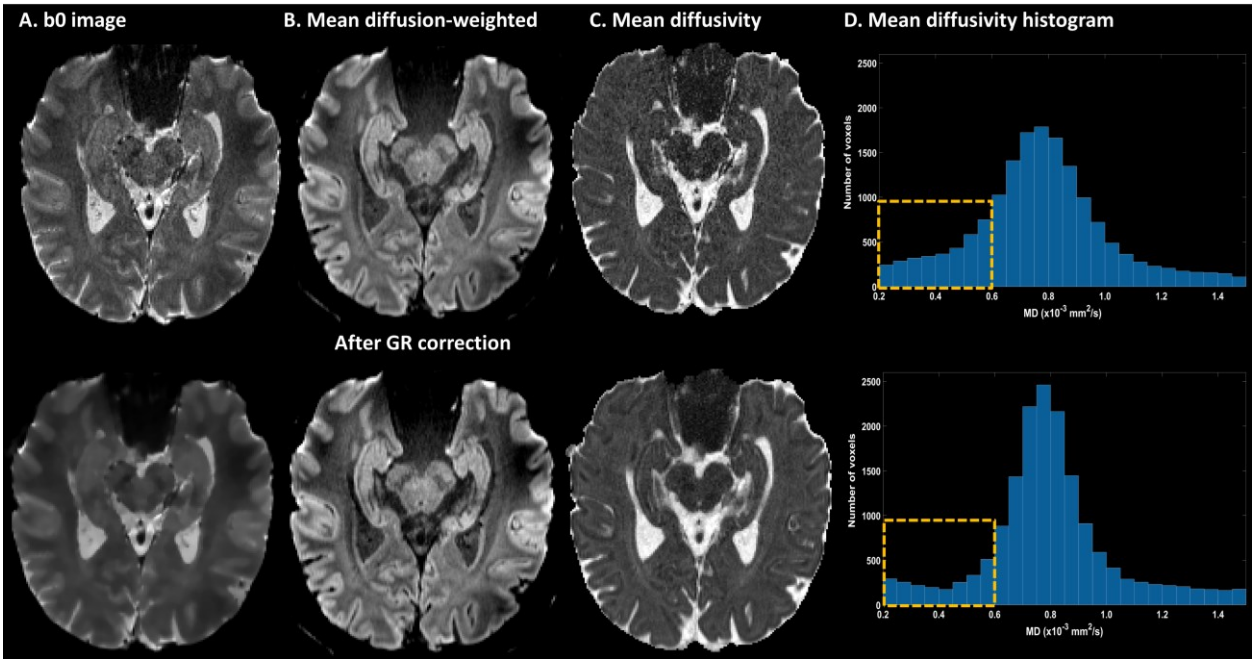

Figure 2.1. Axial (A) b0 and (B) mean DWI slices before and after GR correction. GR artifact can be primarily visualized as dark lines around the ventricles. GR is lessened (but not completely removed) after the correction using the TV approach. However, GR correction smoothed the b0 image and not the mean DWIs resulting in a false MD increase in the stratum lacunosum moleculare as seen in (C). (D) MD histograms corresponding to the respective slices suggest that the number of voxels with lower MD values (< 0.6 x 10^{-3} mm^2/s) is reduced following GR correction.

Diffusion MRI is particularly sensitive to subject motion (e.g. head motion, pulsating flow, etc.) as it can introduce large and unpredictable phase shifts in the spins and may result in an overestimation of MD values.[138] Also, motion or distortions can cause misalignment between the diffusion images which would suggest that each voxels on each diffusion images may not

necessarily come from the same brain region. Eddy currents are produced as a result of rapidly switching diffusion gradients which can induce currents in the conducting surfaces of the scanner (e.g. shields, tubes, etc.). These currents set up magnetic field gradients that remain after the primary gradients are switched off, resulting in image distortions. These distortions are particularly prominent in the EPI sequence (e.g. shearing and scaling artifacts).[154] Motion, eddy current and EPI distortions corrections are included in a single step in ExploreDTI.[155] Average residual error maps of the tensor fit can be used to assess the effect of motion, eddy current and EPI distortion artifacts (Figure 2.2). In this dataset, these maps revealed higher residual error in the middle part of the brain (where the hippocampi are located) compared to the cortex (Figure 2.2). This is because the sensitivity of the 64-channel RF head coil (mounted around the subject's head) decreases as the distance from the coil increases. As a result, the brain regions further away from the coil exhibit worse SNR and higher residual errors from the tensor fit. The last step was diffusion tensor parameter estimation using the linear least square algorithm to obtain mean DWIs, FA, and MD maps as previously demonstrated in Figure 1.7.

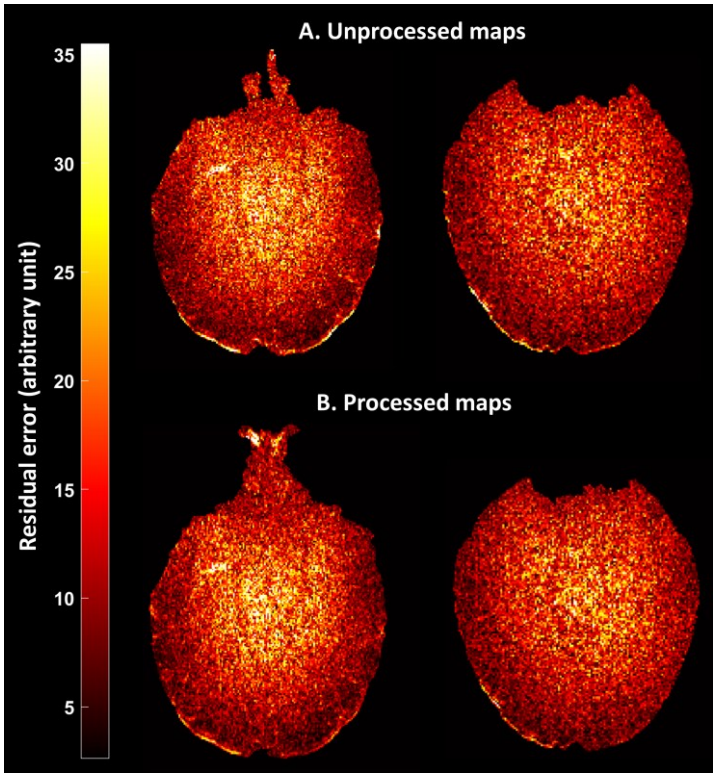

Figure 2.2 Average residual error maps of the tensor fit from two control subjects (A) before and (B) after motion, EPI distortion and eddy current correction. Higher values represent poorer fit. Since the subjects' motion was limited, residual errors are only slightly better after processing (mostly in cortical areas). The middle part of the brain where the hippocampi are demonstrate worse residuals from the tensor fitting compared to the cortex. This can be explained by a reduction in the sensitivity of the 64-channel head coil and SNR in regions furthest away from the coil (e.g. the middle parts).

2.4 T2 relaxometry Processing

There are two main methods to simulate signal decay in a multi-echo spin echo sequence: Bloch equations and extended phase graph (EPG) algorithm. Each method models the spin echo pathway in a different way but both aim to measure T2 and refocusing flip angles by the fitting process.[144] Quantitative T2 maps in this study were computed using a hybrid model of EPG-based indirect and stimulated echo compensation[156] with Shinnar-Le Roux approximation of slice profiles (Figure 2.3).[157] The EPG algorithm computes echo signal amplitude given T1, T2, inter-echo spacing and refocusing angles.[158] The original description of EPG did not account for imperfect

slice profiles which can be a major source of stimulated echoes[156] (discussed in section 1.4.2). A reverse solution to EPG algorithm allows for calculation of T2 values using the echo train amplitudes. A new method was then introduced to compensate for the effect of slice profiles in the EPG algorithm by estimating the distribution of flip angles using the Fourier transform of the RF pulse shape.[156] This method estimates a decay curve with echo train amplitudes integrated over the slice profile. Later it was shown that the Fourier estimation of slice profiles may result in overestimation of the flip angle profile and T2 values. As a result, a hybrid model using EPG with Shinnar-Le Roux (an algorithm that can be used to calculate RF pulse) approximation of slice profiles was employed.[157] This method has been implemented in MATLAB ("StimFitImg_slrpulseshape" script based on these studies[156, 157]) which can compute quantitative T2 maps from MESE scans.

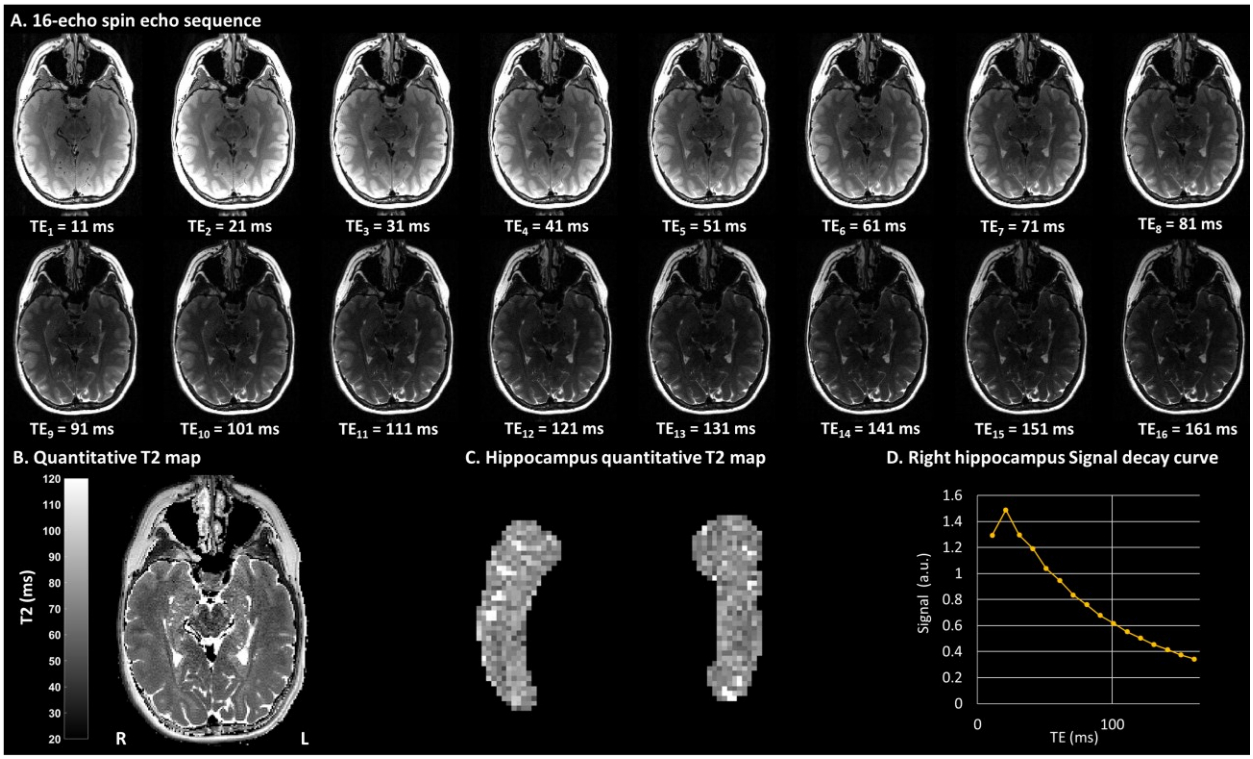

Figure 2.3. (A) 16-echo spin echo T2 sequence acquired at 3T with inter-echo interval of 10 ms. (B) Corresponding quantitative T2 map computed using the EPG-based stimulated echo compensation method in StimFit. (C) Quantified T2 map of the segmented hippocampus with the same scale used in (B). (D) plot of signal intensity over echo time (TE) of the right hippocampus extracted from the 16-echo spin echo sequence.

2.5 Registration

Registration refers to alignment of one MRI data (source image) with another (target image) to ensure spatial overlap of the voxels. The scans can be from different imaging modalities (e.g. MRI and PET) of one subject, from the same modality (e.g. MRI-MRI) of different subjects, or from the same modality and subject (e.g. longitudinal MRI). Registration techniques can be divided into two broad categories: linear and non-linear. Linear registration introduces global changes in the image (e.g. translation, rotation, zooming) while non-linear registration introduces local deformations to match one image with another. There are numerous algorithms within each category tailored to different purposes. Freely available neuroimaging software (e.g. FSL, SPM)

have built-in registration methods, yet choosing an appropriate algorithm and registration parameters (e.g. cost function, interpolation method, degree of freedom, etc.) can be difficult and is usually performed through trial and error.

In this work, repeated MRI acquisitions (mean DWIs and echo-summed T2-weighted images) of the same subject were co-registered to allow within-individual comparison between scan 2 and scan 1. There were several challenges specific to this dataset. First, the MRI acquisitions did not cover the whole-brain as only a small slab of 20 slices along the long axis of the hippocampus were acquired. Most registration techniques have been developed for whole-brain acquisitions by making universal assumptions about the brain (e.g. the head is shaped like an ellipsoid). In this specific sub-volume MRI dataset, some of these assumptions could not be made. For example, the ellipsoid shape of the brain was not visible in the coronal and sagittal planes of the slab acquisition. Consequently, cost functions that do not make such assumptions such as Mutual Information, Correlation Ratio, Least Square, etc. were tested in FSL/FLIRT v6.0.[174] The default FLIRT commend (Correlation Coefficient cost function, spline interpolation, 12 degree of freedom) produced better results among the other variations (e.g. changing the cost functions and/or interpolation methods). However, registration inconsistencies were still observed in the brain of many TLE patients (Figure 2.4). Further, the surgical cavity in a subset of patients that underwent surgical resection of the temporal lobe significantly disrupted the registration algorithms causing failure of the procedure (e.g. an empty output file).

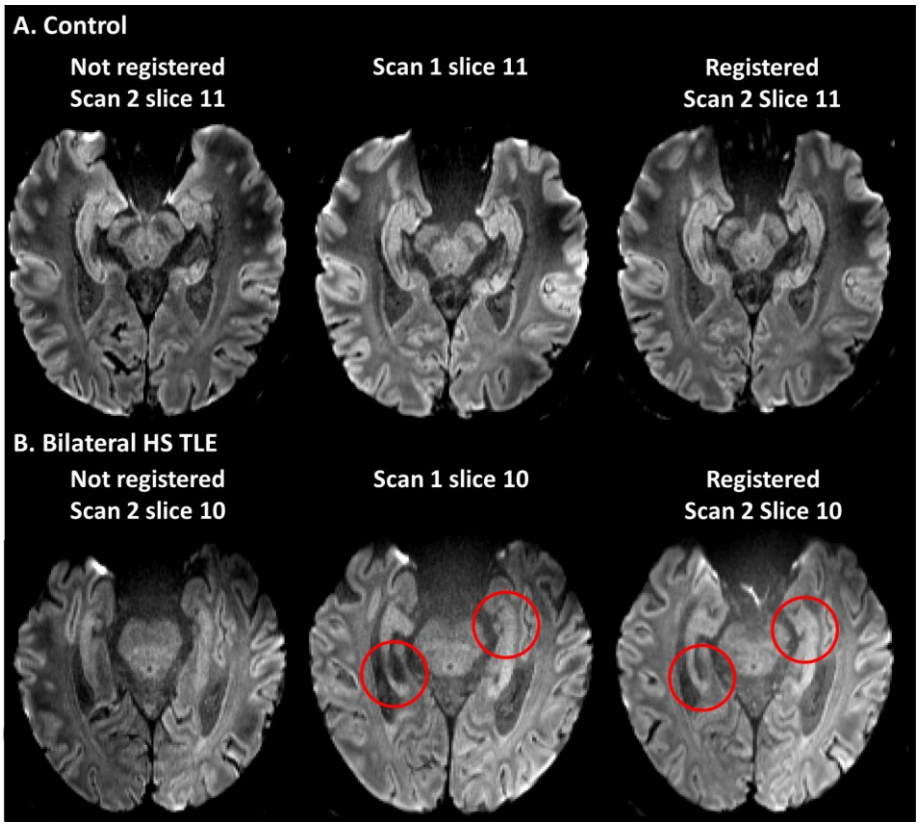

Figure 2.4. Longitudinal registration of mean DWIs (using FSL FLIRT: Correlation Coefficient, spline interpolation, 12 degree of freedom) in a (A) control resulted in accurate spatial correspondence between the images while registration inconsistencies (red circles) were still observed in a (B) TLE patient with bilateral HS.

As a result of the discussed challenges, prior to co-registration, Crop Volume module in 3D Slicer[166] was used to either crop mean DWI into the two hemispheres or extract a box region around the hippocampus given the need to exclude the surgical resection cavity in surgical patients (Figure 2.5). For consistency, this method was applied to all subjects (including non-surgical subjects). Co-registration of the cropped hemispheres did not produce consistent results in some subjects (e.g. cropped out parts or the entire output file). Conversely, co-registration of cropped hippocampus DWIs resulted in excellent correspondence between the two scans. This method was consequently used in Chapter 3 to assess changes between the two scans. There are, however, three limitations: first, this method is very specific to this dataset and is unlikely to work on other

datasets. Second, extraction of the box region around the hippocampus was time-consuming as it was performed manually. Third, while the size of the box ROI was kept the same, its location had to be changed in a few cases as the subject's head and location in the scanner (and accordingly the location of the hippocampus) differed from one MRI data to another.

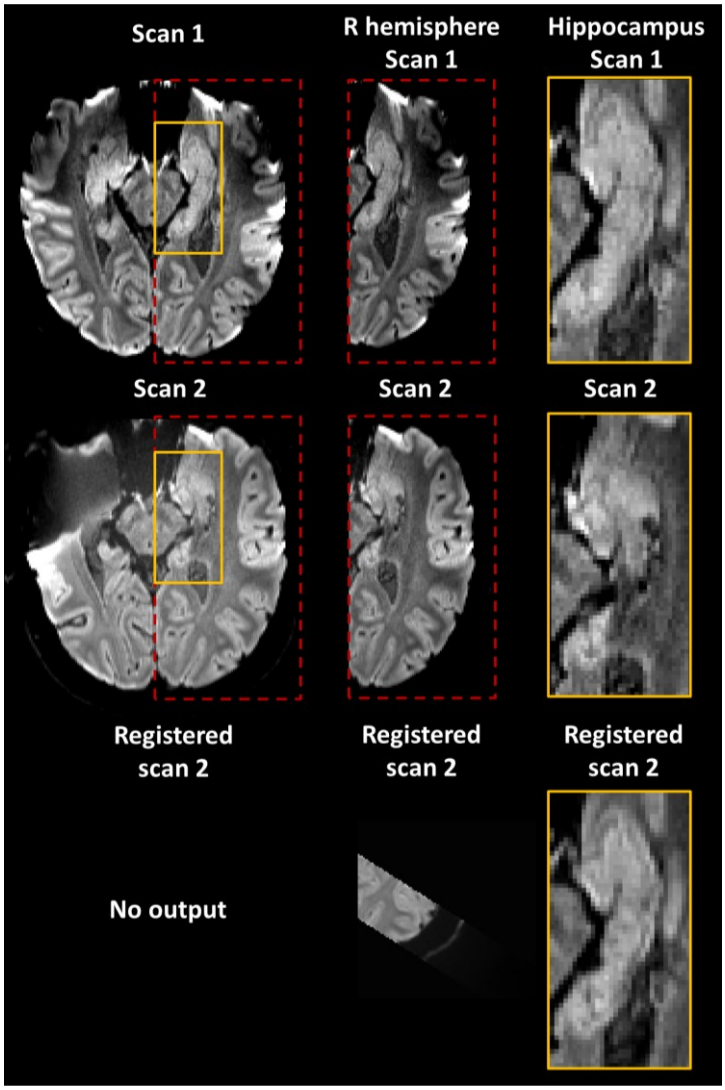

Figure 2.5. Mean DWI slices from a TLE patient that underwent surgical resection of the anterior temporal lobe after scan 1. Left column: co-registration of the two scans failed to produce any results. Middle column: co-registration of the extracted left hemisphere (red dotted box) did not achieve spatial correspondence between the two scans. Right column: co-registration of the extracted hippocampus (yellow boxes) resulted in excellent correspondence between the scans.

2.6 Hippocampus Segmentation

Manual segmentation refers to the delineation of a region of interest on MR images by an individual. While manual segmentation is considered the gold-standard method to analyze a structure of interest, it is time-consuming and requires expertise in the anatomy of the structure.[159] Manual segmentation of the hippocampus is subject to inter- and intra-rater variability and a very large degree of heterogeneity in the volume of the hippocampus among different studies.[160] The European Alzheimer's Disease Consortium (EADC) and Alzheimer's Disease Neuroimaging Initiative (ADNI) centers developed the Harmonized Protocol (HarP) for hippocampus segmentation to account for this heterogeneity.[161] The HarP has demonstrated high inter- and intra-rater reliability[162] even when utilized by inexperienced but compliant tracers.[163]

In this work, whole-hippocampus was segmented according to the HarP on native mean DWIs and separately retraced on echo-summed T2-weighted images acquired along the long axis of the hippocampus. Since this protocol was developed for standard T1-weighted MPRAGE acquired along the anterior and posterior commissures line, Durvery hippocampus atlas was used as a complementary guide.[21]

Segmentation was performed in ITK-SNAP v3.6.0[164] as it provided 3D visualization of the ROI (a requirement in the HarP) to better guide the procedure (Figure 2.6; refer to Appendix A for a complete example of a segmented hippocampus). Hippocampi were segmented in two sequential stages: 1- initial tracing of the hippocampus on the coronal slices, 2- confirmation/modification of the ROIs using all planes (e.g. coronal, axial, sagittal, 3D reconstructed structure). The segmentation started on the middle coronal section of the hippocampus body where a clear view of the dentate gyrus and cornu ammonis (the interlocking “C” relation) could be achieved. The ROIs were then drawn anteriorly and posteriorly with special attention to exclude CSF on the

dorsal boundary. The most rostral slice was defined as the first tissue (e.g. either alveus/fimbria or gray matter tissue; depending on whichever could be visualized) underneath the amygdala. Sagittal and axial slices were particularly useful in separating the amygdala (on the anterior and lateral sides of the hippocampus) from the hippocampus. On axial mean DWIs, the amygdala often appeared as a round gray matter structure with small CSF pockets separating the hippocampus head and amygdala—visualization of the amygdala was more difficult on echo-summed T2 images. The most caudal slice was determined on the coronal section as the last gray matter structure seen inferomedially to the lateral ventricle. Another anatomical landmark on mean DWIs (and to a lesser extent on T2 images) was the SLM which appeared as a dark band along the length of the hippocampus. While these landmarks were sufficient in most cases, visualization of the hippocampus anatomy was sometimes difficult on most rostral or caudal sections—particularly in HS TLE patients with marked atrophy/loss of internal structure/SLM. In such cases, other available scans such as high-resolution ($0.5 \times 0.5 \times 1$ mm^3) coronal T2-weighted scans were used to guide the segmentation.

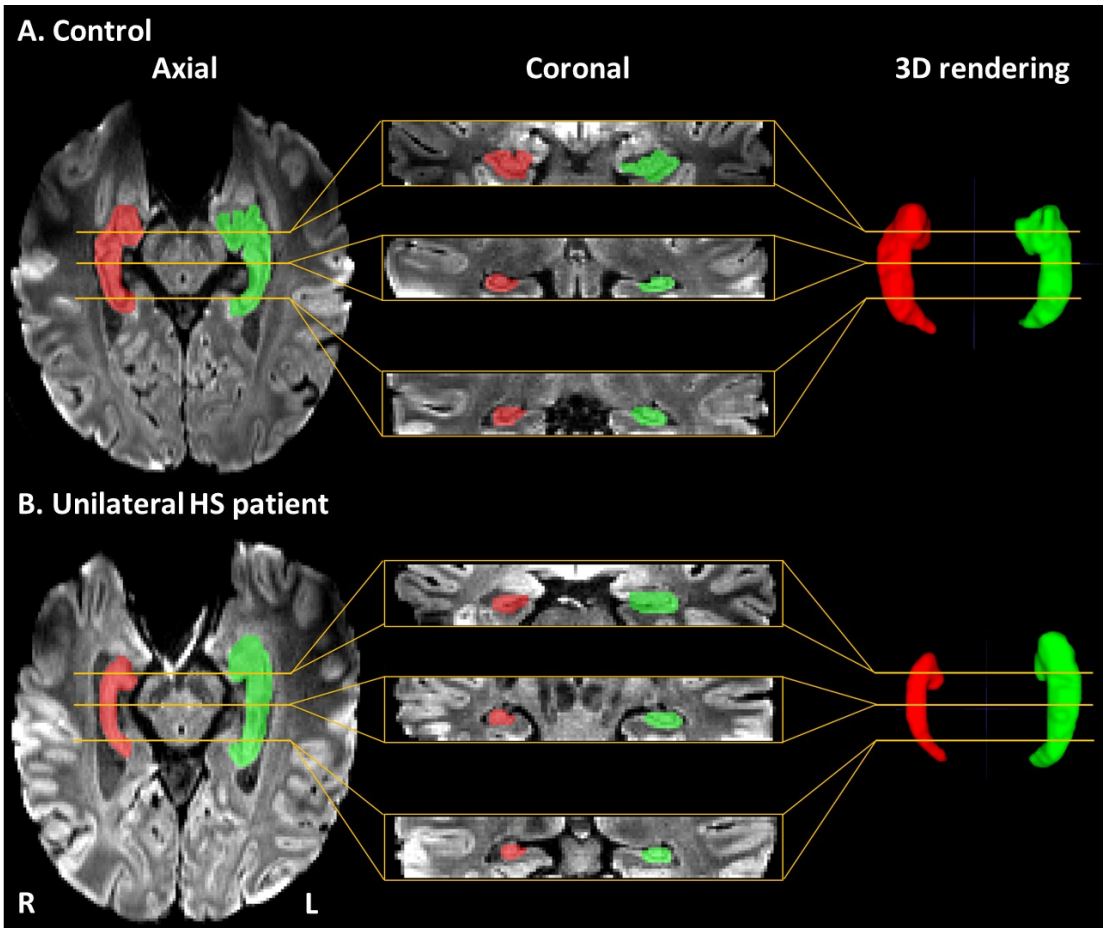

Figure 2.6. Examples of the hippocampus ROIs in a (A) control and (B) unilateral HS patient. The middle coronal section is approximately the first slice on which the ROIs were drawn. The 3D rendering view shown in the right column provides a guide to the protocol (e.g. making sure the gross hippocampal 'seahorse' shape is maintained).

2.7 Curved Multiplanar Reformatting

Curved multiplanar reformatting (CMPR) is a post-processing technique that can improve visualization of complex tubular three-dimensional structures such as blood vessels and trachea.[165] In the CMPR process, the conventional cross-sectional planes (e.g. axial, coronal, sagittal) are modified (e.g. tilted) with respect to the anatomy of the structure to establish the best visualization of the region of interest. As discussed in 1.1.1, the hippocampus is a complex tubular structure. Visualization of the hippocampus head and tail using MRI is particularly challenging due to its

curvatures at the junctions of body-head and body-tail. However, recall that the interlocking C relation between dentate gyrus and cornu ammonis remains consistent throughout the length of the hippocampus regardless of this arc. As demonstrated before,[22] applying CMPR to the hippocampus can maintain the characteristic interlocking C relation across the entire length of the hippocampus.

In this work, CMPR was used to facilitate a comparison between MRI and histology results. Post-surgical histology specimens were consistently obtained from the hippocampal head-body junction. The histology specimens were sectioned in the coronal plane to allow the neuropathologist to assess the degree of neuron loss and gliosis in CA1 and CA4 subfields. However, the "coronal" MRI slices from the head-body junction appear folded which limits the detection of hippocampal subfields CA1 and CA4 (Figure 2.7A). CMPR allows for reconstruction of the MRI slices transverse to the long axis of the hippocampus to enable visualization of CA1 (localized on the lateral aspect) and CA4 (localized on in the mesial regions) subregions. CMPR was performed in 3D Slicer v4.11[166] using the Reformat Module. The coronal plane was manually adjusted obliquely at the head-body hippocampal junction to maintain a tangential orientation with respect to the hippocampus curve and to achieve the best representation of the "interlocking C" relationship between the cornu ammonis and dentate gyrus (Figure 2.7B).

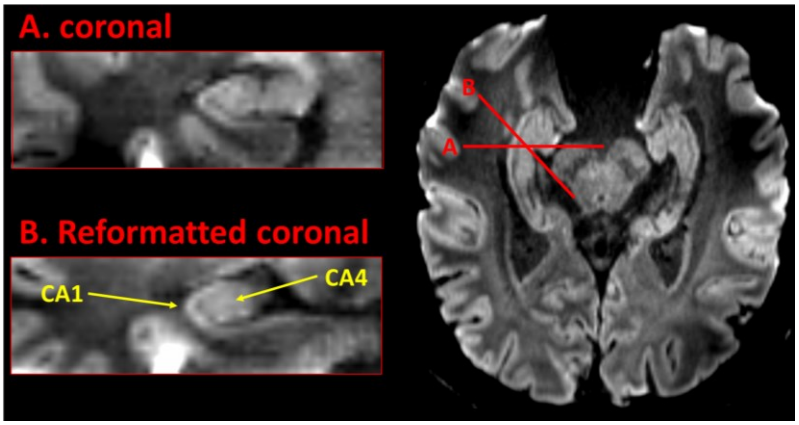

Figure 2.7 (A) Poor representation of cornu ammonis and dentate gyrus on a hippocampal coronal section at the head-body junction. (B) CA1 (lateral regions) and CA4 (mesial regions) are easily identified when the angle of the coronal plane is tilted with respect to the hippocampal curvature.

3. Longitudinal Hippocampal Diffusion-Weighted Imaging and T2 Relaxometry Demonstrate Regional Abnormalities Which are Stable and Predict Subfield Pathology in Temporal Lobe Epilepsy[1]

3.1 Introduction

Temporal lobe epilepsy (TLE) is the most common form of focal epilepsy. While only 20% of TLE patients respond to medications,[3] anterior temporal lobe resection including the hippocampus can provide seizure freedom with resultant improvements in quality of life. However, long-term surgical outcome studies demonstrate that approximately 50% of patients experience seizure recurrence.[4] Finding more accurate predictors of surgical success pre-operatively is imperative to advance treatment options and improve outcomes in TLE patients.

Hippocampal sclerosis (HS) is the most common underlying etiology in drug-resistant TLE[3, 25] and is categorized into three subtypes based on histological assessment of neuronal loss and gliosis of hippocampal subfields.[5, 25] The International League Against Epilepsy (ILAE) HS subtypes include: Type 1 HS with neuronal loss in CA1 and CA4, Type 2 HS with prominent neuronal loss in CA1 and Type 3 HS with prominent neuronal loss in CA4.[25] Notably, post-surgical success has been demonstrated to correlate with HS subtypes.[5, 6, 97, 167-170] Since HS subtype is

[1] Chapter has been submitted for publication elsewhere, Adel SAA, Treit S, Abd Wahab W, Little G, Schmitt L, Wilman AH, Beaulieu C, Gross DW. "Longitudinal Hippocampal Diffusion-Weighted Imaging and T2 Relaxometry Demonstrate Regional Abnormalities Which Are Stable and Predict Subfield Pathology in Temporal Lobe Epilepsy"

currently diagnosed on surgical histology,[5, 167, 168] it has not been possible to use this information to improve the prediction of surgical outcomes prospectively prior to surgery.[97, 167, 168, 170]

While conventional clinical magnetic resonance imaging (MRI) can reliably detect HS (volume loss and elevated T2-weighted signal),[6, 171] it has not been possible to diagnose HS subtypes using standard in-vivo MRI.[3-6, 25] Diffusion tensor imaging (DTI) indirectly evaluates brain microstructure[139, 172] and has demonstrated elevated mean diffusivity (MD) in the ipsilateral hippocampus of TLE patients with HS,[86, 89, 91, 173] correlating with lower pyramidal neuron density in CA4/dentate gyrus (DG).[61] Given the low spatial resolution of most research DTI acquisitions designed for whole-brain (e.g. 2 mm isotropic; 8 mm^3 voxel volumes), it has been difficult to evaluate diffusion changes in hippocampal subregions. Recently, high-resolution (1 mm isotropic) DTI of the human hippocampus using a clinically relevant protocol (~6 minutes at 3T)[148] has shown focal diffusion abnormalities of the hippocampus pre-surgery that agreed with subfield neuron loss in post-surgical histology in a pilot sample of 4 TLE patients.[94] However, to characterize and validate TLE diffusion findings using high-resolution DTI, a larger sample size of patients with post-surgical histology is required. Increased quantitative T2 relaxation time has also been shown to correlate with neuronal loss in CA1 and CA3,[117] gliosis in DG[109] and granule cell dispersion.[116] Whether diffusion and T2 MRI provide complementary data regarding underlying structural abnormalities in the TLE hippocampus is not known.

It is also unclear whether hippocampal volume, quantitative T2 and diffusion subfield abnormalities persist or worsen in TLE and what the impact of temporal lobe surgery is on the contralateral hippocampus. Some previous longitudinal MRI studies have suggested progressive atrophy of the sclerotic hippocampus[71, 72, 150] as well as post-operative reduction in volume and an increase in MD of contralateral non-resected hippocampus.[80, 81, 99, 100] However, these findings are

not supported by other MRI and histological studies[82, 127, 128, 151] which suggest limited change over time in the hippocampus. Thus, more studies with a longitudinal design are needed to explore these inconsistencies and to improve understanding of structural changes following epilepsy surgery.

The current longitudinal imaging study of 19 patients and 19 healthy controls acquired high-resolution 1 mm isotropic DTI and 1.1 × 1.1 × 1 mm^3 quantitative T2 to assess whole and focal MRI changes of the ipsilateral and contralateral hippocampus over ~2.6 years in TLE patients (8 of whom had hippocampal resection). To provide insight into focal diffusion abnormalities, the location of pre-operative MD abnormalities of the hippocampus was compared to focal T2 abnormalities and areas identified as abnormal (e.g. containing neuron loss) in subfield histopathology following surgery.

3.2 Methods

3.2.1 Participants/Study Demographics

This study included 19 controls (mean age 44±13 years; 18-70 years; 10 females) and 19 patients with TLE (mean age 43±13 years; 18-71 years; 9 females). Of this cohort, 12 patients and 10 controls were recruited from our previous cross-sectional study.[94] All controls were recruited through advertising and had no self-reported history of epilepsy, neurological and psychiatric illnesses, or contraindications to MRI. TLE Patients were referred by the neurologists at the University of Alberta Hospital Epilepsy Clinic based on ictal semiology, ictal and interictal EEG and MRI being consistent with a diagnosis of TLE. All subjects provided written informed consent prior to participation. This study was approved by the Health Research Ethics Board at the University of Alberta.

Patients with TLE were subdivided into unilateral HS (n=11), bilateral HS (n=2) and non-HS (n=6) based on qualitative review of the clinical MRI by a neuroradiologist (Table 3.1). Non-HS

patients showed no evidence of hippocampal atrophy, loss of internal hippocampal architecture or other structural abnormalities, except for one patient who had a low grade ganglioglioma (diagnosed on histopathology) with normal hippocampi on MRI (and no evidence of hippocampal pathology on surgical histology).

Table 3.1. Characteristics and demographics of 19 TLE patients

ID	HS Classification (clinical MRI)	Sex	Age at scan 1 (years)	Scan gap (years)	Age of seizure onset (years)	Disease duration (years)	Telemetry Results	Surgery Type	Gap surgery – Scan 2 (years)	Pathology	Engel Outcome[a]
1	Non-HS	Male	47	2.5	18	29	Bilateral	n/a	n/a	n/a	n/a
2	Non-HS	Male	51	2.5	45	6	Right	n/a	n/a	n/a	n/a
3	Non-HS	Male	53	3.5	51	2.0	Right	n/a	n/a	n/a	n/a
4	Non-HS	Male	34	2.4	28	6	Left	n/a	n/a	n/a	n/a
5	Non-HS	Male	29	2.3	18	11	Left	n/a	n/a	n/a	n/a
6	Non-HS	Female	18	4.0	17	1.0	Right	Right ATL	4.0	Non-HS (Glioma grade 1)	IA
7	Unilateral – Right	Male	44	3.9	2	42	Right	Right ATL	2.5	Type 1 HS	IA
8	Unilateral – Right	Female	39	2.0	28	11	Right	Right SAH	2.0	Type 2 HS	IA
9	Unilateral – Left	Female	19	1.4	6	13	Left	Left ATL	1.4	Type 2 HS	ID
10	Unilateral – Left	Male	28	1.7	4	24	Left	Left ATL	1.1	Type 2 HS	IA
11	Unilateral – Left	Female	54	2.4	37	17	Left	Left ATL	1.6	Type 2 HS	IIIA
12	Unilateral – Left	Female	47	2.7	27	20	Left	Left ATL	2.7	Type 2 HS	IIIA
13	Unilateral – Left	Male	43	4.4	33	10	Left	Left SAH	3.1	Type 2 HS	IA
14	Unilateral – Right	Female	47	2.9	9	37	Right	n/a	n/a	n/a	n/a
15	Unilateral – Right	Female	71	2.7	18	53	Right	n/a	n/a	n/a	n/a
16	Unilateral – Left	Female	44	1.0	7	37	Left	n/a	n/a	n/a	n/a
17	Unilateral – Left	Male	49	2.4	44	5	Left	n/a	n/a	n/a	n/a
18	Bilateral	Male	59	2.6	5	54	Bilateral	n/a	n/a	n/a	n/a
19	Bilateral	Female	36	2.4	0.7	35	Bilateral	n/a	n/a	n/a	n/a

[a]Engel outcomes for eight surgical patients were determined within four months of their post-operative scans.

3.2.2 Image Acquisition

All 38 subjects underwent two research MRI scans with an inter-scan gap of 2.6±0.8 years (1-4.4 years) for TLE patients and 2.7±0.8 years (1-4 years) for controls. Eight out of 19 TLE patients (seven unilateral HS and one non-HS patient with ganglioglioma) had hippocampal resection surgery at 6.6±7.5 months (1 day-18 months) after scan 1 and then had a follow-up scan at 2.3±1.0 years (1-4 years) after their surgery.

All MRI images were acquired on a Siemens Prisma 3T as per Treit *et al*.[148] Diffusion images were acquired with single-shot 2D EPI (GRAPPA R2; 6/8 PPF; A/P phase encode), FOV 220 × 216 mm^2, matrix 220 × 216, 20 slices at 1 × 1 × 1 mm^3 resolution with no interpolation, TE 72 ms, TR 2800 ms, b 500 s/mm^2, 10 averages of 10 gradient directions and 10 b0s in 5:18 minutes. The slices were manually aligned along the long axis of the hippocampus using a whole-brain 3D T1-weighted MPRAGE for reference (0.85 mm^3 isotropic; 3:39 minutes). A subset of 16 TLE patients and 9 controls also underwent T2 multi-echo spin echo relaxometry scans with 20 slices, 16 echoes, TE 10.7-171.2 ms, 10 ms inter-echo spacing, TR 3560 ms, 1.1 × 1.1 × 1 mm^3, 5:47 minutes. T2 relaxometry scans were acquired along the long axis of the hippocampus (in the same plane as the diffusion acquisition).

Gibbs-ringing, eddy current and motion corrections, and tensor parameter estimations were performed in ExploreDTI v4.8.6 to obtain mean diffusion-weighted image (DWI), MD and FA maps. Quantitative T2 maps from multi-echo spin echo acquisition were computed using a hybrid model of extended phase graph (EPG)-based indirect and stimulated echo compensation[156] with Shinnar-Le Roux approximation of slice profiles.[157]

3.2.3 Hippocampus Segmentation

Whole-hippocampi were manually segmented on mean DWIs in native space using ITK-snap v3.6.0[164] by a single user (author SAA), blinded to subject group and longitudinal scan number.

Similarly, hippocampi were traced again by author SAA on echo-summed T2-weighted images. The segmentation protocol followed the guidelines outlined in Alzheimer's Disease Neuroimaging Initiative Harmonized Protocol,[162] including the fimbria/alveus in the procedure but excluding the subiculum. To exclude cerebrospinal fluid (CSF)-containing voxels, an MD threshold of 1.5×10^{-3} mm^2/s and T2 threshold of 150 ms (determined based on the lower range of MD and T2 in lateral ventricles) were applied. The volume, MD, FA and T2 were obtained for the whole-hippocampus. The intra-rater dice coefficient (DC) for author SAA was 0.93±0.01 and intraclass correlation coefficient (ICC) for hippocampus volume was 0.98 (0.96-0.99 CI) as measured in 12 subjects (six controls and six TLE) randomly chosen from the sample. Inter-rater reliability between two authors (SAA and ST) showed strong DC (0.83±0.03) and ICC (0.91, 0.64-0.97 CI) scores in the same 12 subjects (Table 3.2).

Table 3.2. Hippocampus manual segmentation intra- and inter-rater reliability.

Reliability	Groups	DICE (SD)	ICC (CI)
Intra-rater	Control (n=6)	0.94 (0.02)	0.94 (0.70-0.99)
	TLE (n=6)	0.93 (0.01)	0.98 (0.87-0.99)
	Total (n=12)	0.93 (0.01)	0.98 (0.96-0.99)
Inter-rater	Control (n=6)	0.85 (0.02)	0.80 (0.64-0.96)
(2 raters)	TLE (n=6)	0.82 (0.04)	0.90 (0.71-0.98)
	Total (n=12)	0.83 (0.04)	0.91 (0.64-0.97)

3.2.4 Registration

To directly compare hippocampal regional changes between the scans, longitudinal mean DWIs for each subject were co-registered using FSL/FLIRT v6.0.[174] Prior to co-registration, 3D Slicer v4.11[166] was used to extract a box region around the hippocampus as a new extracted mean DWI volume given the need to exclude the surgical resection cavity in surgical patients, as this area would significantly disrupt the registration algorithm (Figure 3.1). For consistency, this method was applied to all subjects (including non-surgical subjects) and the same transformation was applied to MD using trilinear interpolation. The same method was applied on echo-summed T2-weighted images to co-register longitudinal T2 maps.

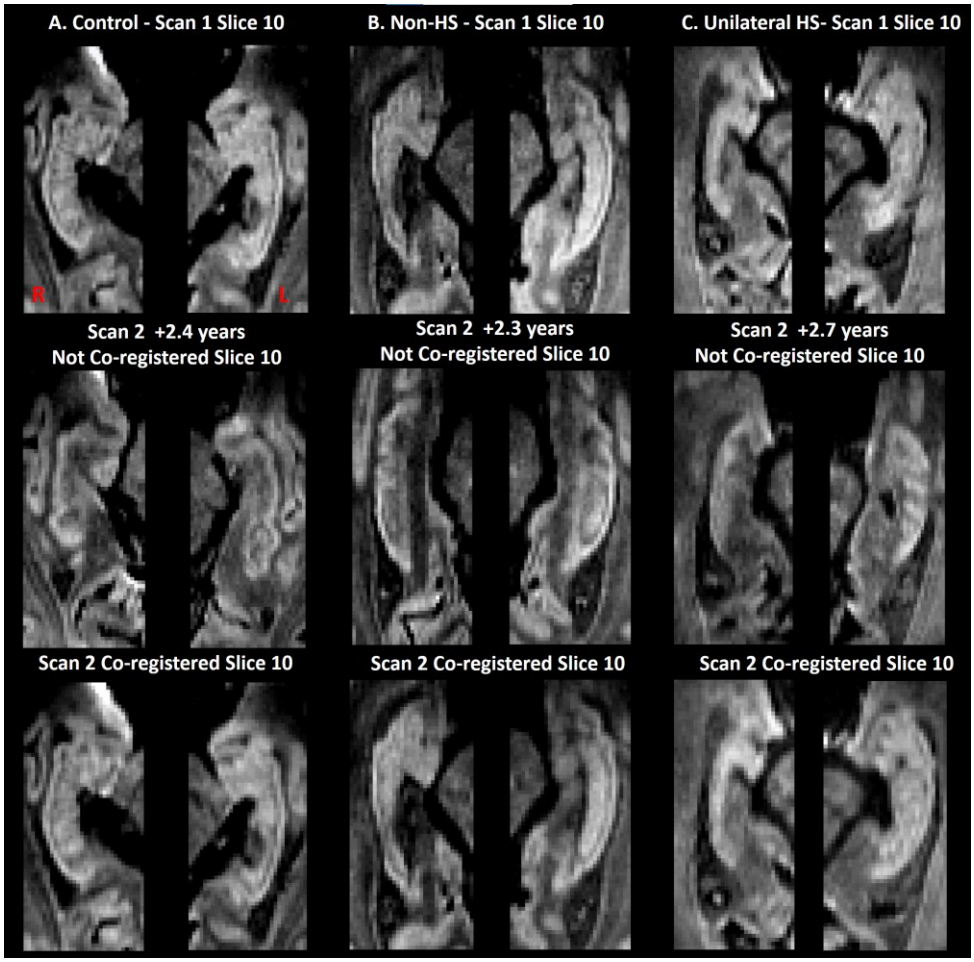

Figure 3.1 Longitudinal co-registration of processed mean diffusion-weighted images (b = 500 s/mm^2) resulted in correspondence of the two scans in a representative (A) control, (B) non-HS and (C) right unilateral HS participant.

3.2.5 Identification of Focal MD and T2 Abnormalities

To characterize focal MD abnormalities at scan 1, a MD threshold of 1.1×10^{-3} mm^2/s was applied, representing two standard deviations (SD) above mean MD ($0.78 \pm 0.17 \times 10^{-3}$ mm^2/s) of 19 controls (38 hippocampi). Similarly, regional T2 abnormalities were defined as voxels above a T2 threshold value of 95 ms (2 SD above the control mean, 71±12 ms) measured in 9 controls (18 hippocampi). This identified the location and extent (expressed as percent of the hippocampus volume with abnormal voxels) of hippocampal MD and T2 elevations.

3.2.6 Regional MD Changes Between the Scans

To characterize the expected range of inter-scan variability in regional MD maps, a reliability analysis was performed by scanning six healthy subjects (mean age 30±4.9 years; 22-35 years; 3 females) two or three times each over a period of 6±3.8 days (1-17 days) using the high-resolution DTI protocol. This allowed for an estimation of the scan-rescan reliability and the level of noise (e.g. processing and registration variability, etc.) in closely spaced serial scans. Difference MD maps were created by subtracting co-registered hippocampal MD maps for each subject. Voxel-by-voxel MD subtraction maps of the six healthy subjects demonstrated a small mean range of -0.06×10^{-3} to $+0.05 \times 10^{-3}$ mm^2/s between the serial scans.

3.2.7 Statistical Analysis

Statistical tests were performed in SPSS v28 (SPSS Corp, 2021) and Prism (GraphPad Software, 2021). Two independent repeated-measures ANOVA (RM-ANOVA) designs were prepared with scans 1 and 2 as repeated factors, hippocampal MRI measures (volume, MD, FA, T2) as dependent variables and inter-scan interval as a covariate. The first RM-ANOVA assessed the trajectories of MRI measures in the controls (bilateral hippocampi of 19 healthy subjects, n=38), non-HS (contralateral hippocampus of 11 unilateral HS and 11 hippocampi of six non-HS TLE patients (one hippocampus was surgically removed); n=22) and HS (ipsilateral hippocampus of four

unilateral HS without surgery and hippocampi of two bilateral HS TLE patients; n=8) (Figure 3.2A). The second RM-ANOVA compared the contralateral hippocampus of TLE patients with and without surgery (Figure 3.2B). One non-HS and both bilateral HS patients were excluded due to demonstration of independent bilateral seizure onset during inpatient EEG-video telemetry (Table 3.1). The groups included surgery (contralateral hippocampus of seven unilateral HS and one non-HS patients; n=8) and non-surgery (contralateral hippocampus of four unilateral HS who did not undergo resection and four non-HS patients; n=8). T2 was available in a subset with group numbers shown in Figure 3.2 . Pairwise comparisons adjusted with a Sidak correction for multiple comparisons were conducted for RM-ANOVAs with significant omnibus effect. Whole-hippocampus measures were plotted against scan number, mean control measurements and two SD boundaries to assess individual longitudinal changes. Pearson's correlations tested the relationship between whole-hippocampus volume, MD, FA, and T2 with age of seizure onset and disease duration.

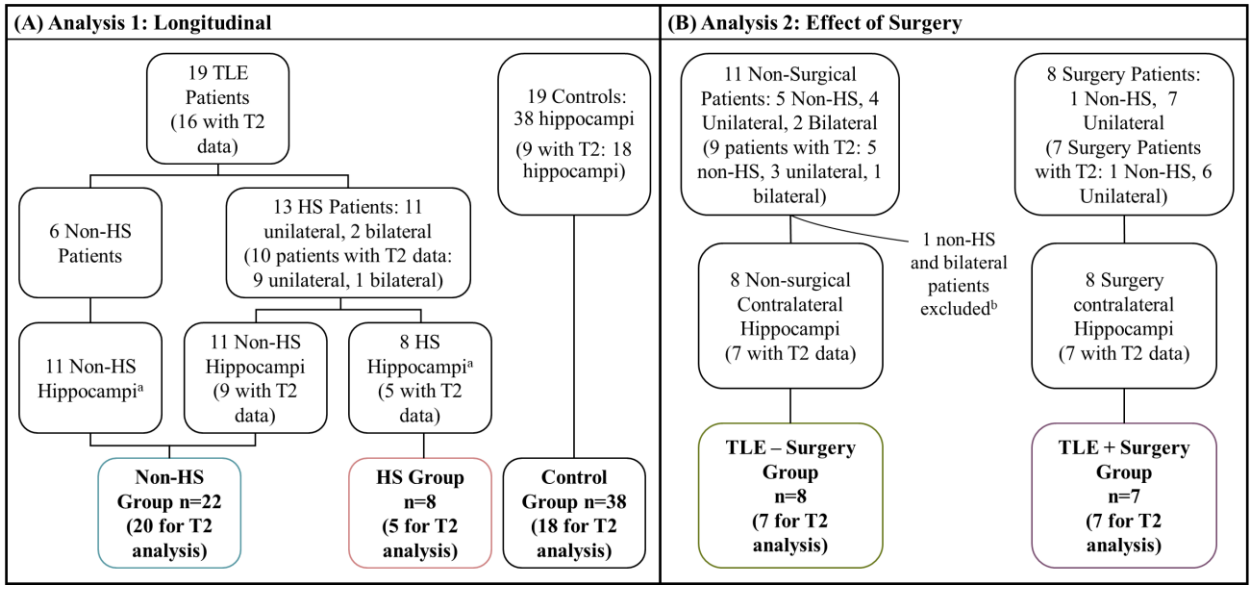

Figure 3.2 Flow chart of the hippocampus groups selected for the repeated-measures ANOVA to assess trajectories of volume, MD, FA and quantitative T2. (A) Analysis 1 was conducted to assess trajectories of volume, MD, FA and T2 in the control, non-HS and sclerotic hippocampi. (B) Analysis 2 assessed the effect of surgery on the contralateral hippocampus of HS and non-HS patients. [a]One non-HS patient and seven of 11 unilateral HS patients underwent surgical removal of the ipsilateral hippocampus following their first scan and therefore longitudinal analysis could not be performed on the resected hippocampi. [b]One non-HS and bilateral HS patients were excluded due to demonstration of independent bilateral seizure onset during inpatient EEG-video telemetry.

3.2.8 Histology

Histological samples of the hippocampus were available for eight TLE patients who underwent surgical resection of the anterior temporal lobe and had pre- and post-operative scans. While the exact location of the histology sample taken from the hippocampus could not be determined, based on the standard surgical procedure used by the neurosurgeon, the histology sample was consistently taken from the posterior head and anterior body of the hippocampus. The histological tissues were analyzed by a neuropathologist (LS) blinded to the clinical information. Neuronal nuclei (NeuN) stain was used as a marker of neuronal loss. The HS subtypes were assigned based on the degree of neuronal loss in CA1 and CA4 subfields as per ILAE criteria[25].

As the pathological specimens were obtained at the hippocampal head-body junction, the comparison to MD and T2 abnormalities was also focused on this region. Based on anatomical knowledge, it was assumed that the CA1 subfield is located in the lateral aspect of the hippocampus and that the CA4 subfield is located in the mesial hippocampus.[21] To facilitate the analysis of CA1 and CA4 at the head-body junction, where the hippocampus curves mesially, 3D Slicer was used to manually perform curved multiplanar reformatting on mean DWI and echo-summed T2-weighted images.[22] This enabled reconstruction of diffusion and T2 slices transverse to the long axis of the hippocampus and allowed identification of CA1 and CA4 with normal or elevated MD and T2 (Figure 3.8). Sensitivity, specificity, positive predictive value (PPV) and negative predictive value (NPV) of MD and T2 to identify subfield pathology were independently determined. False negatives were defined as subfields with histological diagnosis of neuron loss and normal MD and T2. False positives were defined as subfields without neuron loss and abnormally elevated MD and T2.

3.3 Results

3.3.1 Whole-hippocampus MRI Measures Remain Stable

There was a significant effect of group (control, non-HS, HS) on volume ($F(2) = 32.1$, $P < 0.001$), MD ($F(2) = 84.2$, $P < 0.001$), FA ($F(2) = 11.7$, $P < 0.001$) and T2 ($F(2)=27.2$, $P < 0.001$). Post-hoc tests revealed significantly lower volume (by 46%, $P < 0.001$), higher MD (by 23%, $P < 0.001$), lower FA (by 15%, $P < 0.001$) and higher T2 (by 19%, $P < 0.001$) in the HS hippocampi compared to the control (Figure 3.3). The control and non-HS hippocampi did not significantly differ in any of the MRI measures (Table 3.3). There were no statistically significant differences in hippocampal volumes, MD, and T2 between scan 1 and 2 for any groups. There was a significant interaction effect between the groups and repeat scans for hippocampal FA ($F(2) = 3.49$, $P = 0.038$). Post-hoc

analysis showed that hippocampal FA in the HS group at scan 2 was significantly higher (by ~8-20%, P = 0.022) compared to scan 1 (Table 3.3). There were no significant correlations between MRI measures of sclerotic hippocampi with either age of seizure onset or disease duration at either scan.

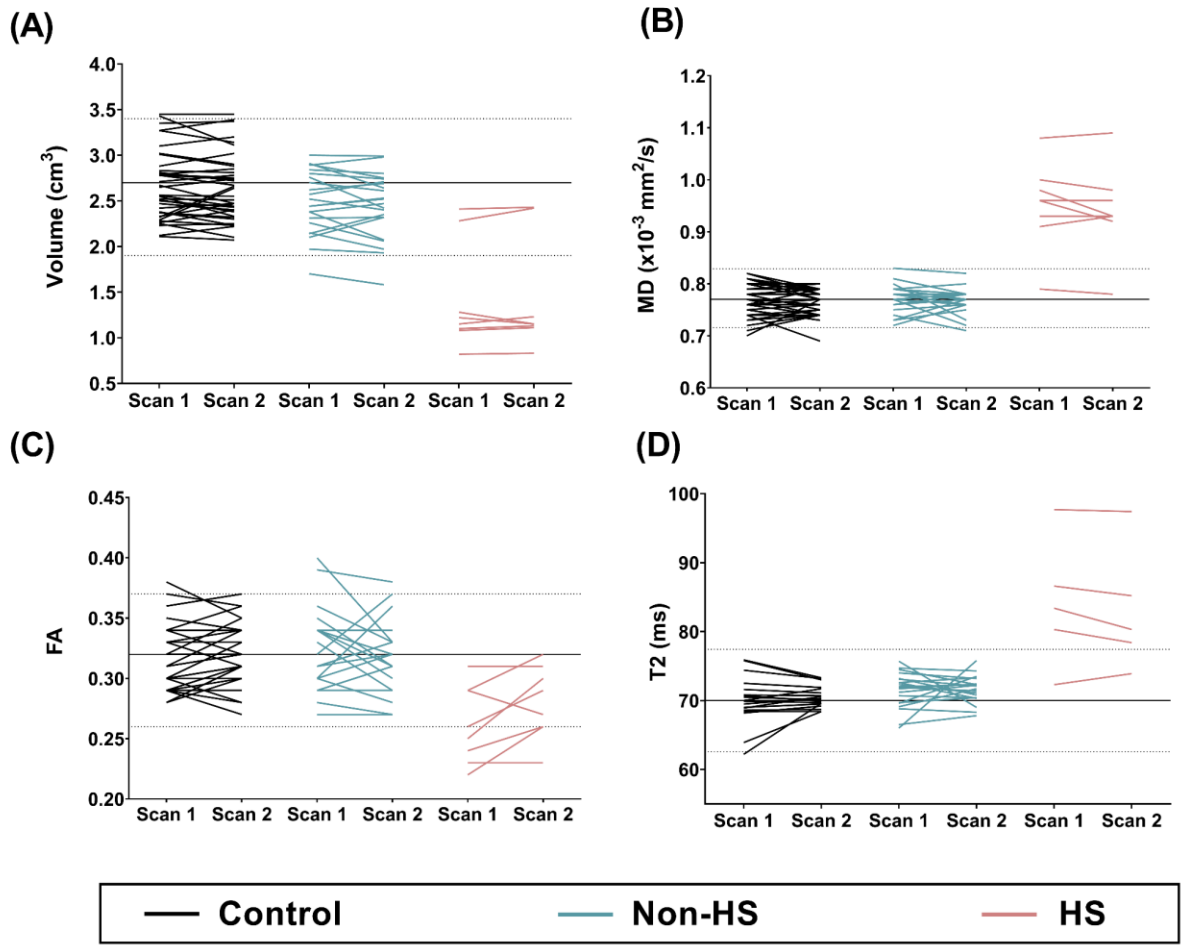

Figure 3.3 Within-individual longitudinal changes of (A) volume, (B) MD, (C) FA and (D) T2 for whole-hippocampi of all subjects across two scans ~2.6 years apart plotted against mean control (solid line) and 2 SD (dotted lines) at both scans. Volume, MD, FA and T2 of non-HS group generally remained within 2 SD of the mean control values at both scans. The HS group demonstrated lower volume in 6/8, higher MD in 7/8, lower FA in 4/8 and higher T2 in 4/5 (scan 1) compared to the control group. The volume, MD and T2 differences remained consistent between the scans. FA increased by 8-20% in 5/8 HS hippocampi, but was still lower than 2 SD of controls in 3/8 patients.

Table 3.3. Whole-hippocampus MRI measures and quantification of thresholded MRI abnormalities of the sclerotic hippocampi.

	Whole-Hippocampus MRI Measure (mean ± SD)										***Thresholded MRI Abnormalities***
	Analysis 1						**Analysis 2**				***(mean ± SD)***
Group	Control (n=38)		Non-HS (n=22)		HS(n=8)		TLE – Surgery (n=8)		TLE + Surgery (n=8)		HS (n=15)[b]
Scan	1	2	1	2	1	2	1	2	1	2	1
Volume (cm^3)	2.7 ±0.4	2.6 ±0.4	2.5 ±0.3	2.4 ±0.4	1.4 ±0.6*	1.4 ±0.6*	2.5 ±0.4	2.5 ±0.5	2.4 ±0.4	2.5 ±0.3	0.3 ±0.3
MD ($x10^{-3}$ mm^2/s)	0.77 ±0.03	0.77 ±0.02	0.77 ±0.03	0.77 ±0.02	0.95 ±0.08*	0.94 ±0.08*	0.77 ±0.03	0.77 ±0.01	0.78 ±0.02	0.76 ±0.02	1.22 ±0.02
FA	0.32 ±0.03	0.32 ±0.02	0.32 ±0.03	0.32 ±0.03	0.26 ±0.03*	0.28 ±0.03*†	0.32 ±0.03	0.31 ±0.02	0.32 ±0.02	0.33 ±0.03	0.24 ±0.02
T2 (ms)[a]	70 ±3	70 ±2	72 ±2	72 ±2	84 ±9*	83 ±9*	72 ±2	71 ±2	72 ±2	71 ±3	107 ±2

[a]T2 relaxometry data was available in a subset of 16 patients and 9 controls with hippocampus group sizes of $n_{Control} = 18$, $n_{Non\text{-}HS} = 20$, $n_{HS} = 5$, $n_{TLE\text{-}surgery} = 7$, $n_{TLE+surgery} = 7$.
[b]This analysis pooled sclerotic hippocampi (n=15) of all HS patients (11 unilateral and 2 bilateral HS patients) at scan 1
*Significant difference ($p<0.05$) from controls based on pairwise comparisons at each scan from repeated-measures ANOVA
†Significant difference ($p<0.05$) from scan 1 for each group based on pairwise comparisons from repeated-measures ANOVA

3.3.2 Heterogeneous Regional MD Abnormalities of the Sclerotic Hippocampus Persist Over Time

High-resolution DTI demonstrated substantial heterogeneity of MD values within hippocampal subregions for HS patients (Figure 3.4). Hippocampi of non-HS patients (Figure 3.4B, E) showed comparable MD (~0.8×10^{-3} mm^2/s) to the controls (Figure 3.4A) whereas sclerotic hippocampi in HS patients showed "hotspots" with regional elevations of MD (>1.1×10^{-3} mm^2/s shown in orange and red in Figure 3.4C, D, F-H).

To identify regions of abnormally high MD at scan 1, a threshold value of 1.1×10^{-3} mm^2/s (2 SD above mean control) was applied while excluding voxels attributed to CSF. The percent of voxels with MD above this threshold was minimal in the controls (mean 5±2% of voxels, range 1-9%) and non-HS groups (mean 4±1%, range 1-7%). Conversely, 22±17% (range 4-59%) of

sclerotic hippocampi volume contained voxels with elevated MD (Figure 3.5). MD elevations were diffuse along the long axis of the hippocampus (e.g. Figure 3.4C, D-left hippocampus) in 8/15 sclerotic hippocampi, predominantly localized to the head (e.g. Figure 3.4D-right hippocampus, G, H) in 5/15 sclerotic hippocampi, and were not evident in 2/15 sclerotic hippocampi. MD elevations were localized to the lateral regions in four hippocampi which was suggestive of Type 2 HS (CA1 abnormalities; e.g. Figure 3.4G, H) and localized to both lateral and mesial regions in nine hippocampi which was suggestive of Type 1 HS (CA1 and CA4 abnormalities; e.g. Figure 3.4C, D, F).

Longitudinal analysis of repeated scans indicated that regional MD abnormalities were consistent over time. MD subtraction maps (scan 2 – scan 1) for TLE patients and control subjects fell in the expected range of scan-rescan noise as determined in six healthy subjects with closely spaced serial scans. This provided quantitative evidence that there is little to no regional hippocampal MD change between the two scans in healthy controls and TLE patients over ~2.6 year.

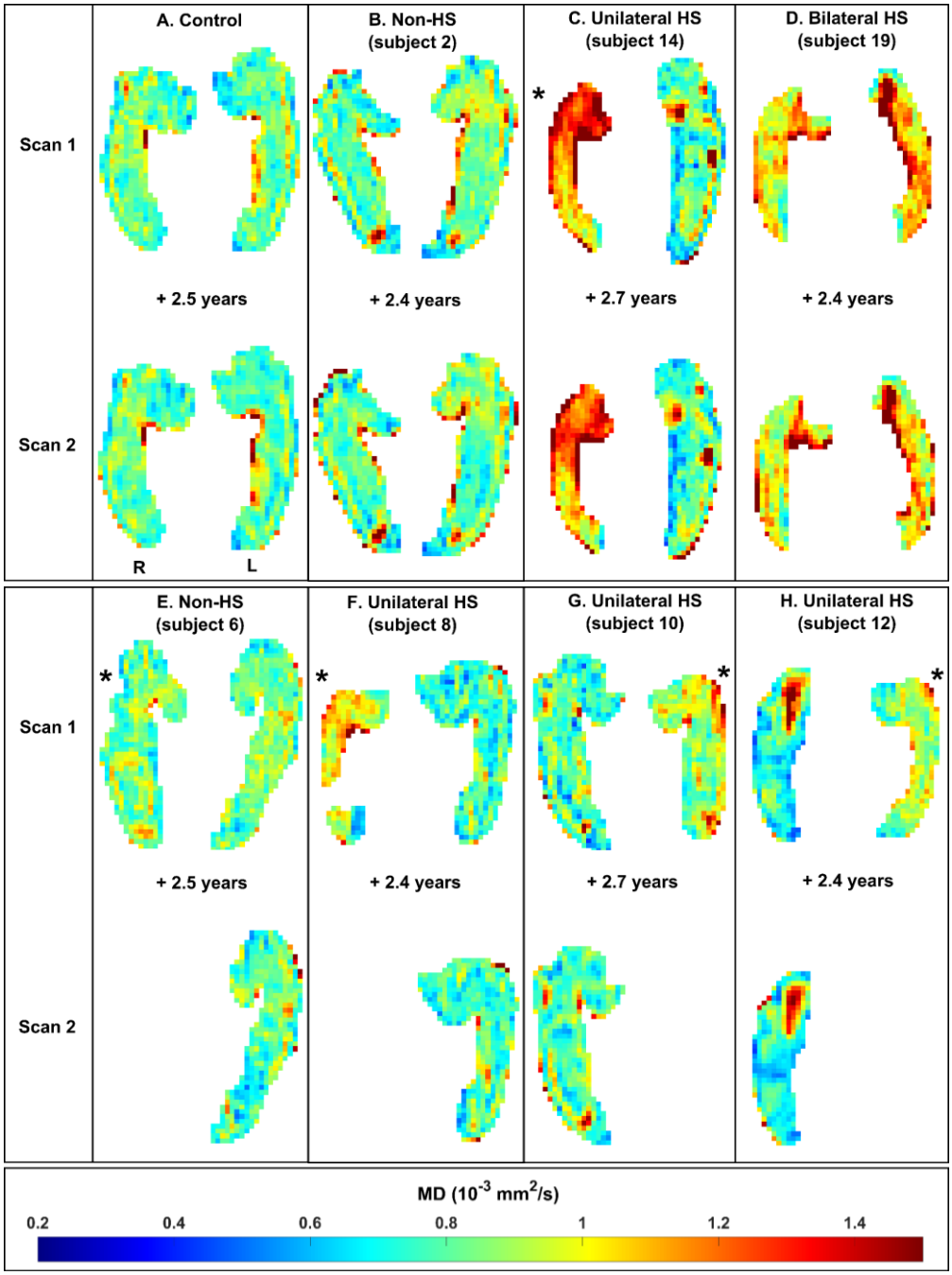

Figure 3.4 The top panel demonstrates longitudinal co-registered MD maps of the hippocampi from a representative (A) control (28 years old), (B) non-HS, (C) right unilateral HS TLE, and (D) bilateral HS TLE. Regional MD maps demonstrate excellent spatial correspondence between longitudinal scans ~2.6 years apart. The non-HS hippocampi (B) are comparable to the control (mostly green 0.8×10^{-3} mm^2/s) and remain unchanged between the two scans. The ipsilateral hippocampus (indicated by *) of (C) and sclerotic hippocampi of (D) show widespread elevated MD (above 1.1×10^{-3} mm^2/s) throughout the entire hippocampus that remain consistent between the scans. The contralateral hippocampus in (C) shows a focal increase of MD within the hippocampus head which remains consistent between the scans. The bottom panel demonstrates longitudinal MD maps of four representative (E-H) surgical patients. The MD of the contralateral hippocampus in all examples remains consistent and unchanged between the scans. Non-lesional patient (E) shows hippocampal MD within the control range. Regions of elevated MD are present in the ipsilateral hippocampus (*) of (F-H) and contralateral hippocampus of (H). Note that the maps are not scaled to size between patients, but are scaled the same left/right.

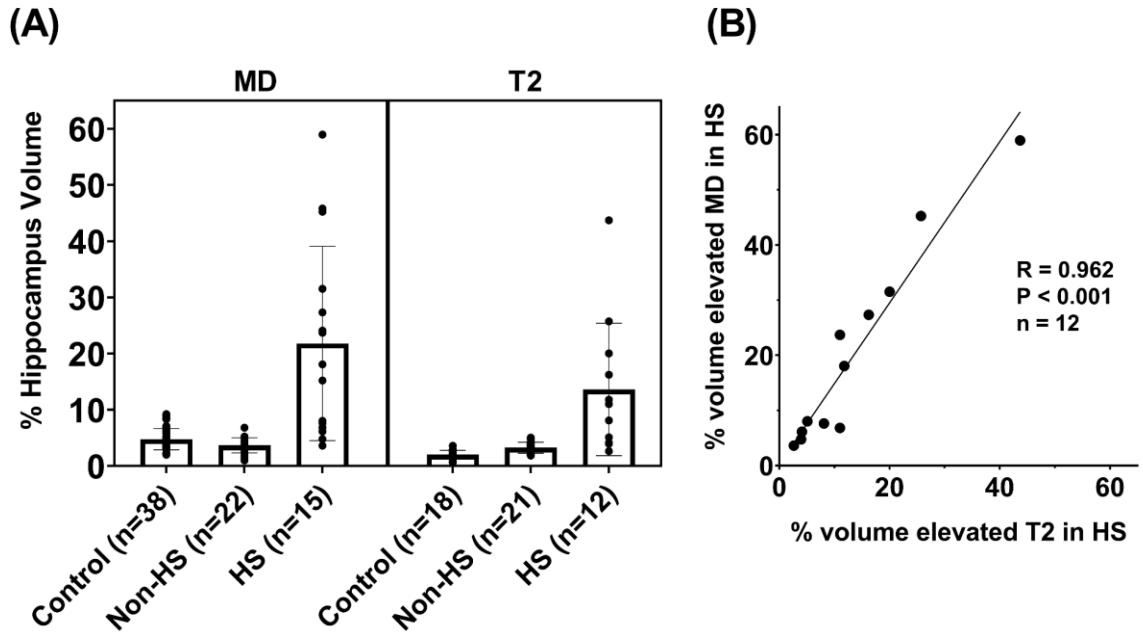

Figure 3.5 (A) Percent hippocampus volume with MD elevations (above 1.1×10^{-3} mm^2/s or 2 SD above the controls) and high T2 (above 95 ms or 2 SD above the controls) in control, non-HS and HS groups at scan 1. Recall that all voxels attributed to CSF (above 1.5×10^{-3} mm^2/s) were not counted. While the control and non-HS groups showed a small percentage of regions with elevated MD and T2, sclerotic hippocampi showed ~22% MD and ~13% T2 elevated regions. (B) The percent hippocampus volume of elevated MD and T2 of the sclerotic hippocampi correlated linearly with each other in 12 TLE patients at scan 1, although the volume on MD was greater than the volume of T2 per patient.

3.3.3 Regional T2 Relaxometry Increases Correspond to Regions with Elevated MD

Quantitative T2 maps from multi-echo relaxometry were acquired in 16 TLE patients and 9 controls. The percent of hippocampal voxels with regions of abnormally high T2 (>95 ms or above 2 SD of mean controls while also excluding CSF-containing voxels) at scan 1 was 2±1% (range 1-4%) in control, 3±1% (range 2-5%) in non-HS and 14±12% (range 3-44%) in HS (Figure 3.5). Regions of elevated T2 were diffuse along the long axis of the hippocampus in 4/12 sclerotic hippocampi (e.g. Figure 3.6C), regional and predominately localized on the head in 6/12 sclerotic hippocampi (e.g. Figure 3.6B), and were not evident in 2/12 sclerotic hippocampi. T2 elevations

were localized to the lateral regions of two hippocampi (suggestive of Type 2 HS), to the mesial regions of one hippocampus (suggestive of Type 3 HS) and to both lateral and mesial regions in seven hippocampi (suggestive of Type 1 HS; e.g. Figure 3.6B, C).

Regions of elevated hippocampal T2 demonstrated excellent spatial overlap with regions of high MD (Figure 3.6). While the extent of MD elevated regions (~22%) was larger than T2 elevated regions (~14%), there was a significant correlation ($R = 0.962$, $P < 0.001$) between percent hippocampal regions with high MD and T2 in sclerotic hippocampi (Figure 3.5).

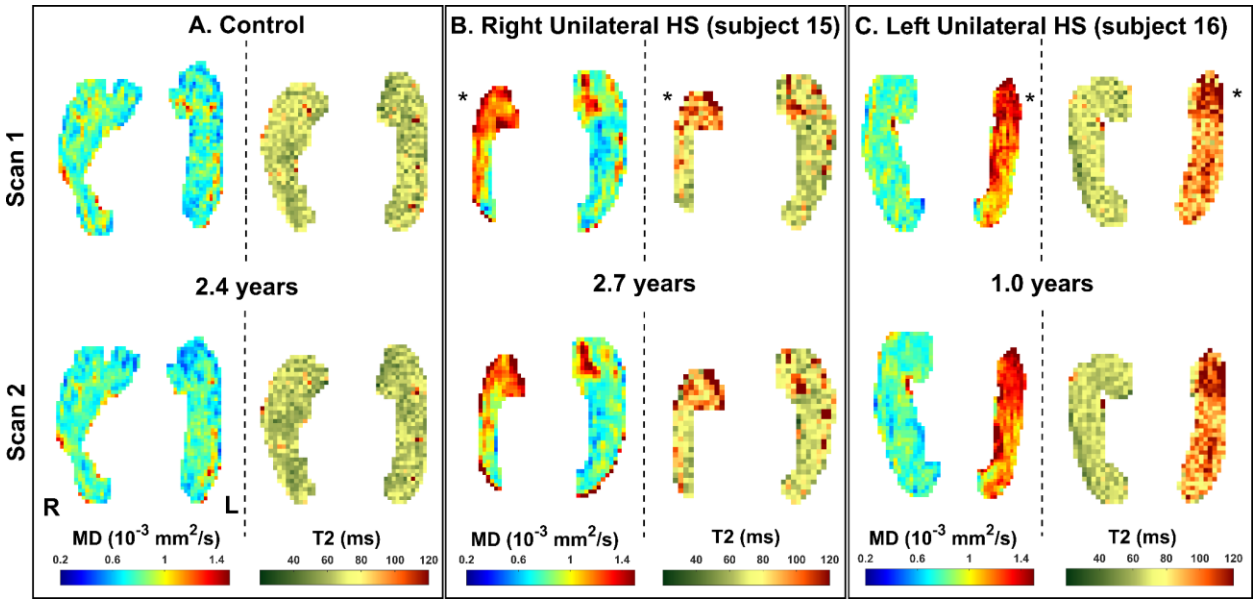

Figure 3.6 Regional MD and T2 maps of the hippocampus in a representative (A) control (32 years old) and two unilateral HS patients. Regions of elevated T2 (above 95 ms) were present in the ipsilateral (indicated by *) hippocampus of (B) and (C) and contralateral head of hippocampus of (B). These elevated T2 regions overlapped with regions of high MD and remained consistent between the longitudinal scans. Note that the maps are not scaled to size between patients, but are scaled the same left/right.

3.3.4 Focal Regions of Elevated MD and T2 in Contralateral Hippocampus

While whole-hippocampal MD and T2 of non-HS hippocampi did not differ from the controls, focal regions of elevated MD were detected in 4/11 contralateral hippocampi of unilateral HS

patients (e.g. Figure 3.4H). Regions of elevated T2 were also detected in the contralateral hippocampi of the same four patients (Figure 3.6B). In all cases, regional elevations of MD and T2 were localized to the mesial hippocampal head (suggesting CA4 abnormalities).

3.3.5 MRI and Histological Assessment of Surgical Patients

Surgery did not result in a significant difference for volume, MD, FA and T2 in the contralateral whole-hippocampus 2.3±1.0 years after surgery (Figure 3.7). MD subtraction maps of the contralateral hippocampus in eight surgical patients showed little to no change between the two scans (not shown).

Subject 6 had a brain tumour with no evidence of HS on clinical MRI and the histology showed normal neuron density in CA1 and CA4 (Figure 3.8A). All seven surgical patients with evidence of HS on clinical MRI had HS confirmed with surgical pathology (one subject with Type 1 HS and six subjects with Type 2 HS; Figure 3.8B, C).

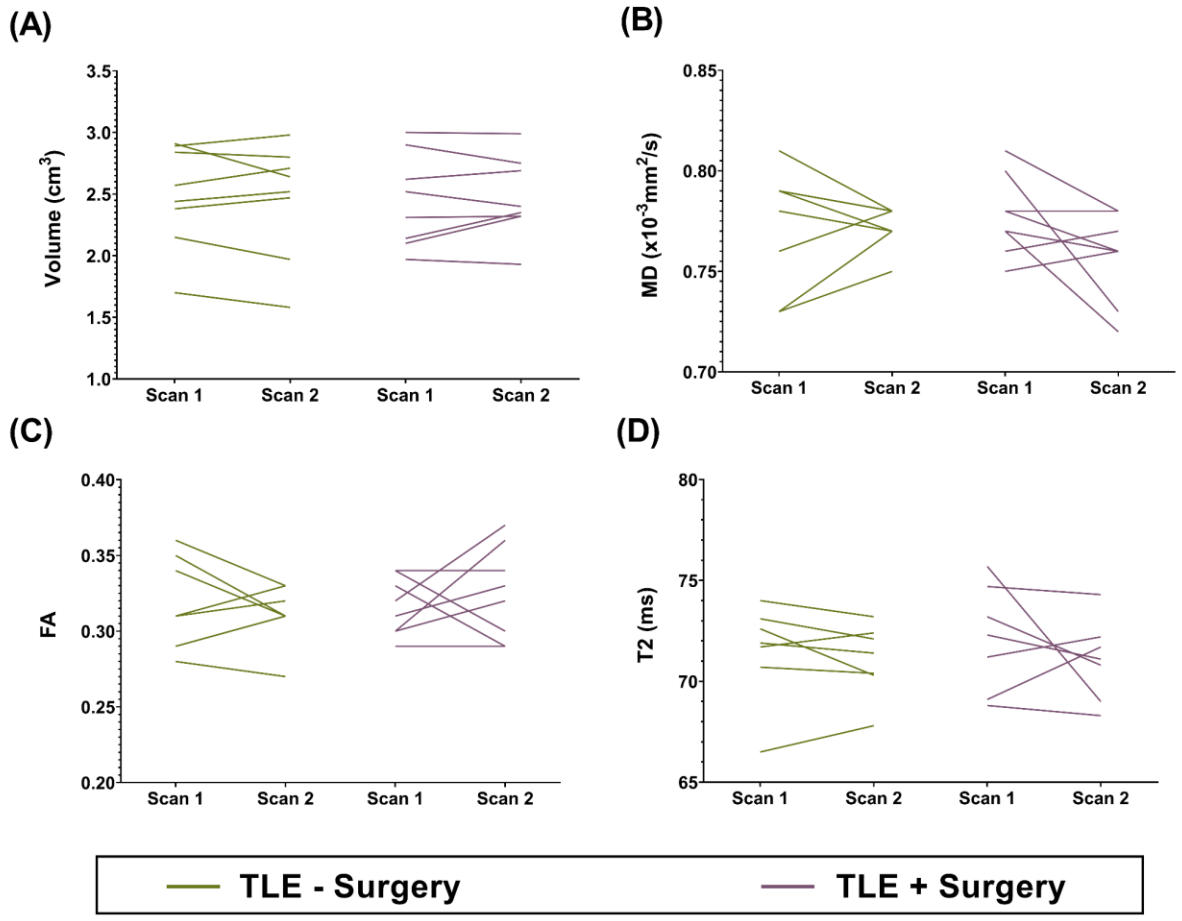

Figure 3.7 Within-individual longitudinal changes in (A) volume, (B) MD, (C) FA and (D) T2 of the contralateral hippocampus for the TLE groups without and with surgical transection of the other hippocampus ~2.6 years after scan 1 or surgery. There were no consistent changes in any parameters for either group between the two scans.

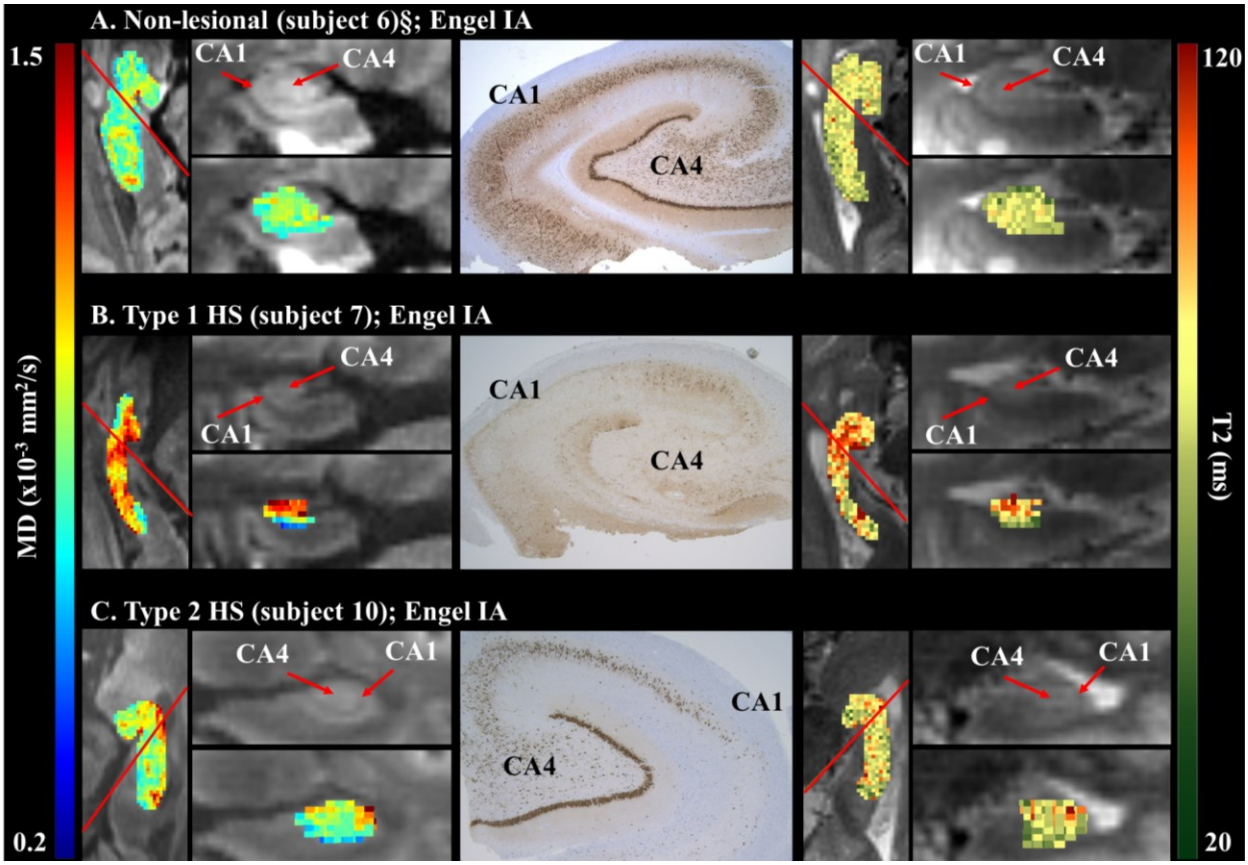

Figure 3.8 Comparison of pre-surgical MD (superimposed on mean DWI) and quantitative T2 maps (superimposed on echo-summed T2-weighted images) with NeuN (marker of neuronal loss) histology of 3 subjects who underwent surgical resection of the hippocampus. The HS subtypes were assigned by the neuropathologist (coauthor LS) blinded to the clinical information. The histology specimen analyzed was consistently obtained from the posterior head and anterior body of the hippocampus (where the red lines were manually oriented to reconstruct the coronal MRI slices). (A) Non-lesional hippocampus showing typical MD and T2 values (mostly green) and normal neuronal density (dark brown). (B) Type 1 HS with elevated MD and T2 (orange and red) in both CA1 and CA4 regions agreeing with Type 1 HS diagnosis. (C) Type 2 HS (neuronal loss in CA1) with MD and T2 elevations in only CA1. (§) denotes the subject reported in our previous study[88].

3.3.6 Pre-surgical Regional Elevated MD and T2 Correspond with NeuN Loss on Post-Surgical Histology

Based on the pathologist's assessment of post-surgical histology in eight surgical patients (16 subfields in total), 8/16 subfields were classified as normal (CA1 and CA4 in the tumour case and

CA4 for seven Type 2 hippocampi) and 8/16 subfields were classified as abnormal (CA1 and CA4 for Type 1 HS hippocampus, CA1 for seven Type 2 hippocampi).

Regional MD abnormalities (>1.1 × 10^{-3} mm^2/s) in the pre-surgical ipsilateral hippocampus correctly identified 7/8 subfields with reduced neuronal density, demonstrating 88% sensitivity. Likewise, 7/8 subfields with normal neuronal density had normal MD (~0.8 × 10^{-3} mm^2/s), yielding 88% specificity. Regional MD values were normal in 1/8 subfields with neuron loss (false negative) and abnormally elevated in 1/8 subfield without neuron loss (false positive), yielding 88% PPV and 88% NPV. Regional T2 abnormalities (>95 ms) identified 6/8 subfields with neuron loss, yielding 75% sensitivity and regions with normal T2 (~71 ms) identified 7/8 normal subfields, yielding 88% specificity. Regional T2 values were normal in 2/8 subfields with neuron loss (false negatives) and abnormally elevated in 1/8 subfields without neuron loss (false positive), yielding 86% PPV and 78% NPV. Overall, regional patterns of MD and T2 agreed with HS subtype diagnosis in 6/8 and 5/8 surgical patients, respectively.

3.4 Discussion

Hippocampal sclerosis is the most common pathology in medically intractable TLE and the presence of HS is associated with improved seizure free outcome with temporal lobe resection.[6, 169] However, HS is not homogeneous and has a tremendous amount of variability between patients with respect to the extent of pathological changes within different hippocampal subregions[5] and along the long axis of the hippocampus,[48, 175] as well as the presence of pathology in the hippocampus contralateral to the seizure focus.[46-48] Given that approximately 50% of patients have seizure recurrence following surgery on long-term follow up,[4] it is reasonable to hypothesize that differences in surgical outcomes could be driven by this pathological heterogeneity. This hypothesis is supported by the demonstration of differences in surgical outcomes for different HS

subtypes.[97, 167, 168, 170] These studies highlight the importance of developing noninvasive methods to accurately detect subhippocampal pathological changes in-vivo as part of surgical planning. While MRI has been demonstrated to detect HS with a high accuracy at the whole-hippocampal level,[6, 171] the ability to detect subhippocampal abnormalities with conventional MRI is limited. High-resolution DTI (1 mm isotropic) has shown focal MD abnormalities of the hippocampus pre-surgery that corresponded with subfield neuron loss in post-surgical histology in 4 TLE patients.[94] In the current study we have expanded our observations to a larger cohort of 8 TLE patients with post-surgical histology and included longitudinal analysis in order to gain further insights into the underlying mechanisms responsible for regional changes in MD of the hippocampus.

Regional MD elevations were stable over the 2.6 year time period of the study and did not change in the contralateral hippocampus of surgical patients, ~2.3 years after surgery. These observations suggest that the regional MD changes are associated with structural abnormalities as opposed to functional changes (such as fluid shifts) which could also result in elevation of MD. Previous longitudinal hippocampal DTI studies post-surgery are limited. In contrast to our findings, two surgical studies demonstrated changes in MD in the post-operative contralateral hippocampus however with conflicting findings (one showing an increase in MD[99] and other showing a decrease[100]). Differences in the timing of post-operative scans and the methodology (in particular the spatial resolution of scans and looking at regional as opposed to whole-hippocampal measures) could explain the conflicting findings.

Consistent with the pathological literature[46-48] we observed considerable heterogeneity in the extent of MD abnormalities along the long axis of the hippocampus (Figure 3.4), within the lateral and mesial hippocampus (suggestive of variability in pathological involvement of different hippocampal subfields) as well as in the involvement of the contralateral hippocampus (e.g. Figure

3.4H). Of note contralateral MD hippocampal abnormalities were not observed at a whole-hippocampal level and were only seen regionally. When comparing pre-surgical regional MD abnormalities to post-surgical histology, MD identified subfield neuron loss with excellent sensitivity and specificity (e.g. Figure 3.8B and C).

While visual detection of increased T2-weighted signal can reliably identify HS in TLE patients,[6, 171] quantification of T2 relaxation time can detect subtle hippocampal abnormalities with higher accuracy.[57, 107] However, T2 relaxometry studies have been limited by the low spatial resolution of acquisitions and while recent studies[57, 107, 116] acquired T2 scans with high in-plane resolutions (e.g. 0.43×0.43 mm^2), these studies still acquired thick slices (4 mm or above) which can result in missed lesions/abnormalities on a regional hippocampal level. Further, these studies used a dual-echo sequence and did not account for stimulated echoes which leads to an overestimation of T2 values.[156, 176] In our study, focal hippocampal T2 abnormalities were demonstrated using a 16-echo T2 sequence with stimulated echo compensation and thin 1 mm slices (1.21 mm^3 voxel volume). These regional abnormalities strongly correlated with the MD findings (Figure 3.6) and also had good sensitivity and excellent specificity in detecting subfield pathology (Figure 3.8B, C). These observations suggest that MD and quantitative T2 provided complementary information regarding hippocampal structural changes. Of interest the extent of the focal abnormalities demonstrated with MD was 1.5× greater than T2 which is consistent with our observation of MD having higher sensitivity than T2 in detecting hippocampal subfield pathology.

In summary, our findings demonstrate that high resolution DTI and quantitative T2 relaxometry can demonstrate structural abnormalities associated with hippocampal sclerosis at a subhippocampal level ipsilateral and contralateral to the seizure focus. While the cohort of patients

that underwent surgery was limited, both MD and T2 accurately predicted HS subtype. Both DTI and T2 acquisitions were acquired at 3T in under 6 minutes making them clinically feasible, potentially providing the opportunity to diagnose precise HS subtypes as well as subtle or regional contralateral hippocampal abnormalities, which could also affect surgical outcomes, preoperatively.

4. Conclusions

The results of this thesis address the current inconsistency in the literature regarding longitudinal changes of the hippocampus in TLE patients, with some studies showing progression of hippocampal damage while others not supporting this notion. We demonstrated the first longitudinal application of high-resolution ($1 \times 1 \times 1$ mm^3) diffusion MRI and ($1.1 \times 1.1 \times 1$ mm^3) T2 relaxometry at 3T in a cohort of TLE patients (eight of whom underwent surgery) to assess the stability of focal diffusion and T2 changes in bilateral hippocampus over ~2.6 years. The results show stability of MD and quantitative T2 abnormalities over the time period of the study and no post-operative changes in the contralateral hippocampus of surgical patients. These results indicate that the regional diffusion changes are likely associated with structural abnormalities as opposed to functional changes which could also result in transient elevation of MD. Methodological differences in MRI acquisitions (e.g. spatial resolution), hippocampal segmentation (e.g. exclusion of the subiculum in the protocol) and the timing of the follow-up/post-operative scans could explain the inconsistencies in the literature.

Our diffusion and T2 relaxometry acquisitions with greatly improved spatial resolution compared to the previous studies allowed us to compare the location of pre-operative diffusion abnormalities of the hippocampus with focal T2 abnormalities and post-surgical subfield histopathology in HS patients. Focal regions of diffusion and T2 abnormalities were detected in bilateral hippocampi of TLE patients with HS. These regions strongly correlated in terms of localization and the extent of abnormality. These findings suggest that diffusion and quantitative T2 provide complementary information regarding hippocampal structural changes. However, compared to quantitative T2, MD was found to be a more sensitive predictor of post-surgical HS

subtype (e.g. neuron loss assessed by NeuN stain). Both high-resolution diffusion and T2 acquisitions were acquired using a clinically feasible protocol (at 3T with each in under 6 minutes), and allowed detection of heterogeneous ipsilateral and subtle contralateral hippocampal abnormalities. In summary, these results support the potential clinical utility of high-resolution hippocampal diffusion and T2 relaxometry imaging in precise characterization of HS subtypes that may have significant implications for surgical patient selection.

The limitations in this study provide opportunities for future investigations. First, while the number of patients with post-surgical histology (n=8) was twice of that in our previous high-resolution DTI study (n=4)[94], there is still a need for a larger sample of patients with post-surgical histology as two subjects were reported in both studies. Also, the small number of surgical patients limited our ability to establish correlations between the HS subtypes predicted by the MRI measures and the surgical outcomes, particularly since only 1/8 patients were diagnosed with Type 1 HS and no patients were diagnosed with Type 3 HS. Further work with a larger number of surgical patients with available HS subtype diagnoses is required. As an aside, it would be interesting to identify hippocampal regions of abnormally high MD and T2 that may predict neuropsychological outcomes (e.g. memory, cognitive) following the surgery.

Second, direct comparisons of focal MD and T2 elevations with histology were not possible due to availability of limited specimens from anterior ipsilateral hippocampus. Curved multiplanar reformatting was applied at hippocampal head-body junction (where the histology was taken) in an attempt to address this limitation. Nevertheless, the MRI-histology component of this study was descriptive and qualitative. Future studies are needed to evaluate correlations between MD and T2 and a quantified degree of neuron loss in hippocampal subfields.

Third, registration between the diffusion and T2 relaxometry data of each subject could not be achieved—possibly due to the presence of different distortions in the echo-planar sequence (diffusion) and the multi-echo spin echo sequence (T2). Registration of hippocampal DTI and T2 acquisitions would allow a direct comparison between the location of focal diffusion and T2 abnormalities in the sclerotic hippocampus of TLE patients.

Fourth, the spatial resolution of DTI and T2 relaxometry scans can be further enhanced to allow improved visualization of hippocampal subfields. While 1 mm isotropic resolution allowed for visualization of the hippocampal internal structure (e.g. SLM) on mean DWIs, accurate estimation of diffusion and T2 parameters in the hippocampal subfields (e.g. CA1, dentate gyrus) at this resolution is still limited due to insufficient resolution and partial volume effect. To address this issue, hippocampal DTI and T2 relaxometry scans can be optimized and acquired on a MRI scanner at higher field strength (> 3T). Since SNR is proportional to both field strength and voxel volume, an increase in field strength allows for a reduction in voxel volume (achieving higher spatial resolution).

References

1. Singh A, Woelfle R, Chepesiuk R, Southward C, Antflick J, Cowan K, et al. Canadian epilepsy priority-setting partnership: Toward a new national research agenda Epilepsy & Behavior. 2022 2022/05/01/;130:108673.

2. Engel J, Jr. What can we do for people with drug-resistant epilepsy? The 2016 Wartenberg Lecture Neurology. 2016 Dec 6;87:2483-2489.

3. Semah F, Picot MC, Adam C, Broglin D, Arzimanoglou A, Bazin B, et al. Is the underlying cause of epilepsy a major prognostic factor for recurrence? Neurology. 1998 Nov;51:1256-1262.

4. de Tisi J, Bell GS, Peacock JL, McEvoy AW, Harkness WF, Sander JW, et al. The long-term outcome of adult epilepsy surgery, patterns of seizure remission, and relapse: a cohort study Lancet. 2011 Oct 15;378:1388-1395.

5. Blumcke I, Pauli E, Clusmann H, Schramm J, Becker A, Elger C, et al. A new clinico-pathological classification system for mesial temporal sclerosis Acta Neuropathol. 2007 Mar;113:235-244.

6. Wieser HG, Epilepsy ICoNo. ILAE Commission Report. Mesial temporal lobe epilepsy with hippocampal sclerosis Epilepsia. 2004 Jun;45:695-714.

7. Engel J, Pedley TA. Epilepsy : a comprehensive textbook. 2nd ed ed. Philadelphia: Lippincott Williams & Wilkins; 2008.

8. Fisher RS, van Emde Boas W, Blume W, Elger C, Genton P, Lee P, et al. Epileptic seizures and epilepsy: definitions proposed by the International League Against Epilepsy (ILAE) and the International Bureau for Epilepsy (IBE) Epilepsia. 2005 Apr;46:470-472.

9. Berg A. Mortality in Epilepsy Epilepsy Curr. 2001 Sep;1:28.

10. Bandstra NF, Camfield CS, Camfield PR. Stigma of epilepsy Can J Neurol Sci. 2008 Sep;35:436-440.

11. Proposal for revised classification of epilepsies and epileptic syndromes. Commission on Classification and Terminology of the International League Against Epilepsy Epilepsia. 1989 Jul-Aug;30:389-399.

12. Gross DW. Diffusion tensor imaging in temporal lobe epilepsy Epilepsia. 2011 Jul;52 Suppl 4:32-34.

13. Haneef Z, Lenartowicz A, Yeh HJ, Levin HS, Engel J, Jr., Stern JM. Functional connectivity of hippocampal networks in temporal lobe epilepsy Epilepsia. 2014 Jan;55:137-145.

14. Bartolomei F, Wendling F, Regis J, Gavaret M, Guye M, Chauvel P. Pre-ictal synchronicity in limbic networks of mesial temporal lobe epilepsy Epilepsy Res. 2004 Sep-Oct;61:89-104.

15. Berg AT, Berkovic SF, Brodie MJ, Buchhalter J, Cross JH, van Emde Boas W, et al. Revised terminology and concepts for organization of seizures and epilepsies: report of the ILAE Commission on Classification and Terminology, 2005-2009 Epilepsia. 2010 Apr;51:676-685.

16. Blumcke I, Spreafico R. Cause matters: a neuropathological challenge to human epilepsies Brain Pathol. 2012 May;22:347-349.

17. Blair RD. Temporal lobe epilepsy semiology Epilepsy Res Treat. 2012;2012:751510.

18. Brodie MJ, Zuberi SM, Scheffer IE, Fisher RS. The 2017 ILAE classification of seizure types and the epilepsies: what do people with epilepsy and their caregivers need to know? Epileptic Disord. 2018 Apr 1;20:77-87.

19. Bartsch T, Wulff P. The hippocampus in aging and disease: From plasticity to vulnerability Neuroscience. 2015 Nov 19;309:1-16.

20. Bird CM, Burgess N. The hippocampus and memory: insights from spatial processing Nat Rev Neurosci. 2008 Mar;9:182-194.

21. Duvernoy HM, Cattin F, Risold PY. The human hippocampus: functional anatomy, vascularization and serial sections with MRI. 4th edition ed2013.

22. Gross DW, Misaghi E, Steve TA, Wilman AH, Beaulieu C. Curved multiplanar reformatting provides improved visualization of hippocampal anatomy Hippocampus. 2020 Feb;30:156-161.

23. Rajmohan V, Mohandas E. The limbic system Indian J Psychiatry. 2007;49:132-139.

24. Small SA, Schobel SA, Buxton RB, Witter MP, Barnes CA. A pathophysiological framework of hippocampal dysfunction in ageing and disease Nat Rev Neurosci. 2011 Sep 7;12:585-601.

25. Blumcke I, Thom M, Aronica E, Armstrong DD, Bartolomei F, Bernasconi A, et al. International consensus classification of hippocampal sclerosis in temporal lobe epilepsy: a Task Force report from the ILAE Commission on Diagnostic Methods Epilepsia. 2013 Jul;54:1315-1329.

26. Aulicka S, Ceska K, Sana J, Siegl F, Brichtova E, Oslejskova H, et al. Cytokine-chemokine profiles in the hippocampus of patients with mesial temporal lobe epilepsy and hippocampal sclerosis Epilepsy Res. 2022 Feb;180:106858.

27. de Lanerolle NC, Kim JH, Williamson A, Spencer SS, Zaveri HP, Eid T, et al. A retrospective analysis of hippocampal pathology in human temporal lobe epilepsy: evidence for distinctive patient subcategories Epilepsia. 2003 May;44:677-687.

28. de Lanerolle NC, Lee TS. New facets of the neuropathology and molecular profile of human temporal lobe epilepsy Epilepsy Behav. 2005 Sep;7:190-203.

29. Sutula T. Seizure-Induced Axonal Sprouting: Assessing Connections Between Injury, Local Circuits, and Epileptogenesis Epilepsy Curr. 2002 May;2:86-91.

30. Thom M. Review: Hippocampal sclerosis in epilepsy: a neuropathology review Neuropathol Appl Neurobiol. 2014 Aug;40:520-543.

31. Zimmer TS, David B, Broekaart DWM, Schidlowski M, Ruffolo G, Korotkov A, et al. Seizure-mediated iron accumulation and dysregulated iron metabolism after status epilepticus and in temporal lobe epilepsy Acta Neuropathol. 2021 Oct;142:729-759.

32. Blumcke I. Neuropathology of focal epilepsies: a critical review Epilepsy Behav. 2009 May;15:34-39.

33. Magloczky Z, Freund TF. Impaired and repaired inhibitory circuits in the epileptic human hippocampus Trends Neurosci. 2005 Jun;28:334-340.

34. Devinsky O, Vezzani A, O'Brien TJ, Jette N, Scheffer IE, de Curtis M, et al. Epilepsy Nature Reviews Disease Primers. 2018 2018/05/03;4:18024.

35. Kwan P, Arzimanoglou A, Berg AT, Brodie MJ, Allen Hauser W, Mathern G, et al. Definition of drug resistant epilepsy: consensus proposal by the ad hoc Task Force of the ILAE Commission on Therapeutic Strategies Epilepsia. 2010 Jun;51:1069-1077.

36. Chen Z, Brodie MJ, Liew D, Kwan P. Treatment Outcomes in Patients With Newly Diagnosed Epilepsy Treated With Established and New Antiepileptic Drugs: A 30-Year Longitudinal Cohort Study JAMA Neurology. 2018;75:279-286.

37. Brodie MJ, Dichter MA. Antiepileptic drugs N Engl J Med. 1996 Jan 18;334:168-175.

38. Spencer D, Burchiel K. Selective amygdalohippocampectomy Epilepsy Res Treat. 2012;2012:382095.

39. Engel J, Jr., McDermott MP, Wiebe S, Langfitt JT, Stern JM, Dewar S, et al. Early surgical therapy for drug-resistant temporal lobe epilepsy: a randomized trial Jama. 2012 Mar 7;307:922-930.

40. Chandra PS, Ramanujam B, Tripathi M. Surgery for Drug-Resistant Epilepsy in Children N Engl J Med. 2018 Jan 25;378:399.

41. Engel J Jr, Van Ness PC, Rasmussen TB, Ojemann LM. O. Outcome with respect to epileptic seizures. Surgical treatment of the epilepsies. New York: Raven Press; 1993. p. 609–621.

42. Hu WH, Zhang C, Zhang K, Meng FG, Chen N, Zhang JG. Selective amygdalohippocampectomy versus anterior temporal lobectomy in the management of mesial temporal lobe epilepsy: a meta-analysis of comparative studies J Neurosurg. 2013 Nov;119:1089-1097.

43. Radhakrishnan K, So EL, Silbert PL, Jack CR, Jr., Cascino GD, Sharbrough FW, et al. Predictors of outcome of anterior temporal lobectomy for intractable epilepsy: a multivariate study Neurology. 1998 Aug;51:465-471.

44. Janszky J, Janszky I, Schulz R, Hoppe M, Behne F, Pannek HW, et al. Temporal lobe epilepsy with hippocampal sclerosis: predictors for long-term surgical outcome Brain. 2005;128:395-404.

45. Tezer FI, Akalan N, Oguz KK, Karabulut E, Dericioglu N, Ciger A, et al. Predictive factors for postoperative outcome in temporal lobe epilepsy according to two different classifications Seizure. 2008 2008/09/01/;17:549-560.

46. Babb TL. Bilateral pathological damage in temporal lobe epilepsy Can J Neurol Sci. 1991 Nov;18:645-648.

47. Margerison JH, Corsellis JA. Epilepsy and the temporal lobes. A clinical, electroencephalographic and neuropathological study of the brain in epilepsy, with particular reference to the temporal lobes Brain. 1966 Sep;89:499-530.

48. Thom M, Liagkouras I, Martinian L, Liu J, Catarino CB, Sisodiya SM. Variability of sclerosis along the longitudinal hippocampal axis in epilepsy: a post mortem study Epilepsy Res. 2012 Nov;102:45-59.

49. Shah AK, Mittal S. Invasive electroencephalography monitoring: Indications and presurgical planning Ann Indian Acad Neurol. 2014 Mar;17:S89-94.

50. Ho SS, Berkovic SF, Berlangieri SU, Newton MR, Egan GF, Tochon-Danguy HJ, et al. Comparison of ictal SPECT and interictal PET in the presurgical evaluation of temporal lobe epilepsy Ann Neurol. 1995 Jun;37:738-745.

51. Ponisio MR, Zempel JM, Day BK, Eisenman LN, Miller-Thomas MM, Smyth MD, et al. The Role of SPECT and PET in Epilepsy AJR Am J Roentgenol. 2021 Mar;216:759-768.

52. Sidhu MK, Duncan JS, Sander JW. Neuroimaging in epilepsy Curr Opin Neurol. 2018 Aug;31:371-378.

53. Bernasconi A, Cendes F, Theodore WH, Gill RS, Koepp MJ, Hogan RE, et al. Recommendations for the use of structural magnetic resonance imaging in the care of patients with epilepsy: A consensus report from the International League Against Epilepsy Neuroimaging Task Force Epilepsia. 2019 Jun;60:1054-1068.

54. Jackson GD, Connelly A, Duncan JS, Grunewald RA, Gadian DG. Detection of hippocampal pathology in intractable partial epilepsy: increased sensitivity with quantitative magnetic resonance T2 relaxometry Neurology. 1993 Sep;43:1793-1799.

55. Kuzniecky R, de la Sayette V, Ethier R, Melanson D, Andermann F, Berkovic S, et al. Magnetic resonance imaging in temporal lobe epilepsy: pathological correlations Ann Neurol. 1987 Sep;22:341-347.

56. Berkovic SF, Andermann F, Olivier A, Ethier R, Melanson D, Robitaille Y, et al. Hippocampal sclerosis in temporal lobe epilepsy demonstrated by magnetic resonance imaging Ann Neurol. 1991 Feb;29:175-182.

57. Vos SB, Winston GP, Goodkin O, Pemberton HG, Barkhof F, Prados F, et al. Hippocampal profiling: Localized magnetic resonance imaging volumetry and T2 relaxometry for hippocampal sclerosis Epilepsia. 2020 Feb;61:297-309.

58. Louis S, Morita-Sherman M, Jones S, Vegh D, Bingaman W, Blumcke I, et al. Hippocampal Sclerosis Detection with NeuroQuant Compared with Neuroradiologists AJNR Am J Neuroradiol. 2020 Apr;41:591-597.

59. Jack CR, Jr., Sharbrough FW, Cascino GD, Hirschorn KA, O'Brien PC, Marsh WR. Magnetic resonance image-based hippocampal volumetry: correlation with outcome after temporal lobectomy Ann Neurol. 1992 Feb;31:138-146.

60. Princich JP, Donnelly-Kehoe PA, Deleglise A, Vallejo-Azar MN, Pascariello GO, Seoane P, et al. Diagnostic Performance of MRI Volumetry in Epilepsy Patients With Hippocampal Sclerosis Supported Through a Random Forest Automatic Classification Algorithm Front Neurol. 2021;12:613967.

61. Goubran M, Bernhardt BC, Cantor-Rivera D, Lau JC, Blinston C, Hammond RR, et al. In vivo MRI signatures of hippocampal subfield pathology in intractable epilepsy Hum Brain Mapp. 2016 Mar;37:1103-1119.

62. Van Paesschen W, Revesz T, Duncan JS, King MD, Connelly A. Quantitative neuropathology and quantitative magnetic resonance imaging of the hippocampus in temporal lobe epilepsy Ann Neurol. 1997 Nov;42:756-766.

63. Mizutani M, Sone D, Sano T, Kimura Y, Maikusa N, Shigemoto Y, et al. Histopathological validation and clinical correlates of hippocampal subfield volumetry based on T2-weighted MRI in temporal lobe epilepsy with hippocampal sclerosis Epilepsy Res. 2021 Nov;177:106759.

64. Jardim AP, Corso JT, Garcia MT, Gaca LB, Comper SM, Lancellotti CL, et al. Hippocampal atrophy on MRI is predictive of histopathological patterns and surgical prognosis in mesial temporal lobe epilepsy with hippocampal sclerosis Epilepsy Res. 2016 Dec;128:169-175.

65. Steve TA, Gargula J, Misaghi E, Nowacki TA, Schmitt LM, Wheatley BM, et al. Hippocampal subfield measurement and ILAE hippocampal sclerosis subtype classification with in vivo 4.7 tesla MRI Epilepsy Res. 2020 Mar;161:106279.

66. Alhusaini S, Doherty CP, Scanlon C, Ronan L, Maguire S, Borgulya G, et al. A cross-sectional MRI study of brain regional atrophy and clinical characteristics of temporal lobe epilepsy with hippocampal sclerosis Epilepsy Res. 2012 Mar;99:156-166.

67. Kalviainen R, Salmenpera T, Partanen K, Vainio P, Riekkinen P, Pitkanen A. Recurrent seizures may cause hippocampal damage in temporal lobe epilepsy Neurology. 1998 May;50:1377-1382.

68. Pai A, Marcuse LV, Alper J, Delman BN, Rutland JW, Feldman RE, et al. Detection of Hippocampal Subfield Asymmetry at 7T With Automated Segmentation in Epilepsy Patients With Normal Clinical Strength MRIs Front Neurol. 2021;12:682615.

69. Theodore WH, Bhatia S, Hatta J, Fazilat S, DeCarli C, Bookheimer SY, et al. Hippocampal atrophy, epilepsy duration, and febrile seizures in patients with partial seizures Neurology. 1999 Jan 1;52:132-136.

70. Spencer SS, McCarthy G, Spencer DD. Diagnosis of medial temporal lobe seizure onset: relative specificity and sensitivity of quantitative MRI Neurology. 1993 Oct;43:2117-2124.

71. Briellmann RS, Berkovic SF, Syngeniotis A, King MA, Jackson GD. Seizure-associated hippocampal volume loss: a longitudinal magnetic resonance study of temporal lobe epilepsy Ann Neurol. 2002 May;51:641-644.

72. Fuerst D, Shah J, Shah A, Watson C. Hippocampal sclerosis is a progressive disorder: a longitudinal volumetric MRI study Ann Neurol. 2003 Mar;53:413-416.

73. Conz L, Morita ME, Coan AC, Kobayashi E, Yasuda CL, Pereira AR, et al. Longitudinal MRI volumetric evaluation in patients with familial mesial temporal lobe epilepsy Front Neurol. 2011;2:5.

74. Alvim MK, Coan AC, Campos BM, Yasuda CL, Oliveira MC, Morita ME, et al. Progression of gray matter atrophy in seizure-free patients with temporal lobe epilepsy Epilepsia. 2016 Apr;57:621-629.

75. Quigg M, Bertram EH, Jackson T. Longitudinal distribution of hippocampal atrophy in mesial temporal lobe epilepsy Epilepsy Res. 1997 May;27:101-110.

76. Bonilha L, Halford JJ, Morgan PS, Edwards JC. Hippocampal atrophy in temporal lobe epilepsy: the 'generator' and 'receiver' Acta Neurol Scand. 2012 Feb;125:105-110.

77. Kreilkamp BAK, Weber B, Elkommos SB, Richardson MP, Keller SS. Hippocampal subfield segmentation in temporal lobe epilepsy: Relation to outcomes Acta Neurol Scand. 2018 Jun;137:598-608.

78. Quigg M, Bertram EH, Jackson T, Laws E. Volumetric magnetic resonance imaging evidence of bilateral hippocampal atrophy in mesial temporal lobe epilepsy Epilepsia. 1997 May;38:588-594.

79. Keller SS, Roberts N. Voxel-based morphometry of temporal lobe epilepsy: an introduction and review of the literature Epilepsia. 2008 May;49:741-757.

80. Fernandes DA, Yasuda CL, Lopes TM, Enrico G, Alessio A, Tedeschi H, et al. Long-term postoperative atrophy of contralateral hippocampus and cognitive function in unilateral refractory MTLE with unilateral hippocampal sclerosis Epilepsy Behav. 2014 Jul;36:108-114.

81. Elliott CA, Gross DW, Wheatley BM, Beaulieu C, Sankar T. Progressive contralateral hippocampal atrophy following surgery for medically refractory temporal lobe epilepsy Epilepsy Res. 2016 Sep;125:62-71.

82. Li W, Jiang Y, Qin Y, Zhou B, Lei D, Zhang H, et al. Structural and functional reorganization of contralateral hippocampus after temporal lobe epilepsy surgery Neuroimage Clin. 2021;31:102714.

83. Assaf BA, Mohamed FB, Abou-Khaled KJ, Williams JM, Yazeji MS, Haselgrove J, et al. Diffusion tensor imaging of the hippocampal formation in temporal lobe epilepsy AJNR Am J Neuroradiol. 2003 Oct;24:1857-1862.

84. Chiang S, Levin HS, Wilde E, Haneef Z. White matter structural connectivity changes correlate with epilepsy duration in temporal lobe epilepsy Epilepsy Res. 2016 Feb;120:37-46.

85. Ercan K, Gunbey HP, Bilir E, Zan E, Arslan H. Comparative Lateralizing Ability of Multimodality MRI in Temporal Lobe Epilepsy Dis Markers. 2016;2016:5923243.

86. Focke NK, Yogarajah M, Bonelli SB, Bartlett PA, Symms MR, Duncan JS. Voxel-based diffusion tensor imaging in patients with mesial temporal lobe epilepsy and hippocampal sclerosis Neuroimage. 2008 Apr 1;40:728-737.

87. Gonçalves Pereira PM, Oliveira E, Rosado P. Apparent diffusion coefficient mapping of the hippocampus and the amygdala in pharmaco-resistant temporal lobe epilepsy AJNR Am J Neuroradiol. 2006 Mar;27:671-683.

88. Hugg JW, Butterworth EJ, Kuzniecky RI. Diffusion mapping applied to mesial temporal lobe epilepsy: preliminary observations Neurology. 1999 Jul 13;53:173-176.

89. Liacu D, de Marco G, Ducreux D, Bouilleret V, Masnou P, Idy-Peretti I. Diffusion tensor changes in epileptogenic hippocampus of TLE patients Neurophysiol Clin. 2010 Jun;40:151-157.

90. Lui YW, Nusbaum AO, Barr WB, Johnson G, Babb JS, Orbach D, et al. Correlation of apparent diffusion coefficient with neuropsychological testing in temporal lobe epilepsy AJNR Am J Neuroradiol. 2005 Aug;26:1832-1839.

91. Nazem-Zadeh MR, Schwalb JM, Elisevich KV, Bagher-Ebadian H, Hamidian H, Akhondi-Asl AR, et al. Lateralization of temporal lobe epilepsy using a novel uncertainty analysis of MR diffusion in hippocampus, cingulum, and fornix, and hippocampal volume and FLAIR intensity J Neurol Sci. 2014 Jul 15;342:152-161.

92. Salmenpera TM, Simister RJ, Bartlett P, Symms MR, Boulby PA, Free SL, et al. High-resolution diffusion tensor imaging of the hippocampus in temporal lobe epilepsy Epilepsy Res. 2006 Oct;71:102-106.

93. Thivard L, Lehéricy S, Krainik A, Adam C, Dormont D, Chiras J, et al. Diffusion tensor imaging in medial temporal lobe epilepsy with hippocampal sclerosis Neuroimage. 2005 Nov 15;28:682-690.

94. Treit S, Little G, Steve T, Nowacki T, Schmitt L, Wheatley BM, et al. Regional hippocampal diffusion abnormalities associated with subfield-specific pathology in temporal lobe epilepsy Epilepsia Open. 2019 Dec;4:544-554.

95. Wieshmann UC, Clark CA, Symms MR, Barker GJ, Birnie KD, Shorvon SD. Water diffusion in the human hippocampus in epilepsy Magn Reson Imaging. 1999 Jan;17:29-36.

96. Yoo SY, Chang KH, Song IC, Han MH, Kwon BJ, Lee SH, et al. Apparent diffusion coefficient value of the hippocampus in patients with hippocampal sclerosis and in healthy volunteers AJNR Am J Neuroradiol. 2002 May;23:809-812.

97. Coras R, Milesi G, Zucca I, Mastropietro A, Scotti A, Figini M, et al. 7T MRI features in control human hippocampus and hippocampal sclerosis: an ex vivo study with histologic correlations Epilepsia. 2014 Dec;55:2003-2016.

98. Sala-Padro J, Miró J, Rodriguez-Fornells A, Quintana M, Vidal N, Plans G, et al. Hippocampal microstructural architecture and surgical outcome: Hippocampal diffusivity could predict seizure relapse Seizure. 2020 Jan 26;76:84-88.

99. Elliott CA, Gross DW, Wheatley BM, Beaulieu C, Sankar T. Longitudinal hippocampal and extra-hippocampal microstructural and macrostructural changes following temporal lobe epilepsy surgery Epilepsy Res. 2018 Feb;140:128-137.

100. Thivard L, Tanguy ML, Adam C, Clemenceau S, Dezamis E, Lehericy S, et al. Postoperative recovery of hippocampal contralateral diffusivity in medial temporal lobe epilepsy Epilepsia. 2007 Mar;48:599-604.

101. Briellmann RS, Jackson GD, Pell GS, Mitchell LA, Abbott DF. Structural abnormalities remote from the seizure focus: a study using T2 relaxometry at 3 T Neurology. 2004 Dec 28;63:2303-2308.

102. Coan AC, Kubota B, Bergo FP, Campos BM, Cendes F. 3T MRI quantification of hippocampal volume and signal in mesial temporal lobe epilepsy improves detection of hippocampal sclerosis AJNR Am J Neuroradiol. 2014 Jan;35:77-83.

103. Kubota BY, Coan AC, Yasuda CL, Cendes F. T2 hyperintense signal in patients with temporal lobe epilepsy with MRI signs of hippocampal sclerosis and in patients with temporal lobe epilepsy with normal MRI Epilepsy Behav. 2015 May;46:103-108.

104. Mueller SG, Laxer KD, Schuff N, Weiner MW. Voxel-based T2 relaxation rate measurements in temporal lobe epilepsy (TLE) with and without mesial temporal sclerosis Epilepsia. 2007 Feb;48:220-228.

105. Namer IJ, Bolo NR, Sellal F, Nguyen VH, Nedelec JF, Hirsch E, et al. Combined measurements of hippocampal N-acetyl-aspartate and T2 relaxation time in the evaluation of mesial temporal lobe epilepsy: correlation with clinical severity and memory performances Epilepsia. 1999 Oct;40:1424-1432.

106. Namer IJ, Waydelich R, Armspach JP, Hirsch E, Marescaux C, Grucker D. Contribution of T2 relaxation time mapping in the evaluation of cryptogenic temporal lobe epilepsy Neuroimage. 1998 May;7:304-313.

107. Winston GP, Vos SB, Burdett JL, Cardoso MJ, Ourselin S, Duncan JS. Automated T2 relaxometry of the hippocampus for temporal lobe epilepsy Epilepsia. 2017 Sep;58:1645-1652.

108. Woermann FG, Barker GJ, Birnie KD, Meencke HJ, Duncan JS. Regional changes in hippocampal T2 relaxation and volume: a quantitative magnetic resonance imaging study of hippocampal sclerosis J Neurol Neurosurg Psychiatry. 1998 Nov;65:656-664.

109. Briellmann RS, Kalnins RM, Berkovic SF, Jackson GD. Hippocampal pathology in refractory temporal lobe epilepsy: T2-weighted signal change reflects dentate gliosis Neurology. 2002 Jan 22;58:265-271.

110. Briellmann RS, Syngeniotis A, Fleming S, Kalnins RM, Abbott DF, Jackson GD. Increased anterior temporal lobe T2 times in cases of hippocampal sclerosis: a multi-echo T2 relaxometry study at 3 T AJNR Am J Neuroradiol. 2004 Mar;25:389-394.

111. Chen H, Yu G, Wang J, Li F, Li G. Application of T2 relaxometry in lateralization and localization of mesial temporal lobe epilepsy and corresponding comparison with MR volumetry Acta Radiol. 2016 Sep;57:1107-1113.

112. Gonçalves Pereira PM, Oliveira E, Rosado P. Relative localizing value of amygdalo-hippocampal MR biometry in temporal lobe epilepsy Epilepsy Res. 2006 May;69:147-164.

113. Goodkin O, Pemberton HG, Vos SB, Prados F, Das RK, Moggridge J, et al. Clinical evaluation of automated quantitative MRI reports for assessment of hippocampal sclerosis Eur Radiol. 2021 Jan;31:34-44.

114. Peixoto-Santos JE, Kandratavicius L, Velasco TR, Assirati JA, Carlotti CG, Scandiuzzi RC, et al. Individual hippocampal subfield assessment indicates that matrix macromolecules and gliosis are key elements for the increased T2 relaxation time seen in temporal lobe epilepsy Epilepsia. 2017 Jan;58:149-159.

115. Rodionov R, Bartlett PA, He C, Vos SB, Focke NK, Ourselin SG, et al. T2 mapping outperforms normalised FLAIR in identifying hippocampal sclerosis Neuroimage Clin. 2015;7:788-791.

116. Sato S, Iwasaki M, Suzuki H, Mugikura S, Jin K, Tominaga T, et al. T2 relaxometry improves detection of non-sclerotic epileptogenic hippocampus Epilepsy Res. 2016 Oct;126:1-9.

117. von Oertzen J, Urbach H, Blümcke I, Reuber M, Träber F, Peveling T, et al. Time-efficient T2 relaxometry of the entire hippocampus is feasible in temporal lobe epilepsy Neurology. 2002 Jan 22;58:257-264.

118. Van Paesschen W, Duncan JS, Stevens JM, Connelly A. Longitudinal quantitative hippocampal magnetic resonance imaging study of adults with newly diagnosed partial seizures: one-year follow-up results Epilepsia. 1998 Jun;39:633-639.

119. Kandratavicius L, Balista PA, Lopes-Aguiar C, Ruggiero RN, Umeoka EH, Garcia-Cairasco N, et al. Animal models of epilepsy: use and limitations Neuropsychiatr Dis Treat. 2014;10:1693-1705.

120. Curia G, Longo D, Biagini G, Jones RS, Avoli M. The pilocarpine model of temporal lobe epilepsy J Neurosci Methods. 2008 Jul 30;172:143-157.

121. Lévesque M, Avoli M. The kainic acid model of temporal lobe epilepsy Neurosci Biobehav Rev. 2013 Dec;37:2887-2899.

122. Sloviter RS. Hippocampal epileptogenesis in animal models of mesial temporal lobe epilepsy with hippocampal sclerosis: the importance of the "latent period" and other concepts Epilepsia. 2008 Dec;49 Suppl 9:85-92.

123. Bertoglio D, Verhaeghe J, Dedeurwaerdere S, Gröhn O. Neuroimaging in animal models of epilepsy Neuroscience. 2017 Sep 1;358:277-299.

124. Polli RS, Malheiros JM, Dos Santos R, Hamani C, Longo BM, Tannús A, et al. Changes in Hippocampal Volume are Correlated with Cell Loss but Not with Seizure Frequency in Two Chronic Models of Temporal Lobe Epilepsy Front Neurol. 2014;5:111.

125. Wolf OT, Dyakin V, Patel A, Vadasz C, de Leon MJ, McEwen BS, et al. Volumetric structural magnetic resonance imaging (MRI) of the rat hippocampus following kainic acid (KA) treatment Brain Res. 2002 May 3;934:87-96.

126. Mathern GW, Bertram EH, 3rd. Recurrent limbic seizures do not cause hippocampal neuronal loss: A prolonged laboratory study Neurobiol Dis. 2021 Jan;148:105183.

127. Sen A, Thom M, Martinian L, Dawodu S, Sisodiya SM. Hippocampal malformations do not necessarily evolve into hippocampal sclerosis Epilepsia. 2005 Jun;46:939-943.

128. Thom M, Zhou J, Martinian L, Sisodiya S. Quantitative post-mortem study of the hippocampus in chronic epilepsy: seizures do not inevitably cause neuronal loss Brain. 2005 Jun;128:1344-1357.

129. Zhong J, Petroff OA, Prichard JW, Gore JC. Changes in water diffusion and relaxation properties of rat cerebrum during status epilepticus Magn Reson Med. 1993 Aug;30:241-246.

130. Reddy SD, Younus I, Sridhar V, Reddy DS. Neuroimaging Biomarkers of Experimental Epileptogenesis and Refractory Epilepsy Int J Mol Sci. 2019 Jan 8;20.

131. Luna-Munguia H, Marquez-Bravo L, Concha L. Longitudinal changes in gray and white matter microstructure during epileptogenesis in pilocarpine-induced epileptic rats Seizure. 2021 Aug;90:130-140.

132. Boux F, Forbes F, Collomb N, Zub E, Mazière L, de Bock F, et al. Neurovascular multiparametric MRI defines epileptogenic and seizure propagation regions in experimental mesiotemporal lobe epilepsy Epilepsia. 2021 May;62:1244-1255.

133. Laitinen T, Sierra A, Pitkänen A, Gröhn O. Diffusion tensor MRI of axonal plasticity in the rat hippocampus Neuroimage. 2010 Jun;51:521-530.

134. Stejskal EO, E. TJ. Spin diffusion measurements: spin echoes in the presence of a time‐dependent field gradient The journal of chemical physics. 1965;42:288-292.

135. Hahn EL. Spin echos Physical Review. 1950;80:580-594.

136. Le Bihan D, Breton E, Lallemand D, Grenier P, Cabanis E, Laval-Jeantet M. MR imaging of intravoxel incoherent motions: application to diffusion and perfusion in neurologic disorders Radiology. 1986 Nov;161:401-407.

137. Basser PJ, Mattiello J, Lebihan D. Estimation of the Effective Self-Diffusion Tensor from the NMR Spin Echo Journal of Magnetic Resonance, Series B. 1994 1994/03/01/;103:247-254.

138. Le Bihan D, Poupon C, Amadon A, Lethimonnier F. Artifacts and pitfalls in diffusion MRI J Magn Reson Imaging. 2006 Sep;24:478-488.

139. Beaulieu C. The basis of anisotropic water diffusion in the nervous system - a technical review NMR Biomed. 2002 Nov-Dec;15:435-455.

140. Mugler JP, 3rd, Brookeman JR. Rapid three-dimensional T1-weighted MR imaging with the MP-RAGE sequence J Magn Reson Imaging. 1991 Sep-Oct;1:561-567.

141. Damadian R. Tumor detection by nuclear magnetic resonance Science. 1971 Mar 19;171:1151-1153.

142. MacKay AL, Vavasour IM, Rauscher A, Kolind SH, Mädler B, Moore GR, et al. MR relaxation in multiple sclerosis Neuroimaging Clin N Am. 2009 Feb;19:1-26.

143. Tang X, Cai F, Ding DX, Zhang LL, Cai XY, Fang Q. Magnetic resonance imaging relaxation time in Alzheimer's disease Brain Res Bull. 2018 Jun;140:176-189.

144. Lurie DJ. Quantitative MRI of the Brain: Principles of Physical Measurement, 2nd edition PHYSICA MEDICA-EUROPEAN JOURNAL OF MEDICAL PHYSICS. 2020 02/01/;70:206-207.

145. Larsson HB, Frederiksen J, Petersen J, Nordenbo A, Zeeberg I, Henriksen O, et al. Assessment of demyelination, edema, and gliosis by in vivo determination of T1 and T2 in the brain of patients with acute attack of multiple sclerosis Magn Reson Med. 1989 Sep;11:337-348.

146. Carr HY, Purcell EM. Effects of Diffusion on Free Precession in Nuclear Magnetic Resonance Experiments Physical Review. 1954 05/01/;94:630-638.

147. Meiboom S, Gill D. Modified Spin‐Echo Method for Measuring Nuclear Relaxation Times Review of Scientific Instruments. 1958;29:688-691.

148. Treit S, Steve T, Gross DW, Beaulieu C. High resolution in-vivo diffusion imaging of the human hippocampus Neuroimage. 2018 Feb 1;182:479-487.

149. Kalviainen R, Salmenpera T. Do recurrent seizures cause neuronal damage? A series of studies with MRI volumetry in adults with partial epilepsy Prog Brain Res. 2002;135:279-295.

150. Caciagli L, Bernasconi A, Wiebe S, Koepp MJ, Bernasconi N, Bernhardt BC. A meta-analysis on progressive atrophy in intractable temporal lobe epilepsy: Time is brain? Neurology. 2017 Aug 1;89:506-516.

151. Noulhiane M, Samson S, Clemenceau S, Dormont D, Baulac M, Hasboun D. A volumetric MRI study of the hippocampus and the parahippocampal region after unilateral medial temporal lobe resection J Neurosci Methods. 2006 Sep 30;156:293-304.

152. Leemans A JB, Sijbers J, and Jones DK. ExploreDTI: a graphical toolbox for processing, analyzing, and visualizing diffusion MR data In: 17th Annual Meeting of Intl Soc Mag Reson Med2009. p. p. 3537.

153. Perrone D, Aelterman J, Pižurica A, Jeurissen B, Philips W, Leemans A. The effect of Gibbs ringing artifacts on measures derived from diffusion MRI Neuroimage. 2015 Oct 15;120:441-455.

154. Jezzard P, Barnett AS, Pierpaoli C. Characterization of and correction for eddy current artifacts in echo planar diffusion imaging Magn Reson Med. 1998 May;39:801-812.

155. Leemans A, Jones DK. The B-matrix must be rotated when correcting for subject motion in DTI data Magn Reson Med. 2009 Jun;61:1336-1349.

156. Lebel RM, Wilman AH. Transverse relaxometry with stimulated echo compensation Magn Reson Med. 2010 Oct;64:1005-1014.

157. McPhee KC, Wilman AH. Transverse relaxation and flip angle mapping: Evaluation of simultaneous and independent methods using multiple spin echoes Magn Reson Med. 2017 May;77:2057-2065.

158. Hennig J. Multiecho imaging sequences with low refocusing flip angles Journal of Magnetic Resonance (1969). 1988 1988/07/01/;78:397-407.

159. Boccardi M, Ganzola R, Bocchetta M, Pievani M, Redolfi A, Bartzokis G, et al. Survey of protocols for the manual segmentation of the hippocampus: preparatory steps towards a joint EADC-ADNI harmonized protocol J Alzheimers Dis. 2011;26 Suppl 3:61-75.

160. Geuze E, Vermetten E, Bremner JD. MR-based in vivo hippocampal volumetrics: 1. Review of methodologies currently employed Mol Psychiatry. 2005 Feb;10:147-159.

161. Bocchetta M, Boccardi M, Ganzola R, Apostolova LG, Preboske G, Wolf D, et al. Harmonized benchmark labels of the hippocampus on magnetic resonance: the EADC-ADNI project Alzheimers Dement. 2015 Feb;11:151-160 e155.

162. Frisoni GB, Jack CR, Jr., Bocchetta M, Bauer C, Frederiksen KS, Liu Y, et al. The EADC-ADNI Harmonized Protocol for manual hippocampal segmentation on magnetic resonance: evidence of validity Alzheimers Dement. 2015 Feb;11:111-125.

163. Duchesne S, Valdivia F, Robitaille N, Mouiha A, Valdivia FA, Bocchetta M, et al. Manual segmentation qualification platform for the EADC-ADNI harmonized protocol for hippocampal segmentation project Alzheimers Dement. 2015 Feb;11:161-174.

164. Yushkevich PA, Piven J, Hazlett HC, Smith RG, Ho S, Gee JC, et al. User-guided 3D active contour segmentation of anatomical structures: significantly improved efficiency and reliability Neuroimage. 2006 Jul 1;31:1116-1128.

165. Remy J, Remy-Jardin M, Artaud D, Fribourg M. Multiplanar and three-dimensional reconstruction techniques in CT: impact on chest diseases Eur Radiol. 1998;8:335-351.

166. Fedorov A, Beichel R, Kalpathy-Cramer J, Finet J, Fillion-Robin JC, Pujol S, et al. 3D Slicer as an image computing platform for the Quantitative Imaging Network Magn Reson Imaging. 2012 Nov;30:1323-1341.

167. Deleo F, Garbelli R, Milesi G, Gozzo F, Bramerio M, Villani F, et al. Short- and long-term surgical outcomes of temporal lobe epilepsy associated with hippocampal sclerosis: Relationships with neuropathology Epilepsia. 2016 Feb;57:306-315.

168. Jardim AP, Neves RS, Caboclo LO, Lancellotti CL, Marinho MM, Centeno RS, et al. Temporal lobe epilepsy with mesial temporal sclerosis: hippocampal neuronal loss as a predictor of surgical outcome Arq Neuropsiquiatr. 2012 May;70:319-324.

169. Falconer MA, Serafetinides EA. A follow-up study of surgery in temporal lobe epilepsy J Neurol Neurosurg Psychiatry. 1963 Apr;26:154-165.

170. Thom M, Liagkouras I, Elliot KJ, Martinian L, Harkness W, McEvoy A, et al. Reliability of patterns of hippocampal sclerosis as predictors of postsurgical outcome Epilepsia. 2010 Sep;51:1801-1808.

171. Jackson GD, Berkovic SF, Tress BM, Kalnins RM, Fabinyi GC, Bladin PF. Hippocampal sclerosis can be reliably detected by magnetic resonance imaging Neurology. 1990 Dec;40:1869-1875.

172. Basser PJ, Mattiello J, LeBihan D. MR diffusion tensor spectroscopy and imaging Biophys J. 1994 Jan;66:259-267.

173. Sanches P, Fujisao EK, Braga AMS, Cristaldo NR, Dos Reis R, Yamashita S, et al. Voxel-based analysis of diffusion tensor imaging in patients with mesial temporal lobe epilepsy Epilepsy Res. 2017 May;132:100-108.

174. Jenkinson M, Bannister P, Brady M, Smith S. Improved optimization for the robust and accurate linear registration and motion correction of brain images Neuroimage. 2002 Oct;17:825-841.

175. Ogren JA, Bragin A, Wilson CL, Hoftman GD, Lin JJ, Dutton RA, et al. Three-dimensional hippocampal atrophy maps distinguish two common temporal lobe seizure-onset patterns Epilepsia. 2009 Jun;50:1361-1370.

176. Whittall KP, MacKay AL, Li DK. Are mono-exponential fits to a few echoes sufficient to determine T2 relaxation for in vivo human brain? Magn Reson Med. 1999 Jun;41:1255-1257.

Appendix

A. Right hippocampus segmented on coronal mean DWIs from a 30-years old control male control. Segmented slices (1 mm) on two planes orthogonal to the acquisition axial-oblique plane are shown.

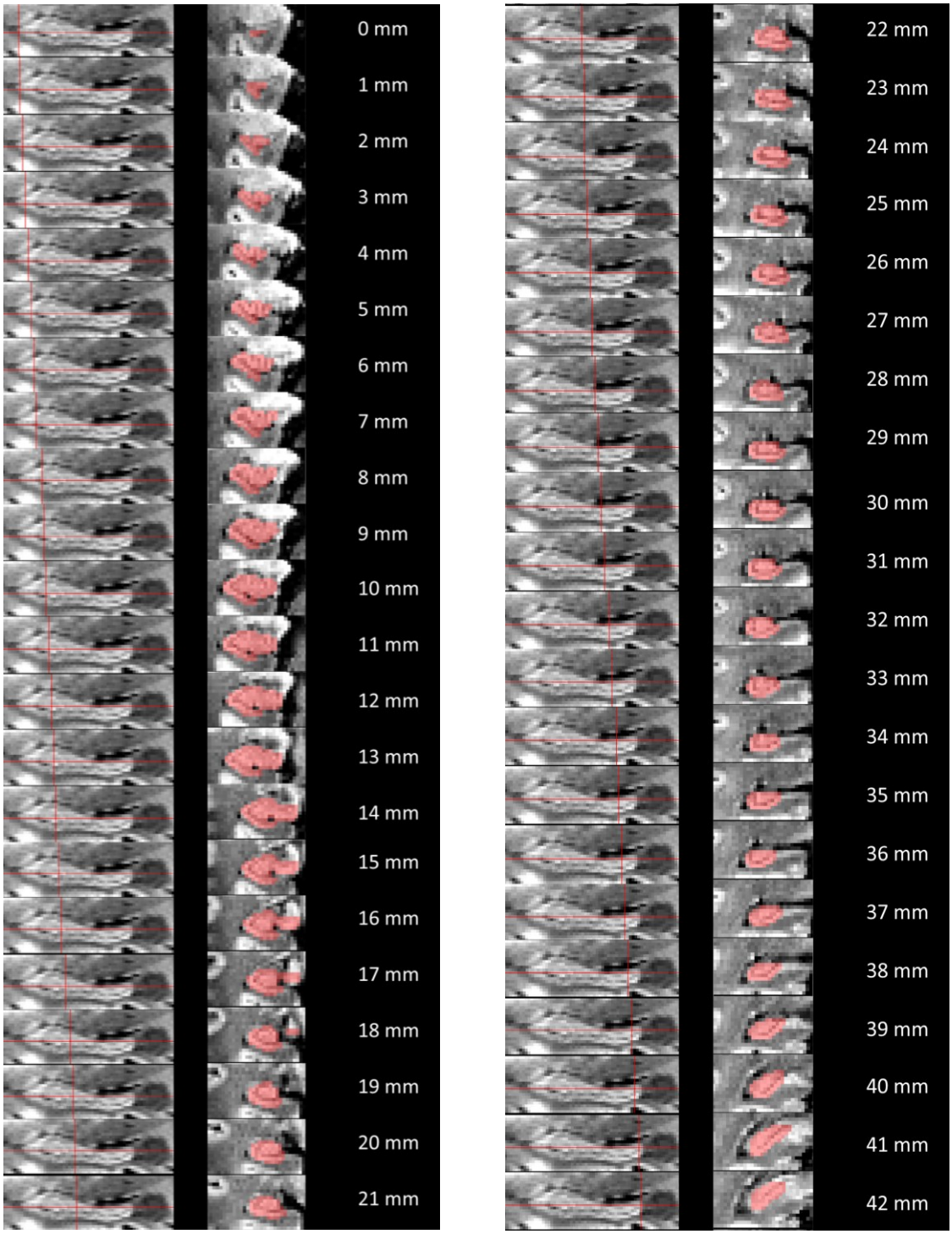

B. The following two figures show longitudinal co-registered regional (i) MD and (ii) T2 maps of all 19 TLE patients (surgical patients 6-13). The patients are numbered consistent with Table 3.1.

i) Mean diffusivity maps of the hippocampus.

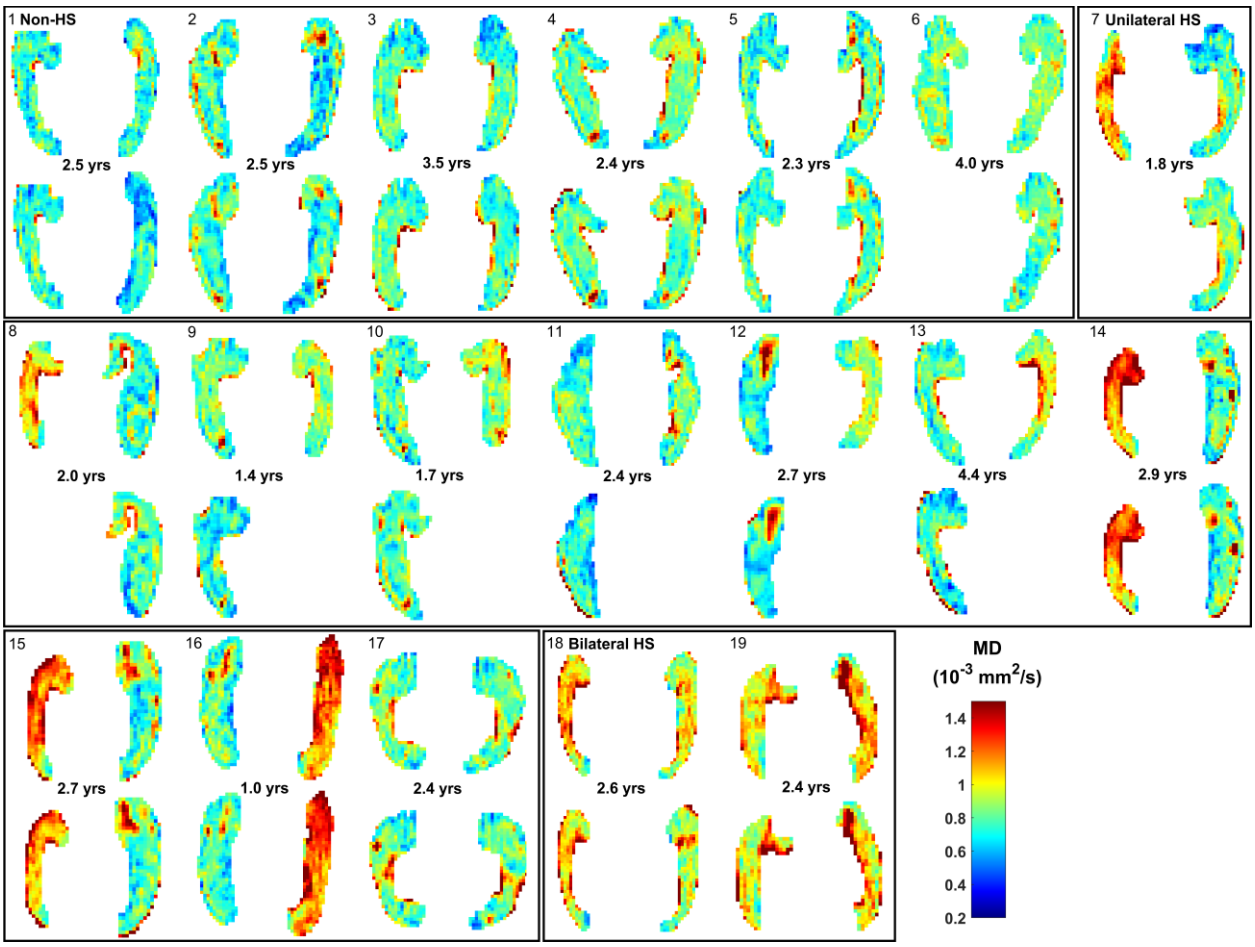

ii) Quantitative T2 maps of the hippocampus.

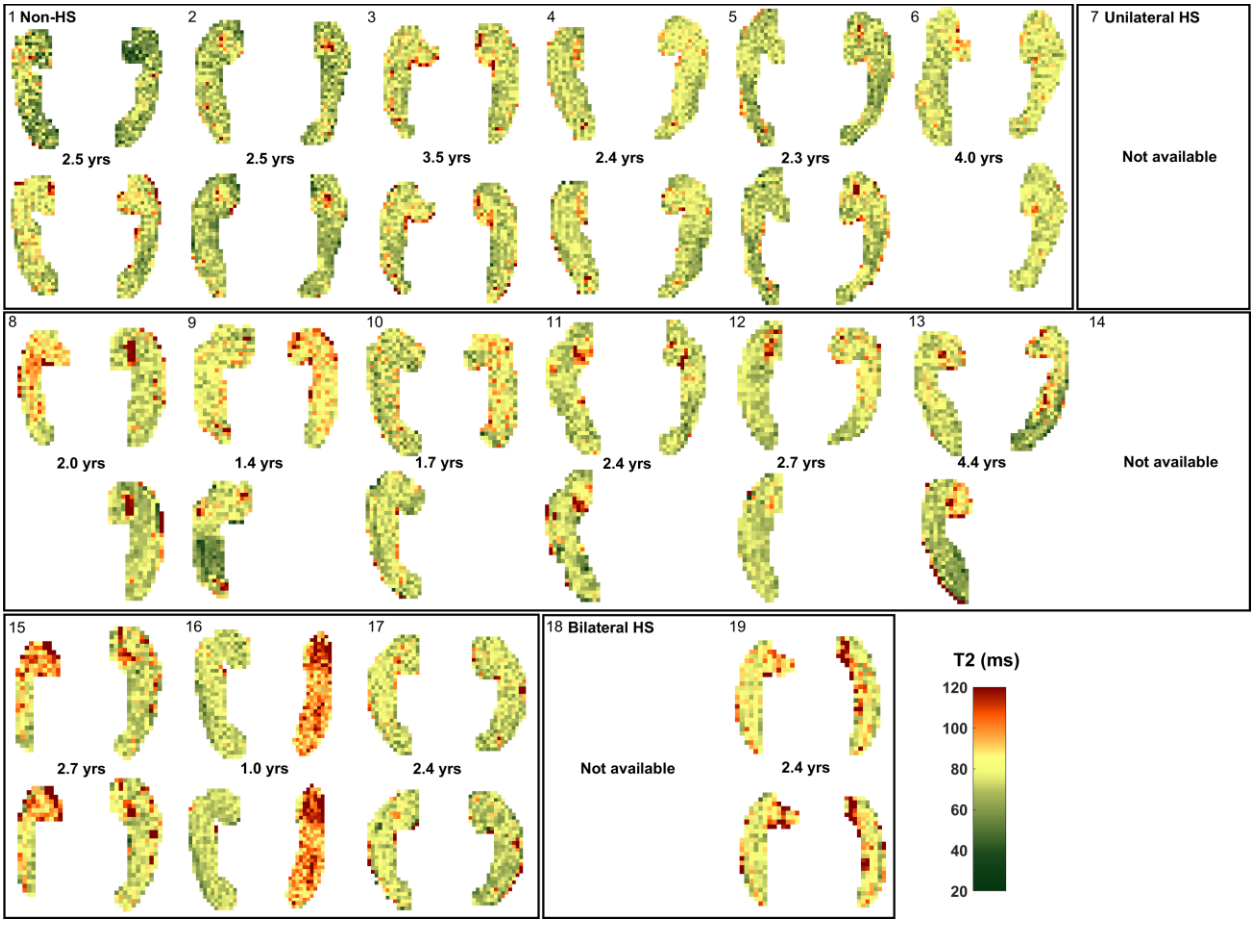

C. Comparison of pre-surgical MD (superimposed on mean DWI) and quantitative T2 maps (superimposed on echo-summed T2-weighted images) with NeuN (marker of neuronal loss) histology of all 8 patients who underwent surgical resection of the hippocampus. Regional patterns of MD agreed with HS subtype diagnosis in 6/8 patients (A, C, D, E, F and H). Regional patterns of T2 agreed with HS subtype diagnosis in 5/8 patients (A, C, D, E, and F). (C) Type 2 HS (neuronal loss in CA1) with MD and T2 elevations in both CA1 and CA4 of the ipsilateral hippocampus. (F) Type 2 HS without MD or T2 elevations in either subfields of the ipsilateral hippocampus. (H) Type 2 HS without T2 elevations in either subfields and MD elevation in CA2 of the ipsilateral hippocampus. Engel outcomes were determined within four months of the post-operative scans: Subjects 6, 7, 8, 10, 13 were assigned Engel IA ("Completely seizure-free"), subject 9 was assigned Engel ID ("Generalized convulsions with antiepileptic drug withdrawal only") and subjects 11 and 12 were assigned IIIA ("Worthwhile seizure reduction"). Subjects 6, 7 and 10 are shown in Figure 3.8. (§) denotes the two subjects reported in our previous study[94].